N-BUTANE ACTIVATION OVER RUTHENIUM AND IRON PROMOTED VPO CATALYSTS

By

Neoentle Masilo

Submitted in fulfillment of the academic

requirements for the degree of

Master of Science in the

School of Pure and Applied Chemistry,

University of KwaZulu-Natal

Durban

February 2009

ABSTRACT

The Fe- and Ru-promoted vanadium phosphorus oxide (VPO) catalysts were synthesized via the organic route in *iso*-butanol to form the VPO precursor, $VOHPO_4 \cdot 0.5H_2O$. The resulting precursor was then activated in a stream of nitrogen to form an amorphous $(VO)_2P_2O_7$, which crystallized after conditioning in the reactor in the presence of *n*-butane. The promoted catalysts were synthesized at 0.1%, 0.3% and 1% loading, pelletized and sieved to give a 300-600 μm pellet size. The catalysts were tested in a fixed-bed continuous flow micro-reactor and the products were analyzed by GC's equipped with a flame ionization detector (FID) to monitor maleic anhydride and *n*-butane and a thermal conductivity detector (TCD) to monitor the carbon oxides.

A range of characterization techniques were employed to determine the influence of the promoting elements on a VPO catalyst and to associate the composition of the catalysts obtained from such techniques with their performance. The characterization techniques used include X-ray diffraction (XRD), BET-surface area, ICP-OES, EDS, ^{31}PNMR, TPR, redox titrations, ATR and SEM to determine the phase composition of the catalysts, the surface area of the promoted catalysts relative to the un-promoted VPO, elemental mole ratios, the reducibility of the catalysts, average vanadium oxidation state, determination of the anions present in the surface of the catalysts and the variations in the morphology of the catalysts, respectively. Optimization of the system involved variation of the GHSV, the reactor temperature and the promoter loading. (Activation of a 0.75% *n*-butane in air mixture was performed at an optimum temperature of 400^{o}C while varying the gas hourly space velocity to establish a range of feed conversions and subsequently determine the activity of each catalyst with respect to *n*-butane conversion).

The promoted catalysts modified the morphology of the catalysts as evidenced by the scanning electron microscopy and the X-ray diffraction patterns. Furthermore an improved conversion was obtained with these catalysts. However, only the 0.1% iron-promoted catalyst improved maleic anhydride yield leading to *ca.* 10% maleic anhydride yield increment. Yields of 46% and 55% were obtained at GHSVs of 2573 and 1450 per hour respectively and a temperature of 400^{o}C. Electronic and structural modifications were encountered leading to an improved catalytic performance. The performance of this catalyst is associated with a vanadyl pyrophosphate phase (XRD), and a limited and controlled amount of V^{5+} species as illustrated in the TPR, and solid state ^{31}P NMR data. Moreover, this modification can be considered both structural and electronic in nature as observed in the SEM images and FTIR spectra of this catalyst. Furthermore, this improved performance is possible at higher conversions 80 to 90% conversion.

DECLARATION 1 - PLAGIARISM

I, Neoentle Masilo declare that

1. The research reported in this thesis, except where otherwise indicated, is my original research.
2. This thesis has never been submitted, in part or in whole for any degree or examination at any other university.
3. This thesis does not contain any other person's data, pictures, graphs or other information unless specifically acknowledged as being sourced from other persons.
4. This thesis does not contain any other person's writing, unless specifically acknowledged as being sourced from other researchers. Where other written sources have been quoted, then:
    a. Their words have been re-written but the general information attributed to them has been referenced
    b. Where their exact words as been used, then their writing has been placed in italics and inside quotation marks, and referenced
5. This thesis does not contain text, graphics or tables copied and pasted from the internet, unless specifically acknowledged, and the source being detailed in the thesis and in the reference sections

Signed……

ACKNOWLEDGEMENTS

I would like to first and foremost extend my gratitude to my sponsoring company, SASOL, for the financial support, and the NRF for financial support during the first year of this degree when I did not have a sponsor. Academically, I would like to thank my supervisor Prof. H. B. Friedrich for his intellectual advice throughout the duration of this project. I would like to appreciate the assistance offered by Mr. M. Mathebula regarding the reactor setup and Dr. E. Changamu for all the advice and encouragement which gave me the strength to advance through the toughest situations. I would also like thank the Head of school Prof. A. Kindness and other staff members for making my stay at this institution manageable. The technical staff members at the University of KwaZulu-Natal made this project a success; I would like to thank Mrs. A. Naidoo and Mrs. B. Soko for assistance with the instruments; Mr. B. Parell for GC-MS analysis; Mr. G. Moodley for his efficient assistance regarding the chemicals; Mr. H. Sishi and Mr. S. Parasram for technical assistance, as well as Mrs. J. Govender for efficient assistance with the orders. Thank you to all my friends, and the rest of the catalysis research group for being family away from home. Lastly, I would like to thank my family, Mercy, Matlhogonolo, Mmathapelo, Katlego and Tusani for all the love, patience and support throughout the duration of this project and God for giving me wisdom and courage.

ABBREVIATIONS

ATR: attenuated total reflectance spectroscopy

AV: average oxidation state

BET: Brenauer-Emmet-Teller

EDX: electron dispersive X-ray spectroscopy

FHWM: full widths at half maximum of reflection (crystal plane)

FID: flame ionization detector

GC: gas chromatograph

GC-MS: gas chromatography-mass spectroscopy

GHSV: gas hourly space velocity

ICP-OES: inductively coupled plasma-atomic emission spectroscopy

MA: maleic anhydride

ppm: parts per million

TAP: temporal analysis of products

TCD: thermal conductivity detector

TPR: temperature programmed reduction

VPD: VPO synthesis via the reduction of $VOPO_4 \cdot 2H_20$

VPO: vanadium phosphorus oxide

XRD: X-ray diffraction

DEFINITIONS AND CALCULATIONS

Average vanadium oxidation state (AV) = 5 - ($KMnO_4$ volume)/($Fe(NH_4)_2(SO_4)_2$ volume)

Gas space hourly space velocity (GHSV) = flow rate (ml. hr^{-1})/Volume of the catalyst bed

Percentage conversion of *n*-butane = n (*n*-butane in – out) x 100/n (*n*-butane in)

Percentage selectivity (MA) = 4 x n MA x 100/1 x n CO + 1 x n CO_2 + 4 x n MA

Percentage yield (MA) = % selectivity (MA) x % conversion (*n*-butane)/100

Carbon mass balance equation = 4 x n MA + n CO + n CO_2 x 100/4 x n (*n*-butane)

Specific activity = % conversion (*n*-butane)/surface area of the catalyst (m^2 g^{-1})

Specific selectivity = % selectivity (MA)/surface area of the catalyst (m^2 g^{-1})

CONTENTS

CHAPTER 1

INTRODUCTION

CHAPTER 2

CRYSTAL STRUCTURE AND MECHANISM OF TRANSFORMATION

CHAPTER 3

EXPERIMENTAL

CHAPTER 4

CHARACTERIZATIONS

CHAPTER 5

RESULTS AND DISCUSSIONS

LIST OF FIGURES

LIST OF TABLES

APPENDICES

CHAPTER 1

INTRODUCTION

1.1 Historical background of Maleic anhydride

Maleic anhydride (cis-butenedioic anhydride or toxilic anhydride) is an organic compound with the formula $C_4H_2O_3$. It is available in its pure state as a white solid with an acrid odor and has a melting point of 53 ^oC. Maleic anhydride is a potent dienophile in Diels-Alder reactions, hydrolyses to yield maleic acid and it is also an excellent ligand for low-valent metal complexes, e.g. $Pt(PPh_3)_2(MA)$ and $Fe(CO)_4(MA)$. This versatile chemical intermediate has numerous industrial uses and is of significant commercial interest worldwide. It is mainly used for the manufacture of unsaturated polyester resins.[1] These laminating resins, produced from maleic anhydride have high structural strength and good dielectric properties, have a variety of applications in automobile bodies, building panels, molded boats, lightweight pipes, bath tubs, etc. Other end products are agricultural chemicals, lubricating oil additives, specialty chemicals, paper reinforcement, lube additives, pharmaceuticals and food additives among others.[2] The applications of maleic anhydride are tabulated in Table1.1. The addition of maleic anhydride to drying oils is also significant, where the required drying time is decreased and the coating quality of lacquers is improved; dispersants derived from maleic anhydride prolong oil change intervals and improve the efficiency of automotive engines. Agricultural applications of MA include its use as herbicides, pesticides, and plant growth regulators.

The production of maleic anhydride is by mainly by vapor phase oxidation of n-butane. Apart from this way of production, maleic anhydride can also be produced as an intermediate from 1,4 butanediol, where it can be used in its crude unrefined state. The demand for this highly functional molecule continues to grow due to its diverse applications, hence the need for research to improve the existing technologies to further optimize production.

1.2 Maleic anhydride products

Table.1.1: The applications of maleic anhydride.

Product family	**Applications**
Unsaturated polyester resins	Boats, synthetic marble, automotive components, building panels, corrosion resistant products, aircraft/aerospace components and bath fixtures.
Food/ pharmaceutical	Fumaric, malic and succinic acids, paper sizing, alkyl resins and animal feed.
Personal care	Copolymer resins, hair spray, adhesives, floor polishes, oil well treating, textile sizing and printing ink.
Oil additives	Ashless dispersants.
Paper/water/intermediate chemicals	Surfactants, scale inhibitors, 1,4- butanediol, THF and γ-butyrolactone.
Detergents	Phosphate builder replacements, and anti re-deposition agents.
Agricultural/ pesticides	Insecticides, fungicides and growth regulators.
Other Applications	Artificial sweeteners, ready mixed concrete and epoxy hardeners

1.3 The selective oxidation of hydrocarbons

The selective oxidation of hydrocarbons is a widely exploited means of producing more valuable products from alkenes, aromatics and some saturated hydrocarbons. The need to develop suitable catalysts for these transformations is of utmost importance. There is a necessity for the particular catalyst to be able to transform those hydrocarbons in a single step by reaction with molecular oxygen, into partially oxidized products.

These can, in turn, be transformed into other highly demanded chemicals. As an example the classification of catalyzed hydrocarbon reactions with oxygen are given in Table.1.2 with an illustrative example for each class of reaction. For class I reactions, where the hydrocarbon is oxidized by dehydrogenation, the process can only become successfully applied if thermodynamics can allow the use

of a lower temperature to prevent complete oxidation of the reactants directly to carbon dioxide. However, the oxidation of a hydrocarbon to give a more saturated molecule (and water) is a thermodynamically favored reaction, due to the high enthalpy of formation of water, hence the necessity to employ a suitable catalyst. As an example, in the oxidative dehydrogenation reaction of *n*-butene with air, butadiene could be selectively formed in good yields at lower temperatures than what could be obtained in direct dehydrogenation. In class II reactions, where oxygen atoms are to be incorporated into an unsaturated molecule while preserving the unsaturation point, the carbon-hydrogen bond on the methyl group adjacent to the unsaturation point is activated via the formation of an allyl-radical, followed by the dehydration and re-oxidation as the final steps in the catalytic cycle.

Table.1.2: Classification of catalyzed reactions of hydrocarbons with oxygen

CLASS I	Oxidative dehydrogenation 1. Dimerization of propene to hexadiene or benzene 2. Dehydrogenation of butane or butene to butadiene 3. Dehydrocyclization of hexane to cyclohexane
CLASS II	Formation of oxygenated products without carbon-carbon bond fission 1. Oxirane / and acetaldehyde from ethene 2. Acrolein, acetone, allyl alcohol, and acrylic acid from propene 3. Maleic anhydride from butadiene; phthalic anhydride from *o*-xylene
CLASS III	Formation of oxygenated products with carbon-carbon bond fission 1. Acetaldehyde and acetic acid from propene 2. Maleic anhydride from benzene; Phthalic anhydride from naphthalene
CLASS IV	Complete oxidation

The formation of a stable л-allyl radical in order to preserve the unsaturation is applicable to propene and higher hydrocarbons, whereas in the case of ethene, the selective oxidation takes place either by direct insertion of an oxygen atom in the double bond or by formation of a temporary chemisorbed complex (as in the synthesis of vinyl acetate on palladium catalysts).[3]

Class III reactions involve the direct oxidation at the double bond, in order to favor the formation of a desired product. This class of reaction, however, results in lower selectivities, and it is also accompanied by carbon loss, e.g. in benzene oxidation to maleic anhydride one-third of the six carbon atoms are lost as carbon oxides. The last class (IV) is most applicable in atmospheric pollution control, whereby carbon monoxide and hydrocarbons can be oxidized to carbon dioxide on noble metal, or oxide catalysts.[3]

1.4 The selective oxidation and transformation of n-butane

Light alkanes have continued to attract tremendous research interest in their catalytic transformation to more valuable chemicals in both the petroleum and petrochemical industries. The value of products that have undergone this type of transformation could be estimated to approximately $40 billion world-wide per annum.[4] An industrially significant and successful process which falls within these classes of catalytic transformations is the 14-electron selective oxidation of *n*-butane to MA over vanadium phosphorus mixed oxide catalysts. This reaction has been considered the only successful industrial process of a selective vapour phase oxidation that uses dioxygen.[5] The process of producing maleic anhydride originated in the early 1930s where the transformation was based on benzene feed-stock over V_2O_5-MoO_3 catalysts. The transformation is illustrated in Fig.1.1

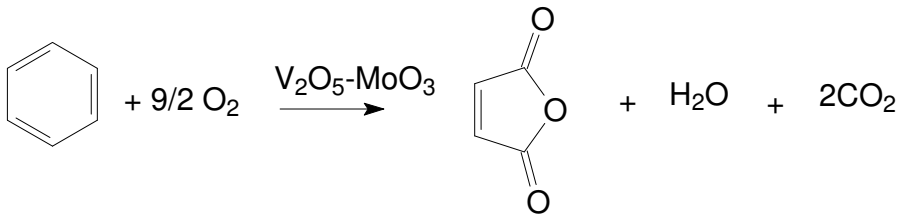

Fig.1.1: Selective oxidation of benzene on V_2O_5-MoO_3 catalysts.

The production from benzene feed-stock became a major concern following the environmental issues associated with this feed-stock. This led to the introduction of environmental legislature which brought about the strict control of benzene emissions from MA plants, prohibiting any traces of benzene emissions to the atmosphere. As a result of this legislature, the existing plants were either shut down or converted to alternative feed-stocks. The C_4-hydrocarbons were tested as an alternative for MA production, and the first catalysts to be tested were the V_2O_5-MoO_3, catalysts used in benzene oxidation. These catalysts resulted in poor selectivity to maleic anhydride, favoring epoxidation and isomerization reactions.[2] Other classes of catalysts which were also tested included: chromia-alumina and Fe_2O_3 promoted with CrO_3 and K_2CO_3.[5] These classes of catalysts, though found to be active in the dehydrogenation of n-butane and n-butenes to butadiene, were not able to complete the transformation to MA. The other catalyst to be

investigated was the vanadium phosphorus oxide catalyst (VPO). This catalyst was reported by Bergman and Frisch in the mid 1960s as a possible catalyst to effect the transformation of *n*-butane to maleic anhydride.[6]

VPO catalysts were then investigated on other C_4 hydrocarbons. Butadiene, *n*-butenes and *n*-butane were all tested for MA production, but despite all the research efforts to focus on C_4 hydrocarbons, it appeared at that time that *n*-butane was still uncompetitive, mainly because of the lower yields compared to the benzene route which was already established and cost effective. However, two important factors arose which resulted in *n*-butane becoming more favorable: The first factor was the reduced costs of *n*-butane, due to the ready availability brought about by the large scale exploitation of natural gas in the United States, and benzene becoming more expensive and scarce due to its applications in the automobile fuels. The second factor was the environmental restriction on atmospheric benzene emissions.[7] These factors contributed to C_4 selective oxidation being favored as opposed to benzene oxidation and the most favorable feed-stock for this transformation was found to be *n*-butane as illustrated in Fig.1.2. Productivity from n-butane is still considered a challenge, under typical industrial conditions (2 mol % *n*-butane in air, 673-723K, and the space velocities of 1000-2600 h^{-1}) the selectivities for fixed-bed production are 67-75 mol% at 70-85 % n-butane conversion.[8]

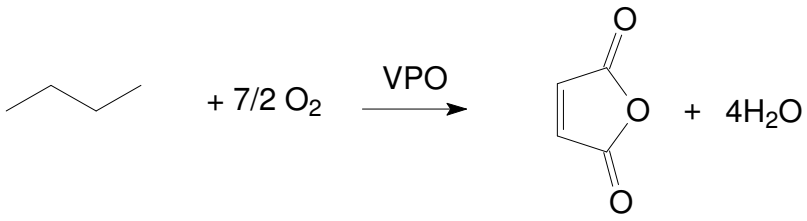

Fig. 1.2: The selective oxidation of n-butane on VPO catalysts.

In general, the production rate of a butane-based plant is 60-70% of a benzene-plant,[6] the utilization of a butane based plant requires larger capital outlays, in particular for larger reactor and recovery units. This downfall, however, can counter balanced by the utilization of other options for the VPO reactor systems. The fluid bed butane-based system is one such option which offers an advantage of operation at higher butane concentrations (up to 4%) and can thus lower original capital costs. Though this may become economically beneficial, the utilization of higher butane concentrations poses problems such as low selectivity and the inherent problems associated with attrition of vanadium phosphorus oxide materials. These factors need to be overcome before this process will become economically employed.[8]

The other interesting alternative is the DuPont transport bed technology which uses the recirculating solid reactor (RSR) developed in the 90's. This reactor operates at lower conversions per pass and with higher selectivities than normally encountered in fixed or fluidized-bed reactors. The DuPont C_4-maleic anhydride transport bed technology employs the redox couple concept, which according to the Mars and van Krevelen mechanism is being utilized by most gas-solid and liquid-solid reactions. In fixed-bed and fluidized-bed reactors oxygen (air) in excess and the reactant are co-fed into the reactor. In this instance the catalyst is supposed to discriminate between the oxidizing and the reducing environment and hence the loss in selectivity results in an excessive oxidizing atmosphere leading to the formation of the total oxidation product CO_2, which is a thermodynamically favored product. In the Dupont RSR technology, the gaseous organic molecules are oxidized in a riser, thus reducing the catalyst. The resulting reduced catalyst is then regenerated by air in a fluidized-bed reactor before entering again the riser and repeating the cycle (Fig.1.3).[9] Apart from the improvement of the novel reactors in the selective oxidation of *n*-butane to maleic anhydride, research has also focused on the inclusion of promoter elements into the VPO catalysts for this reaction. The industrially employed VPO catalysts are usually promoted with metal elements to improve the catalytic activity.[8] In this study a fixed-bed reactor will be used for the hydrocarbon activation, therefore the different kinds of reactors will not be discussed. But much emphasis will be on the inclusion of promoter elements in the VPO catalysis, as that is the aim of this study.

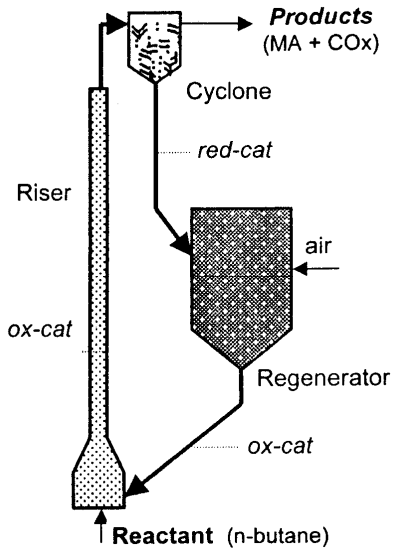

Fig.1.3: Recirculating riser reactor: The catalyst particles circulate in the riser where the reaction take place and in the fluid-bed were it is regenerated in its oxidized and reduced states respectively.[9]

1.5 Catalyst preparation and catalysis

The conventional ways of preparing precursors of VPO catalysts have been by the reduction of V_2O_5 in either aqueous or organic medium using either the hydrochloric acid digestion method or using *iso*-butanol or *iso*-butanol-benzyl alcohol mixtures as the reducing agents, followed by the addition of a stoichiometric amount of *o*-H_3PO_4 according to the required P/V molar ratios. The other route that has been followed previously is the reduction of $VOPO_4{\cdot}2H_2O$ in organic solvents, typically *iso*-butanol. The VPO catalysts are then prepared by the thermal degradation of this precursor, vanadyl hydrogen phosphate hemihydrate, $VOHPO_4{\cdot}0.5H_2O$. The performance of a VPO catalyst mainly depends on (i) the method of precursor synthesis (reducing agents, solvents, synthesis temperature and duration) (ii) Methods used for activation and conditioning of the precursor at high temperature, and (iii) the nature of metal promoters.

1.5.1 The synthesis of $VOHPO_4{\cdot}0.5H_2O$

A general agreement exists in the literature regarding the important parameters to be considered for the synthesis of an optimum VPO catalysts. The following have been reported.[10]

i. The synthesis of a microcrystalline vanadyl hydrogen phosphohemi-hydrate precursor in an alcohol medium preferentially exposing the basal (001) planes and,
ii. A slight excess of phosphorus with respect to stoichiometry known to bind strongly to the surface and not easily removed by simple washings of the precursor in polar solvents.

The most important methods for the preparation of the vanadyl phosphohemi-hydrate precursor include the following:

Preparation in an aqueous medium, (hydrochloric acid digestion method) whereby the V^{5+} (e.g. V_2O_5) species is reduced to V^{4+} in the presence of aqueous hydrochloric acid and *o*-H_3PO_4, followed by evaporation of the solvent to dryness.[11]

i. $V_2O_5 + 2NH_4OH\text{-}HCl + 2H_3PO_4 \rightarrow 2VOHPO_4{\cdot}0.5H_2O + N_2 + 2HCl + 4H_2O$

The synthesis can also be carried out in an organic medium, in this method the V^{5+} compounds are reduced by an anhydrous alcohol, followed by the addition of anhydrous *ortho*-phosphoric acid dissolved

in the same alcohol, followed by the precipitation of $VOHPO_4 \cdot 0.5H_2O$.[10, 12]

ii. $V_2O_5 + EtCHOHMe + 2H_3PO_4 \rightarrow 2VOHPO_4 \cdot 0.5H_2O + EtCOMe + 2H_2O$

The third method utilizes water as a solvent to yield the V^{5+} orthophosphate dihydrate [$VOPO_4.2H_2O$], which is then reduced to the hemi-hydrate in a separate step.

iii. $V_2O_5 + 2H_3PO_4 + H_2O \rightarrow 2VOPO_4 \cdot 2H_2O + H_2O$

$2VOPO_4 \cdot 2H_2O + EtCHOHMe \rightarrow 2VOHPO_4 \cdot 0.5H_2O + EtCOMe + 2H_2$

The organic synthesis route produces the most active and selective catalysts relative to the aqueous preparations because of the higher surface areas obtained in the former preparation. All of the three methods lead to various hydrated vanadyl(IV) hydrogen phosphate phases, $VOHPO_4 \cdot nH_2O$ (n = 0.5, 1, 2, 3, 4) which are all VPO precursors. Among all these precursors, the precursor with n = 0.5 produces the best VPO precursor for *n*-butane to maleic anhydride transformation.[8] Several reducing agents have also been used in the preparation of VPO catalysts. These include $NH_4OH.HCl$, $N_2H_4.2HCl$, ethylene glycol, glycerol, metallic tungsten and mixtures of HCl and $H_2C_2O_4$. Some patents also propose that the phosphorus component be added as a mixture of phosphoric and phosphorus acids, while other patents claim the advantages of using organic solvents and reducing agents. Surface area improvements in the range of (10-30m^2g^{-1}) have been reported for catalysts prepared in *iso*-butanol using anhydrous HCl (g) as a reducing agent, these were characterized by an average oxidation state of ~ 4.2.[2] High surface areas have also been reported when mixtures of *iso*-butanol/benzyl alcohol were used as reducing agents and solvent, but, although high surface areas are reported from the use of many organic reagents, improved catalytic activity does not always follow. When methanol, acetic acid or THF were used, increased surface areas were observed but, contrary to *iso*-butanol, higher reaction temperatures by 50-90 ^oC were required to achieve equivalent activities and selectivities even though BET surface areas were similar.[13] The importance of filtering the vanadium solution before addition of the phosphorus component, in order to remove unreacted vanadia particles greater than 0.04 mm in diameter, when *iso*-butanol is used as a reducing agent and solvent has also been reported.[14] Hutchings and Higgins[15] reported the presence of $VO(H_2PO_4)$ when they prepared catalysts (P:V = 1.2:1) by the HCl digestion method utilizing water as a solvent. They also reported a detrimental effect (reduced surface areas) associated with this compound, but they further concluded that the same compound could be effectively removed by treating the once dried precursor in boiling water or extracting it with di-methyl sulphoxide at 70 ^oC and filtering the resulting slurries hot. The different methods reported above play an important role in controlling the morphology of the catalysts. The morphology of the precursors made by the organic route depends on the

(a) the nature of solvent and reducing agent, (b) the synthesis P/V ratio, and (c) the amount of water present during synthesis.[16] These factors will be elaborated briefly below.

1.5.2 Factors influencing the morphology of the precursors made by the organic route:

a. The nature of the solvent and reducing agents

The morphology of the catalyst can be varied by the introduction of different solvents at a constant P/V, e.g. P/V =1.0. A series of vanadium alkoxy phosphates can be achieved by the use of straight alcohols and branched chain alcohols leading to various morphologies of $(VO)_2H_4P_2O_9$. During $VOPO_4{\cdot}2H_2O$ reflux in *iso*-butanol (VPD route of synthesis), a rosette-type morphology of $(VO)_2H_4P_2O_9$ was achieved; reflux in secondary-butanol, tertiary butanol or ethanol resulted in the formation of non-agglomerated platelets of $(VO)_2H_4P_2O_9$, whereas mixtures of *iso*-butanol/benzyl alcohols favor the rosette-type morphology with more agglomerated platelets relative to pure *iso*-butanol.[10] When the conventional hydrochloric acid digestion method was used, where HCl is used as a reducing agent, a significant amount of water is produced in the system and this requires solvent removal to almost dryness by evaporation to enable the formation of the precursor crystallites. Furthermore, when HCl and oxalic acid are used as reducing agents a higher activation temperature is required relative to what would be utilized for catalysts prepared in the presence of *iso*-butanol as a reducing agent. For methanol, acetic acid or THF, 50-90 ^oC higher reaction temperatures are needed to achieve comparable selectivities and activities relative to *iso*-butanol/benzyl alcohol mixtures.

b. The synthesis P/V ratio

Phosphorus to vanadium ratio in excess of stoichiometry is easily accommodated in the $VOHPO_4{\cdot}0.5H_2O$, precursor for *n*-butane activation to maleic anhydride. The main importance of excess phosphorus in these catalysts is to stabilize the V^{4+} valency relative to V^{5+} and to prevent possible over-oxidation during the hydrocarbon activation.[8, 16] An acceptable P/V ratio for VPO catalysts is between 1.0 and 1.2. Ratios of P/V greater than P/V=2, lead to the formation of trace amounts of an impurity phase $[VO(H_2PO_4)_2]$ which can be observed in the X-ray diffraction patterns. The presence of this phase was confirmed by X-ray line broadening, decrease in surface area and a change of platelet morphology from a distinct morphology of thin platelets randomly aggregated into non-uniformly sized clumps. P/V ratio is an important factor in determining the redox properties of the catalyst, i.e. the reducibility and the

oxidizability of the catalysts; the phase composition and the distribution of vanadium oxidation states in the catalysts. Different phase compositions can result following transformation depending on different P/V ratios. Further elaboration on the phase compositions will be dealt with under activation conditions.

c. The amount of water present during the synthesis

The presence of water during the synthesis of VPO precursors is accompanied by detrimental effects affecting the surface area and hence the catalytic activity. Most authors in the open literature report the addition of tetra ethyl orthosilicate (TEOS) during precursor synthesis to consume, by hydrolysis, the water produced as a by-product of the reaction between *o*-H_3PO_4 and V_2O_5.[17]

1.5.3 The mechanism of $VOHPO_4{\cdot}0.5H_2O$ formation

The mechanism of $VOHPO_4{\cdot}0.5H_2O$ formation has been deduced from the V^{5+} reduction by alcohols. During the oxidation of cyclobutanol as a probe in the mechanism of V^{5+} reduction, the formation γ-hydroxyaldehydes was encountered, providing evidence of a 1-electron process in this reaction. When methyl cyclobutyl ketyl was used as a probe molecule, it was discovered that methyl cyclobutyl ketyl was 10^4 times less active than cyclobutanol giving a clear indication of the importance of the hydroxyl bond in the process. The formation of $ROV(OH)_2(OH_2)_n^{2+}$ (n = 1,2,3,4), an ester of vanadic acid, intermediate suggests that OH bond breaking occurs either prior to or during the rate determining step. The spontaneous formation of vanadate esters was reported by Tracey and Gresser and was observed in the V NMR spectra at pH = 7-11 and a temperature of 398 K. The vanadate ester was found to occur as the tetrahedral monoprotonated anion (HVO_4^{2-}); diprotonared anion ($H_2VO_4^-$) denoted as $V_{i;}$ dimeric ($HO_3VOVO_3H^{2-}$) and the tetrameric ($H_4V_4O_{14}^{4-}$) species. Gresser *et al.*[18] reported the formation of mixed anhydrides of vanadate with phosphates; these can be considered to be the molecular precursors of vanadium phosphate phases. These vanadate esters and phosphovanadates may aid in the V^{5+} reduction by these possible routes:

1 Redox decomposition of the monoalkyl ester of monomeric vanadate generating a free radical species.
2 Redox decomposition of monoalkyl ester of dimeric vanadate, accompanied by two successive one-electron transfers.
3 Redox decomposition of monoalkyl esters of phophovanadate, $[ROV^{5+}O_2\text{-}O\text{-}PO_3H]^{2-}$ leading to the formation of $[V^{4+}O(H_2O)_4OPO_3H]$ species, a precursor to the formation of $VOHPO_4{\cdot}0.5H_2O$.

1.6 Thermal activation of $VOHPO_4 \cdot 0.5H_2O$

During thermal transformation of a $VOHPO_4 \cdot 0.5H_2O$ precursor, several critical factors, e.g. time, temperature and atmosphere of activation; morphology of a precursor phase; P/V ratio; and the presence of defects in structure play an important role in determining the final properties of a VPO catalyst. The transformation of a precursor phase can be effectively activated under inert or oxidizing atmospheres followed by the introduction of a hydrocarbon-air mixture. Activation under inert conditions at temperatures > 673K leads to the formation of a poorly crystalline $(VO)_2P_2O_7$ with little formation of V^{5+} species following the introduction of *n*-butane-air mixture. Calcinations in air are carried out at temperatures less than 673K to give mixtures of $(VO)_2P_2O_7$ and V^{5+} species, these species are reported to form high activity catalysts with low selectivity towards maleic anhydride.[19] Transformations in n-butane-air mixtures lead to complete transformation of the precursor into δ-$VOPO_4$ and $(VO)_2P_2O_7$. These transformations are illustrated in Fig.1.4.

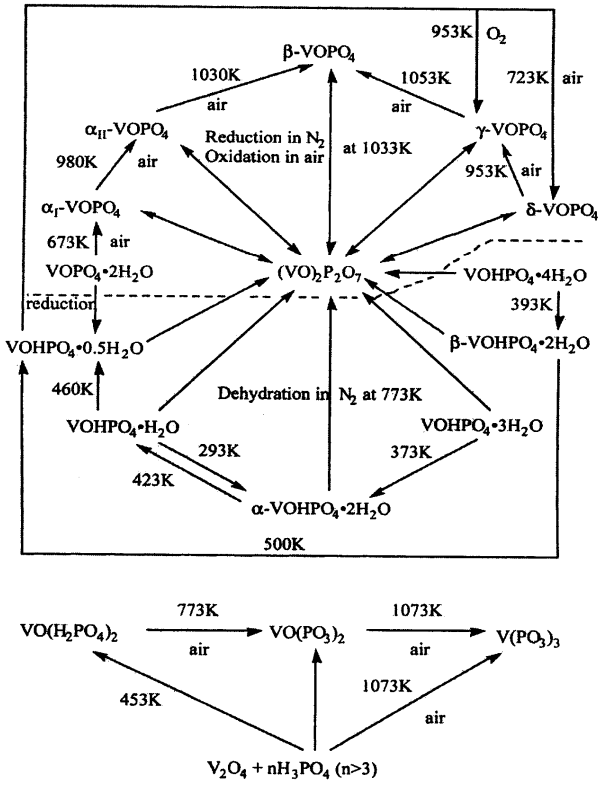

Fig. 1.4: Phase transformation in the VPO system. Reversible redox transformations (top) are separated from irreversible dehydrations (bottom).[20]

This transformation has been reported to proceed through the preservation of V-O-P connectivity, i.e. topotactically, with the precursor morphology being retained following transformation. X-ray diffraction revealed the broadening of the interlayer spacing reflections of (001) relative to the in-plane (130) reflection in the precursor, the same trend was observed in the X-ray diffractogram of the catalysts activated under nitrogen atmosphere, where broadening of the interlayer spacing reflections of the (200) plane relative to the (024) reflection was obtained.[20] Torardi *et al.*[21] explained this topotactic transformation according to the phosphorus inversion mechanism. In this mechanism, the formation of edge-sharing vanadyl dimers occurs as a result of loss of coordinated water. Following this, these vanadyl dimers rearrange from a shared edge to a parallel arrangement of V=O bonds as a result of a concominant decrease in the d-spacing. This rearrangement leads to about 12% expansion of the *a*-lattice parameter, followed by proton transfer from half of the [HPO_4] groups yielding [PO_4] and [H_2O-PO_3] entities. Subsequently water is lost from the latter units allowing full condensation of the layers into a three-dimensional network. A displacement of one of the V atoms in a pair along the *c*-axis toward an apical oxygen atom enables the connection of adjacent layers of the square pyramidal VO_5 pairs, creating edge-sharing vanadyl dimers with a *trans*-arrangement of the vanadyl oxygen along the *c*-axis through the plane of the three basal oxygen atoms bonding to a [PO_4] unit located near the original layer.[21]

Activation in a hydrocarbon-air mixture has proven beneficial in modifying the redox properties of a catalyst. Sobalik *et al.*[22] studied the ability of a VPO system to change its equilibrium solid-state properties as a function of reaction conditions. The effect of different reaction atmospheres and temperatures on the average oxidation state of vanadium was further illustrated by Taufiq-Yap and Saw.[23] where they studied the variation of the average oxidation state for catalysts with P/V ratios of 1.02-1.13 during activation under 1% 1-butene-air flow. The average oxidation state of 4+ was found to increase with temperature to ~ 4.2+.

However when the same catalyst was subjected to slow activation procedures in air, a mixture of the β-phase and α-$VOPO_4$ was formed with an average oxidation state of 4.4+ which decreased to 4.2+ following introduction of the hydrocarbon-air mixture at 430 ^oC. The introduction of the hydrocarbon-air mixture to a previously calcined catalyst functions to condition the catalyst leading to an improved

crystallinity, increased surface area and the reduction of V^{5+}species in the presence of n-butane improving the activity of the catalyst. The presence of V^{5+}species in the catalyst leads to an active but less selective catalyst; therefore a conditioning procedure is required for a catalyst with an optimum behavior. The steady state performance of a catalyst can be obtained after ~ 10 days on-stream. After this time *ca.* 15Å of an amorphous layer covering the surface of the 200 plane disappears, after *ca.* 23 days on stream the 200 plane of $(VO)_2P_2O_7$ extends to the last surface layer in the equilibrated (conditioned) catalyst and this ordering of the $(VO)_2P_2O_7$ leads to a much higher steady state selectivity to maleic anhydride.[24]

1.7 The role played by metal elements in VPO catalysts

Over the years academic and industrial research has focused on the inclusion of metal elements in the VPO formulations with the aim of improving the catalytic performance. A wide variety of metal elements have been tested for the VPO system; the alkali, alkaline earth metals and the transition metals have been investigated to determine their influence on the catalytic properties e.g. Lewis acidity and the redox properties (V^{4+}/V^{5+} balance). It has been reported in the literature that these metal promoters may affect either the structure or the electronic properties of the catalyst during activation to act as structural or electronic promoters. A promoting element may be introduced in various ways to the VPO catalyst, whereby it can be added as a metal or as the salt of the metal under study, within the levels of 0.25-0.5 wt. % corresponding to surface coverage of 0.1-0.2 theoretical mono-layers.[25] At the level below the theoretical monolayer [~ 2-3 wt. %] the promoting element may dissolve within the VPO lattice, forming a two dimensional surface oxide over-layer, this is mainly achieved when soluble promoter salts are introduced directly during $VOHPO_4{\cdot}0.5H_2O$ synthesis. At higher loadings (>3wt. %) the formation of promoter-containing bulk phases, such as oxides or phosphates occurs.

Although the exact role being played by promoters in this system is still poorly understood, from previous studies the following possibilities can be deduced:

i. To control the morphology, whereby there might be a transformation from a rhomboid platelet structure to agglomerated rosettes, or even the reduction in the FHWM of the platelets.[45]
ii. To control the phase composition $(V^{4+}O)_2P_2O_7$ vs. $V^{5+}OPO_4$
iii. Modification of the elemental compositions (P/V) in both the surface and the bulk.
iv. To control the redox properties, as well as modify the V^{4+}/V^{5+} ratio of the catalyst.
v. Improved surface areas with respect to the unpromoted catalyst.

Furthermore, different methods can be used to introduce the metal elements into the VPO system, depending on the preferred location of the promoting element (surface or bulk).

i. During the precursor synthesis together with V_2O_5 and *o*-H_3PO_4.
ii. Impregnation of the precursor prior to thermal activation.
iii. Impregnation into a VPO catalyst following thermal transformation.

These metal elements, once present in the catalyst, can exist in four types of phases, metallic, metallic oxide, metal phosphate and bimetallic phosphate.[26] It has been reported that when alkaline-earth metals are used as promoters, the formation of bi-metal phosphates, such as $M(VO)_2P_2O_7$ and $MVOPO_4$ may take place with the metal being distributed in the empty channels of pyrophosphate of orthophosphate networks.[27] Zazhigalov *et al.*[26] studied the alkali and the alkaline earth metals in VPO catalysts towards the partial oxidation of *n*-butane to maleic anhydride. They studied the incorporation of metals such as Na, K, Cs, Be, Mg, Ca, and Ba. In their study Zazhigalov *et al.*[26] found a decrease in the binding energy (BE) of O1s – electrons in the promoted catalysts, this provided evidence of the increase of the negative charge on oxygen atoms, corresponding to the increase of the basicity of the surface and this was further confirmed by the adsorption of CO_2 on the promoted catalysts relative to the pure un-promoted catalysts. As an illustration, Zazhigalov's finding is included as a plot showing the amount of CO_2 adsorbed on the alkaline-earth metal promoted catalysts as a function of the binding energy of O 1s – photoelectrons (Fig 1.5)[26]

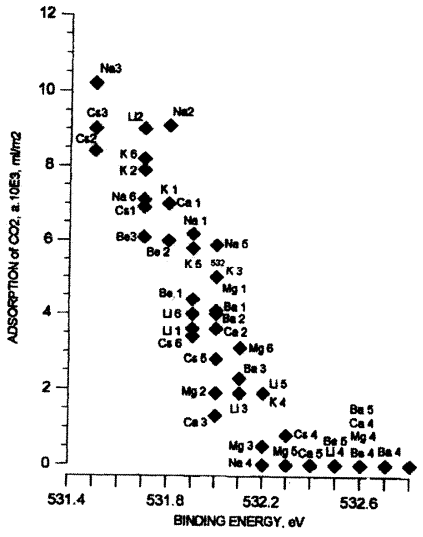

Fig.1.5: The amount of CO_2 adsorbed on V-P-M-O catalysts as a function of the binding energy of O 1s-photelectrons.[26]

Surface phosphorus enrichment was also observed in these catalysts. However, this enrichment of phosphorus occurred at the expense of outward diffusion of over-stoichiometric phosphorus in the pellet, moreover this increase of phosphorus concentration on the surface appears to be accompanied by surface oxygen enrichment leading to an increase in oxygen basicity. Therefore the modification of the acidic properties of the catalyst is established, influencing both the activity and the selectivity of this catalysts.[26]

Metals such as Na, K, and Cs were found to increase the rate of *n*-butane oxidation, whereas Mg, Ba, and Ca improved the selectivity towards maleic anhydride at low metal concentrations e.g. (M/V = 0.02). Several other authors have studied the effect of transition metals in VPO formulations.[24, 36, 38, 44] A wide range of transition metals which have been investigated include Bi, Co, Cr, Fe, Ga, In, Mo, Nb, Pd, Ru, Sb, Th, Zn, and Zr. Some metal elements proved to have promotional effects, while others did not display any promotional effects in the VPO formulations. The most common effect, which most of these elements induce, is an increase in surface areas in the promoted catalysts relative to the un-promoted catalysts and this is often associated with improved catalytic activity.

Zazhigalov *et al*.[26] studied the performance of a Bi-promoted VPO catalyst at a Bi/V loading of 0.1. In their study they reported an increase in the surface phosphate concentration, which enhanced the acidity and the strength of acid sites, improving performance of the catalyst, and hence the selectivity to maleic anhydride. Haber *et al*.[28] studied the effect of bismuth on VPO catalysts; they used three different routes for the preparation of the promoted catalysts. The catalysts were prepared by mixing of VPO precursors with Bi_2O_3 or $BiPO_4$ powder (grinding in agate mortar), by mechanochemical mixing and during the synthesis of the precursor. The properties of the basic $VOHPO_4{\cdot}0.5H_2O$ were not affected by the mere mixing of the precursor and the bismuth powders; this was revealed by XRD and XPS studies whereby the bismuth compounds remained unchanged, Bi_2O_3 and $BiPO_4$, after mixing. In the second method they introduced bismuth into the catalyst during the synthesis of the catalyst precursor, and they found that this method resulted in a slight decrease of the surface area but the intensity of the (001) plane of $VOHPO_4{\cdot}0.5H_2O$ and the surface phosphorus concentration were slightly enhanced. The third method is the mechanochemical treatment which was also found to increase the 0.57 nm intensity line in the XRD patterns, testifying to a relative growth of the (001) plane in the precursor, a plane known to topotactically transform to the (200) plane of the vanadyl pyrophosphate associated with the catalytic activity in the *n*-butane to maleic anhydride selective oxidation. However, relative to the two methods mentioned above, this method resulted in an increase in the surface area, this being confirmed by a decrease in the plate thickness of the precursor. In the mechanochemical treatment, the morphology of the catalyst is affected by the presence of the finely dispersed bismuth. It should also be noted that the introduction of bismuth

increases the number of acidic surface centres and the number of strong acid centres, mainly the bronsted acid sites available as (P-OH), hence improving the selectivity towards maleic anhydride.

Gallium doped catalysts resulted in an improved catalytic behavior, due in part to the improved surface area. A surface area of 25 m^2g^{-1} was reported for the Ga-VPO when compared to 8 m^2g^{-1} in the undoped catalyst. This metal, like other doping metals, modifies the morphology of the catalysts from stacked platelet to agglomerated rosettes as indicated by the dominant (220) reflection relative to the (001) reflection of the precursor. Gallium was found to be uniformly distributed within the hemi-hydrate structure, furthermore at higher loading $GaPO_4$ formed and this compound was reported to be detrimental to the catalytic performance of the catalyst.[29] The structure of gallium in the precursor was found to be octahedral, having six oxygen atoms as neighboring atoms. By considering the crystal structure of $VOHPO_4{\cdot}0.5H_2O$, the only species that have an octahedral co-ordination are the V^{4+} ions. From these observations it can be inferred that Ga^{3+} ions preferentially substitute for V^{4+} in the Ga-doped precursor.[29] Contrary to this, gallium was found in a tetrahedral co-ordination in the tested catalysts, suggesting that during activation Ga^{3+} tends to be redistributed from octahedral to tetrahedral coordinated sites or maybe even surface segregated as $GaPO_4$.

Volta *et al.*[29] further confirmed the co-ordination existence of gallium in VPO catalysts by electrical conductivity measurements. They observed a sharp decrease in the electrical conductivity during the reduction cycle of pure *n*-butane for both the 1% Ga-doped and the undoped catalysts, which reveals that both catalysts are p-type semiconductors. The nature of the 1%-Ga-doped catalyst as a p-type semi-conductor lies solely on the compensating effect of gallium on the initial p-type semi-conductivity of the pyrophosphate. Hence, at 1% loading, gallium effectively acts as an n-type semi-conductor providing more electrons for conduction purposes, counteracting some of the majority charge carriers in the p-type semi conducting pyrophosphate. This means that in order for gallium to act as n-type dopant, Ga^{3+} must substitute onto a site with a valence less than 3+ and the only probable site in the pyrophosphate with a valence less than 3+ is the vanadyl cation $(VO)^{2+}$ in the $(VO)_2P_2O_7$. The radius of the site resulting from a $(VO)^{2+}$ vacancy is $r_{(VO)^{2+}} = 0.195$ nm, and since the radius for Ga^{3+} is $r = 0.062$ nm, the substitution of gallium into the vanadyl cation entities will be relatively easy in terms of the relative size of the cations. In their conclusions, Volta and his associates concluded that gallium at 1% loading improved the performance of the catalysts as compared to the undoped catalysts, whereas at 5% loading it resulted in deleterious effects due the formation of $GaPO_4$ at higher loading as evidenced by the XRD patterns of these catalysts.

Platinum has been incorporated into the layered VPO precursor as H_2PtCl_6 for the hydrogenation of nitrobenzene to aniline and the oxidation of THF to n-butyrolactone. Platinum was incorporated using both the aqueous and the organic preparation methods. The aqueous method resulted in the formation of V^{4+}-V^{5+} dimers with an average oxidation state of +4.65. Platinum in this catalyst was found to exist as Pt^{2+} and the formation of a hydrogen insertion compound has been demonstrated.[30] The organic preparation, however, resulted in both Pt^{2+} and metallic platinum. The catalytic hydrogenation and oxidation test reactions resulted in a lower conversion of the feed relative to Pt/C. The lower conversion was more apparent in the VPO-Pt (prepared by the aqueous route) and this low conversion could be attributed to the lower reducibility of the incorporated platinum. The relatively higher reactivity of the VPO-Pt (prepared by the organic route) can be attributed to the presence of metallic Pt in the sample. It has been reported that the homogeneously catalyzed oxidation of THF by Pt^{2+} salts eliminates the induction period and that metallic Pt enhances the rate of oxidation. However, in the hydrogenation and oxidation reactions Datta *et al.*[30] reported that these platinum incorporated catalysts did not show any activity, but do hold a strong promise as novel heterogeneous catalysts for other oxidation and reduction reactions.

Chromium was chosen and studied as a VPO catalyst promoter, due to its size, electronegativity, "d" character and multiple oxidation states suitable to modify the catalytic behavior of the catalyst. Lombardo *et al.*[31] reported a surface area improvement with chromium addition, as well as the modification in the texture of the catalysts. Although a higher surface area was reported, there was no evidence of correlation between surface area and the catalyst loading. The temperature programmed reduction of the catalysts revealed the presence of isolated V^{5+} species and some V^{5+} containing phases. The acetonitrile adsorption method revealed the presence of strong Lewis acidic sites, which were most apparent in the impregnated catalysts. An optimum concentration was thus established for these catalysts, indicating an optimum balance between acid site abundance and redox sites. Furthermore, Lombardo *et al.*[31, 32] deduced that the increase in the activity of these catalysts is not only attributable to an increase in the surface area as was reported by Hutchings *et al.*[15] They acknowledge an improved surface area with Cr-loading and also conclude that, if they had not investigated different Cr-loading they might have come to the same conclusion

Molybdenum catalysts were synthesized, either by impregnation or co-precipitation in different loadings by Irusta and co-workers.[33] The temperature programmed reduction of these catalysts indicated only the presence of the vanadyl pyrophosphate phase and that the reducibility of the catalysts was not affected by the introduction of molybdenum in these catalysts. The temperature programmed reduction data of these

catalysts demonstrated a reduction peak at 750 ^{o}C, characteristic of V^{4+} to V^{3+} reduction. The FTIR band corresponding to V=O did not shift as it would should there be an incorporation of the more electronegative elements in the VPO lattice. Structural changes were only apparent in the Mo-VPO catalysts prepared by co-precipitation, within the range 1% Mo-VPO to 5% Mo-VPO. The catalysts which were prepared by this kind of method resulted in a decrease of the yield relative to the catalysts prepared by the impregnation method which improved the yield. The improved yield in the impregnated analogues corresponds to the presence of strong Lewis acidic sites on the surface of these catalysts.

Niobium promoted catalysts, prepared by doping VPO catalysts with NbPO, proved to be beneficial by improving the time needed to reach the steady state, which was only 40 hours on stream relative to 120 hours on stream for the un-promoted catalysts. The niobium promoted catalysts led to the formation of different structural changes ("entangled" $VOHPO_4{\cdot}0.5H_2O$, $VOHPO_4{\cdot}0.5H_2O$ "sand roses", and large particles of NbPO were observed in these catalysts). Niobium acted as a structural promoter in this instance improving both the conversion to *n*-butane and the selectivity to maleic anhydride.[34] Volta *et al*.[29] studied the effect of niobium on these catalysts for mild oxidation of *n*-butane. In their study; they reported a promotional catalytic effect of nobium phosphate. They reported the development of strong Lewis acid sites associated with the formation of solid solutions of the type, $(V_{1-x}Nb_xO)_2(P_2O_7)_{1-X}(PO_4)_{2x}$. It was also discovered that constitutional water molecules were lost at 414 ^{o}C in the VNbPO relative to 435 ^{o}C in the unpromoted VPO catalysts. The formation of V^{5+} entities attributed to either V^{5+} species or V^{5+} microdomains and the V^{4+}-V^{5+} dimers was apparent in the VNbPO catalysts. Electrical conductivity measurements revealed the dissolution of Nb^{5+} in the $(VO)_2P_2O_7$ lattice. The electrical conductivity measurements also revealed that doping by niobium results in the formation of n-type semi conducting properties in these catalysts. The n-type doping by Nb can thus be explained in terms of a substitution of V^{4+} by Nb^{5+} in $(VO)^{2+}$ according to the scheme: $[(VO)_2P_2O_7] + [Nb^{5+}] \rightarrow V_{1-x}Nb_xO_2P_2O_{7+x}$, this being made possible by the similar ionic radii of the corresponding cations: Nb^{5+} = 6.4 x 10^{-2} nm, V^{4+} = 5.8 x 10^{-2} nm. Furthermore, it was reported that Niobium is found in close proximity to the vanadyl pyrophosphate, located near a positive hole facilitating C-H bond breaking by surface O^{-} species. Although VNbPO catalysts proved to be beneficial for n-butane activation, the selectivity to maleic anhydride did not follow; only the CO_2/CO product distribution was modified.[34]

The other metal of interest which has been studied and proved to have positive promotional effects for the partial oxidation of n-butane to maleic anhydride on VPO catalysts is cobalt. Zazhigalov[26] and co-workers disclosed that cobalt added in its metallic form to the VPO catalysts modifies the redox properties of a VPO catalyst, improving desorption of maleic anhydride from the catalyst surface, hence the improved

yield in the product using the Co-promoted VPO catalysts. Volta[35] also studied the incorporation of metallic cobalt into the VPO lattice, where he found that the transformation of the precursor into the active phase was delayed, leading to an enhancement of the structural disorder in the inorganic lattice at lower temperatures, stabilizing the amorphous VPO phase, leading to a higher selectivity when compared to the undoped catalysts. Cobalt has also been reported to enhance the surface phosphorus enrichment, modifying the surface acidity of the catalyst by increasing the concentration of the strong lewis acidic sites.[35]

The effect of Co and Fe on VPO catalysts has been studied in detail by several authors. Hutchings *et al.* [36] studied the influence of Co- and Fe-doped catalysts incorporated during the precursor synthesis. They observed that cobalt formed solid solutions within the $VOHPO_4 \cdot 0.5H_2O$ matrix, but following thermal transformation they established that cobalt was insoluble in the $(VO)_2P_2O_7$ matrix and that it migrated to the V^{4+}-V^{5+} disordered phase during thermal transformation of the precursor. It was proposed from these observations that cobalt present on the surface functions as a promoter for the disordered VPO phases, giving an indication of the importance of the disordered phases in the selective oxidation of *n*-butane to maleic anhydride on VPO catalysts. The selectivity to maleic anhydride was reported to be 63 mol% on the cobalt promoted catalyst and only 50 mol% was reported on the un-promoted catalysts at 25% conversion.[36]

In further studies, Co- and Fe-promoted catalysts have been tested as a comparative study, and in this study 5% loading of cobalt was reported to result in the formation of cobalt phosphate present as a separate phase as was seen by the XRD patterns of the catalysts. This resulted in a decrease in maleic anhydride selectivity, thus affecting the promotional effect. In the iron promoted catalysts, the XRD patterns of the precursor revealed a decrease in the relative intensity of the (001) plane relative to the (220) plane. This is a characteristic pattern observed for the catalysts prepared by the reduction of the $VOPO_4 \cdot 2H_2O$ in *iso*-butanol (VPD synthesis). These catalysts also showed a slight formation of the V^{5+} phases as determined by the solid state ^{31}P NMR giving a signal at 0 ppm and 1625 ppm, characteristic of phosphorus in the vicinity of V^{5+} and V^{4+} respectively. The iron promoted catalysts, unlike the cobalt promoted catalysts, was found to have dissolved within the VPO matrix and forming solid solutions of the type $(VO)_{2-x}Fe_xP_2O_7$, acting as an electronic promoter for the $(VO)_2P_2O_7$. It has also been reported that iron may be associated with the disordered phase, and therefore can act in a similar manner as cobalt, promoting the disordered phase. From this it can be deduced that iron's promotional effect may be both structural and electronic in nature.[36] However, although it has been established that iron and cobalt modify the properties of VPO catalysts, thus leading to improved catalytic performance, it also

worthwhile to remember that these catalysts are strongly influenced by the method of preparation. Hutchings *et al.*[36] studied the effect of iron and cobalt using both the VPO and the VPD method of synthesis. They reported a promotional effect associated with both the metals, when the VPO method of synthesis was being utilized. The XRD patterns of the used catalysts revealed the presence of (200), (024), and (032) crystal planes of the vanadyl pyrophosphate in both the un-promoted and the promoted catalysts. The ^{31}P NMR spin echo mapping of these catalysts demonstrated the presence of three signals at (i) 0 ppm (P atoms connected to the V^{5+} in the $VOPO_4$ phases); (ii) at 2400 ppm (P atoms connected to the V^{4+} in the poorly crystallized $(VO)_2P_2O_7$ phase); and (iii) in the 200-1500 ppm range (P atoms connected to the V^{4+}-V^{5+} dimers in a poorly crystalline matrix). The cobalt and iron promoted catalysts displayed similar characteristics, but crystallinity was apparent relative to the unpromoted catalyst. The promoted VPD series, however, displayed rather different characteristics for the iron promoted catalyst, whereby the contribution of the V^{4+}-V^{5+} dimers was more significant (55.1%). This contribution was found to be much lower in the Co-VPD and the VPD catalysts (16.6% and 20.0% respectively). The significance of the method of preparation becomes apparent here, it is apparent that the promotional effect of iron is significant where conversion and selectivity are concerned in the VPO series, but in the VPD series the promotional effect is jeopardized by the high contribution of the dimers in the absence of a crystallized $(VO)_2P_2O_7$.[37]

Iron metal has also been introduced to the VPO catalysts in the presence of cerium, as Fe-Ce mixed oxides. At 5% loading these catalysts increased both the selectivity and the conversion towards maleic anhydride in the absence of gaseous oxygen. This combination of mixed oxides was reported to improve the redox properties of the catalyst. Shen *et al.*[38] suggested that iron increases the reactivity of highly selective lattice oxygen, which is being formed in the presence of cerium in these catalysts. Hutchings and Higgins introduced ruthenium to the VPO formulations in the form of either oxides or nitrates. The metal was introduced by the addition of the salt during the precursor synthesis together with V_2O_5 using the standard non-aqueous preparation method. Promoted catalysts were also prepared by impregnation using the incipient wetness technique. Ruthenium has been utilized in numerous applications as a catalyst, e.g. the Grubbs catalyst for olefin metathesis and the μ_3-oxo trinuclear ruthenium carboxylate complex for the oxidation of alkanes under much milder conditions than would be achieved with other commercial catalysts.[39] Hutchings and Higgins selected ruthenium as a representative of group eight elements, whereby they reported a significant decrease in the primary selectivity (selectivity towards maleic anhydride at zero n-butane conversion) towards maleic anhydride by promoting its over-oxidation. When

an inlet n-butane concentration of 1-2 mol% was used, CO and CO_2 were found to be the only significant by-products and n-butane loss was found to be first order and on this basis they modeled the reaction data by the use of a simplified kinetic scheme involving a series-consecutive reaction scheme of pseudo first-order reactions, where $C_4H_2O_3$ signifies maleic anhydride.[15]

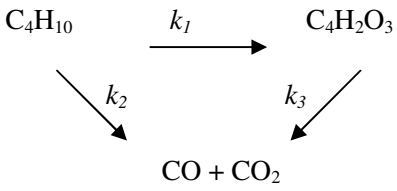

From this simplified model, assuming plug flow conditions, it is possible to calculate three factors:

i. The rate constant for n-butane conversion corrected for surface area ($k_1 + k_2$) / sa (a measure for specific activity).
ii. The primary selectivity S_0 (the selectivity to maleic anhydride at zero conversion).
iii. A measure of selectivity of the catalyst: The relative rates of oxidation of *n*-butane and maleic anhydride.

From these derivations it has been proposed that the relative performance of the promoted catalysts can be determined, thus an improved catalyst would require a high specific activity, (i.e. a high value of $k_1 + k_2$ / sa) and a high maleic anhydride selectivity (i.e. a high value of S_0 and a low value of $k_3 / [k_1 + k_2]$).

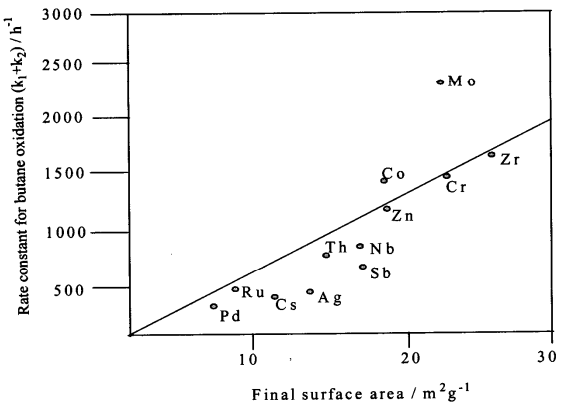

Fig.1.6: Dependence of rate constant for *n*-butane oxidation on the final catalyst surface area.[15]

A plot of the rate constant for *n*-butane conversion ($k_1 + k_2$) versus the final surface area is shown in Fig.1.6. From this plot, it is apparent that the specific activities of the promoted and the un-promoted catalysts are relatively similar, indicating that the presence of these promoters is merely associated with increasing the surface area of the promoted catalysts.

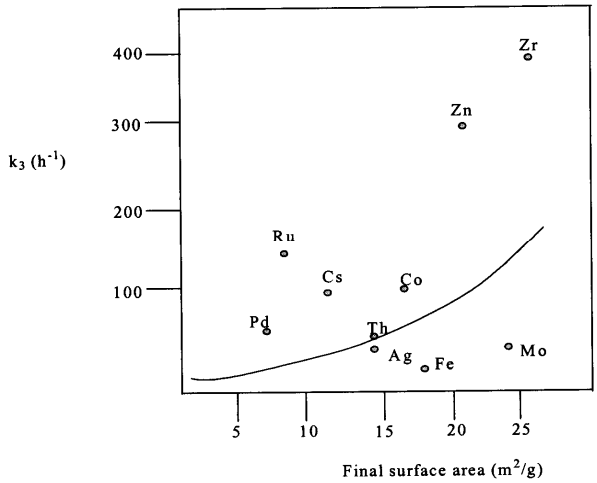

Fig.1.7: Dependence of rate constant for n-butane oxidation on final catalyst surface area (relative rates of MA and *n*-butane oxidation).[15]

The extent of consecutive oxidation of maleic anhydride is given by the magnitude of k_3 and, in general, this is found to increase with surface area (Fig.1.7). Furthermore, the magnitude of k_3 was found to be higher than expected in the 0.03 Ru/V promoted ruthenium catalyst, resulting in loss of selectivity due to over-oxidation.

In the work reported by Hutchings *et al.*[15] only a loading of 0.03 Ru/V was studied and different ruthenium loadings was not reported. They thus concluded that ruthenium does not display any promotional effect based on the results from the simplified kinetic model. The need to investigate different loadings of a metal dopant is necessary since it is possible that the reported loading could have been significant enough to block the active centres of a $(VO)_2P_2O_7$ on the catalyst surface. The interplay between the promoter concentration, promoter coverage on the surface and the catalyst activity are crucial aspects which need to be taken into consideration where the promoted catalysts are concerned. This is illustrated in Fig.1.8, indicating that the promotional effect is highly dependent on concentration and this has been observed for numerous promoted catalysts.

The studies of a K-promoted iron Fischer-Tropsch synthesis catalyst demonstrated that the role of potassium in this instance is to enhance the adsorption and dissociation of CO.[40, 41] This effect was found to be concentration dependent. The concentration dependence of a promoter element has also been demonstrated by Campbell *et al.*[42] in the cesium promoted copper catalyst for the water gas shift reaction. The addition of cesium was found to enhance the rate of reaction at Cs/Cu of loading 0.04. An experimental relationship between the catalyst activity and the promoter concentration was also observed for this work, similar to the predictions made by Bowker (see Fig1.8).

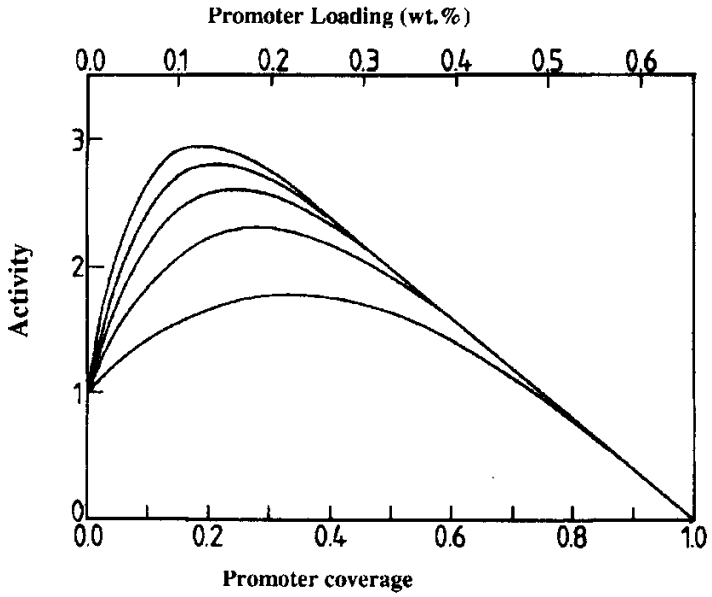

Fig.1.8: The effect of promoter loading and coverage on the activity of a catalyst based on theoretical calculations of Bowker for a catalyst with a surface area of 10 (m^2g^{-1})[43]

Optimum promoter coverage is established, correlating to an optimum catalytic activity. It is apparent from Figure.1.8 that, when the promoter coverage is further increased, loss of activity becomes significant. It is assumed in the figure that the promoted site has four times the turnover frequency of an unpromoted site. The curves of increasing activity correspond to increasing ensembles of 2, 4, 6, 8 and 10 affected sites around the promoter atom.

SCOPE

In an attempt to further optimize a known industrial process of maleic anhydride production, two transition metals, ruthenium and iron, were studied for the n-butane to maleic anhydride transformation while using the unpromoted VPO catalyst as a baseline reference.

REFERENCES

1. I. Krowschwitz and M. Howe-Grant, eds., Wiley, New York, 1991.
2. N. Govender, H. B. Friedrich and M. Mathebula, *Catal. Today*., 2004, **97**, 315.
3. G. C. Bond, eds., *Heterogeneous catalysis: Principles and applications*. Claredon Press. 1987.
4. G. Centi, F. Cavani and F. Trifiro, eds., *Fundamental and applied catalysis*, Kluwer Academic/Planum Publishers: New York, 2001.
5. X. Li, W. Ji, J. Zhao, Z. Zhang and C. Au, *J. Catal*., 2006, **238**, 232.
6. M. Malow, eds., *Hydrocarbon Processing, International*, 1980, **59**, 149.
7. S. Irvin-Monshaw and A. Klein, *Chem. Eng*., 1989, **96**, 35.
8. G. Centi, F. Trifiro, J. B. Ebner and V. M. Franchetti, *Chem. Rev.*, 1988, **88**, 55.
9. E. Bordes, *C. R. Acad. Sci. Paris, Serie IIc, Chemie.*, 2000, **3**, 7255.
10. H. Horowitz, C. M. Blackstone, A. W. Sleight and G. Teufer, *Appl. Catal.*, 1988, **38**, 193.
11. E. Bordes, *Catal. Today.*, 1993, **16**, 27.
12. L. M. Cornaglia, C. A. Sanches and E. A. Lombardo, *Appl. Catal.* A., 1993, **95**, 117.
13. B. J. Barone, in *US Patents.,* 5, 070, 060. (to scientific Design). 1981.
14. N. J. Bremer and D. E. Dria, in *US. Patents.*, 4, 244, 879 (to standard oil company, Ohio). 1981.
15. G. J. Hutchings and R. Higgins, *J. Catal.*, 1996, **162**, 153.
16. B. K. Hodnett, F. Dason and M. O'Connor, *Appl. Catal.*, 1990, **64**, 161.
17. J. P. Harrison, in *U. S. Patents.,* 4, 062, 873. *(to Chevron research. Res. Co)*. 1977.
18. M. J. Gresser and A. S. Tracey, eds., *In Vanadium in Biological systems: Physiology and Biology*, Boston, 1990.
19. L. M. Cornaglia, C. Caspani and E. A. Lombardo, *Appl. Catal.*, 1991, **74**, 15.
20. E. Bordes, *Catal. Today.*, 1987, **1**, 499.
21. C. C. Torardi, Z. G. Li, H. S. Horowitz, W. Liang and M. H. Whangbo, *J. Solid State Chem.,* 1995, **119**, 349.
22. Z. Sobalik, S. Gonzales Carrazan, P. Ruiz, B. Delmon, *J. Catal*., 1999, **185**, 272.
23. Y. H. Taufiq-Yap and C. S. Saw, *Catal. Today*., 2008, **131**, 285.
24. V. V. Guliants, B. Benzinger, S. Sundaresan, N. Yao and I. E. Wachs, *Catal. Lett.*, 1995, **32**, 379.
25. G. J. Hutchings, *Appl. Catal.*, 1991, **72**, 1.

26. V. A. Zazhigalov, J. Haber, J. Stoch, I. V. Bacherikova, G. A. Komashko and A. I. Pyatnitskya, *Appl. Catal.* A.., 1996, **134**, 225.

27. D. Lozano-Calero, S. Bruque, M. A. G. Aeranda, M. Martinez-Lara and L. J. Moreno, *J. Solid State Chem.*, 1993, **103**, 481.

28. V. A. Zazhigalov, J. Harber, J. Stoch and E. Cheburokova, *Catal. Commun.*, 2001, **2**, 375.

29. L. Sartoni, A. Delimitis, J. K. Bartley, A. Burrows, H. Roussel, J. M. Herrmann, J. C. Volta, C. J. Kiely and G. J. Hutchins, *J. Mater. Chem.*, 2006, **16**, 4348.

30. A. Datta and M. A. Agarwal, *J. Mater. Chem.*, 2002, **12**, 1892.

31. B. T. Pierini and E. A. Lombardo, *J. Mat. Chem. Phys.*, 2005, **92**, 197.

32. B. T. Pierini and E. A. Lombardo, *Catal. Today.*, 2005, **107**, 323.

33. S. Irusta, A. Boix, B. Perini, C. Caspani and J. Petunchi, *J. Catal.*, 1999, **187**, 298.

34. J. E. Eon, M. Chavant, P. G. Pries. de Oliveira, A. S. Riche, V. Martin, S. Caldarelli and J. C. Volta, *Catal. Today.*, 2000, **57**, 177.

35. S. Sajip, J. K. Bartley, A. Burrows, C. Rhodes, J. C. Volta, C. J. Kiely and G. J. Hutchings, *Phys. Chem. Chem. Phys.*, 2001, **3**, 2143.

36. S. Sajip, J. K. Bartley, A. Burrows, M. T. Sananes-Shulz, A. Tuel, J. C. Volta, C. J. Kiely and G. J. Hutchings, *New. J. Chem.*, 2001, **25**, 125.

37. M. T. Sananes-Schulz, A. Tuel, G. J. Hutchings and J. C. Volta, *J. Catal.*, 1997, **166**, 388.

38. S. Shen, J. Zhou, F. Zhang, L. Zhou and R. Li, *Catal. Today.*, 2002, **74**, 37.

39. J. B. Binder, J. J. Blank, R. T. Raines, *Org. Lett.*, 2007, **23,** 4885.

40. J. P. Hindermann, G. J. Hutchings and A. Kiennemann, *Catal. Rev. Sci.*, 1993, **35**, 1.

41. R. W. Joyner, eds., *Coadsorption, Promoters and Poisons*, Elsevier, Amsterdam, 1993.

42. J. Nakamura, J. M. Campbell and C. T. Campbell, *J. Chem. Soc. Faraday Trans.*, 1990, **86**, 2725.

43. G. J. Hutchings, *Catal. Lett.*, 2001, **1**, 2.

44. L. M. Cornaglia, S. Irusta, E. A. Lombardo, M. C. Durupty, J. C. Volta. *Catal. Today*., 2003, **78**, 291.

45 V. V.Guliants and A. Carreon, Catalysis., 2005, **18**, 1.

Chapter 2

2.1 Crystal structure of various phases in VPO catalysts

The crystalline structure of the catalysts can be determined through techniques such as X-ray diffraction. The selectivity towards a particular compound in a given reaction is connected with the presence of a specific compound (phase) in the catalyst. In the VPO catalytic system, the active phase has been determined to be the vanadyl pyrophosphate [$(VO)_2P_2O_7$] which is active for both *n*-butane and *n*-butene oxidation to maleic anhydride.

The crystal structure of the vanadyl pyrophosphate involves chains of short and long alternating vanadium-oxygen bonds O=V…O-V…O such that the four equatorial corners are shared with the single tetrahedra in the orthophosphate (PO_4) and the double tetrahedra in the pyrophosphate (P_2O_7).

The structures of VPO catalysts are described according to two kinds of elementary units, a single octahedron and a pair of octahedra.[1]

2.1.1 Single octahedron and pairs of octahedra

In the single octahedron elementary unit, equatorial oxygen shares a corner with one of the orthophosphate groups, while the vanadyl groups occupy the perpendicular directions. Pairs of face-sharing octahedra are connected to corner-sharing tetrahedra (Fig.2.1b) constituting the basic structure of the vanadyl hydrogen phosphorus hemihydrate.

For pairs of octahedra, the V=O bond in each pair is in the cis-position, with the apical oxygen from the water molecule being shared between the two vanadium atoms. The layers of $(VOPO_4)_\infty$ are held intact by strong hydrogen bonds between (HPO_4) and the water molecules. [2, 3]

The number of orthophosphate groups which are reported in the VPO literature includes; $VOPO_4{\cdot}2H_2O$, α_I-$VOPO_4$, α_{II}-$VOPO_4$, and β-$VOPO_4$, among others. The coordination polyhedra in the crystal structures of $VOPO_4{\cdot}2H_2O$, α_I-$VOPO_4$, α_{II}-$VOPO_4$, and β-$VOPO_4$ are given in Fig.2.2, while other VPO phases, such as $VOHPO_4{\cdot}0.5H_2O$, $VO(H_2PO_4)_2$, $VO(PO_3)_2$, $(VO)_2P_2O_7$ and α, β, and γ-$VOPO_4$ are discussed in the next section.

These orthophosphate phases consist of infinite layers of $(VOPO_4)_\infty$, whereby the layers are linked by water molecules in the hydrates: with one H_2O molecule being coordinated to vanadium while the second

water molecule is considered "zeolithic" (Fig.2.2a). The space groups for the α_I-$VOPO_4$ and the α_{II}-$VOPO_4$ is P4 /nmm (F^7_{4h}) and P4 / n (C^3_{4h}); (Fig.2.2b, c) and the β-$VOPO_4$ is characterized by zig-zag chains of octahedra found in the (010 plane), the PO_4 and VO_6 share the same oxygen linked by O=V…O bonds, (Fig.2.2d).

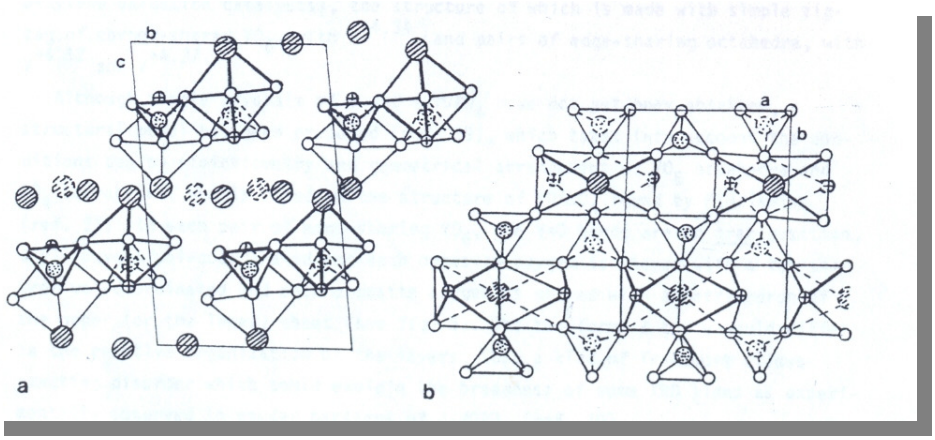

Fig.2.1: Crystal structure of (a) $VOHPO_4 \cdot 4H_2O$; double chains are perpendicular to the figure; (b) layers (010) of $VOHPO_4 \cdot 0.5H_2O$ and (⊛) OH coordinated to P. (⊕) and (⊘) represents the vanadyl oxygen and OH_2 respectively. [1]

$VOHPO_4 \cdot 0.5H_2O$

The precursor for *n*-butane oxidation to maleic anhydride, $VOHPO_4 \cdot 0.5H_2O$ (Fig.2.1b) can be obtained through partial dehydration of $VOHPO_4 \cdot 4H_2O$ (Fig.2.2a), which has a structure closely resembling that of vanadyl orthophosphate dihydrate (Fig.2.2a). The structure of $VOHPO_4 \cdot 4H_2O$ consists of units of alternating tetrahedra and octahedra arranged as a double chain in one direction (Fig.2.2a).

$VO(H_2PO_4)_2$

The elementary units for the $VO(H_2PO_4)_2$ are diagonally linked in the (001) plane; diagonal chains of O-V-O-P-O are formed, with each equatorial oxygen of the octahedron being shared by each tetrahedron and four tetrahedra are bonded by two hydroxyl groups (Fig. 2.3a). The O-V…O-V bonds are found in the perpendicular direction parallel to the hydrogen bonds between the chains of $O_2P(OH)_2$ ensuring the stoichiometry of P/V=2 in this compound.

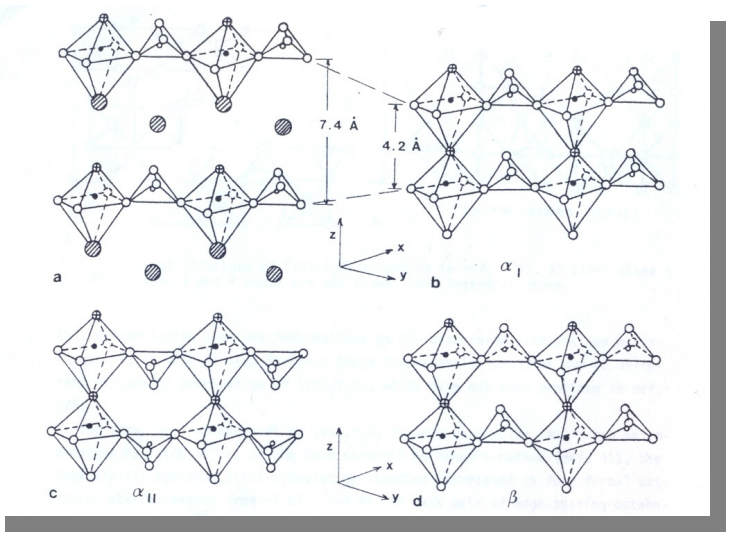

Fig.2.2: Coordination octahedra around V and P in the crystal structure of:

(a) $VOPO_4 \cdot 2H_2O$, (b) α_I-$VOPO_4$, (c) α_{II}-$VOPO_4$, (d) β-$VOPO_4$. Legend: (●) V; (o) P; (O) oxygen; (⊕) vanadyl oxygen; (◍) OH_2 free or coordinated to V.[1]

$VO(PO)_3$

The structure of vanadyl metaphosphate is given in Fig.2.3b, in this structure chains of distorted octahedra [O=V…O=V] and chains of corner sharing (-PO_2-) groups run parallel to each other. Furthermore, short bonds of V=O have also been observed in the UV-vis spectra. [4, 5]

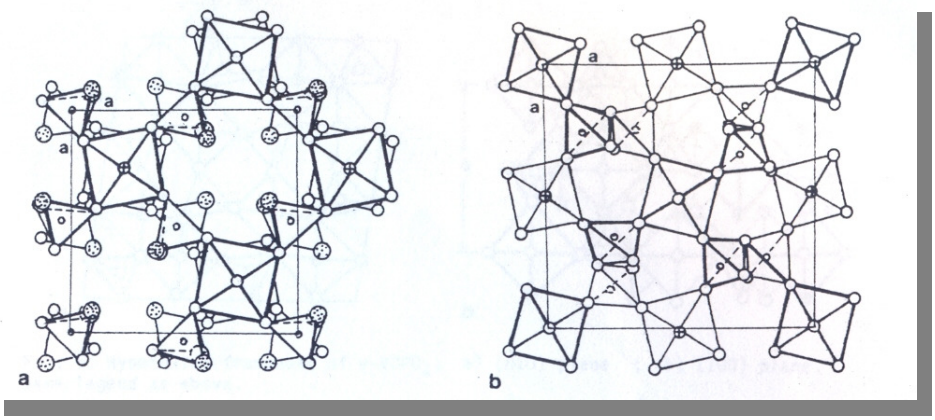

Fig.2.3: Crystal structure of (a) $VO(H_2PO_4)_2$; (b) $VO(PO_3)_2$.[1]

$(VO)_2P_2O_7$

The framework for the vanadyl pyrophosphate structure consist of sheets of edge-sharing VO_6 octahedra, with trans-V=O bonds linked in an equatorial position to the PO_4 terahedra (Fig.2.4a). The sheets are stacked upon each other forming double columns of distorted VO_6 parallel to the bent pyrophosphate groups (Fig.2.4b).

When calculations of the bond strength for the vanadyl pyrophosphate were performed using Brown's method,[1] the four crystallographic sites occupied by vanadium, corresponding to four oxidation states ranging from +3.69 to +4.44, could be determined. For each pair of edge sharing-octahedra, four redox couples are found within the crystalline matrix.

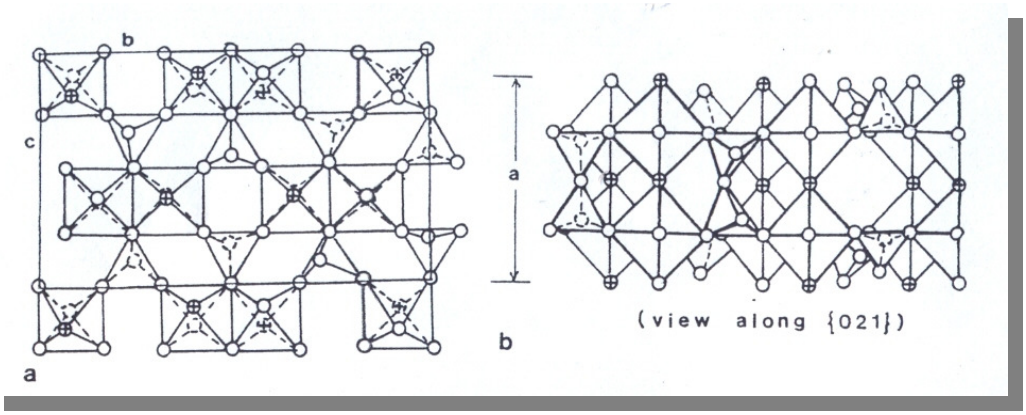

Fig.2.4: Crystal structure of $(VO)_2P_2O_7$.[48] (a) (100) plane; (b) (001) plane.[1]

$VOPO_4$

A structural model for δ-$VOPO_4$ and λ-$VOPO_4$ has been proposed based on the structure of $VOAsO_4$ according to the stoichiometry and the geometrical arrangement of VO_6 octahedra and PO_4 tetrahedra.

Each pair of edge-sharing VO_6 is composed of V=O bonds in transposition, their oxygen is uni-coordinated and each opposite oxygen is shared with a tetrahedron of the upper or lower sheet as shown in Fig.2.5. The relative organization of the layers gives rise to the differences observed in the δ-$VOPO_4$ and λ-$VOPO_4$.[1]

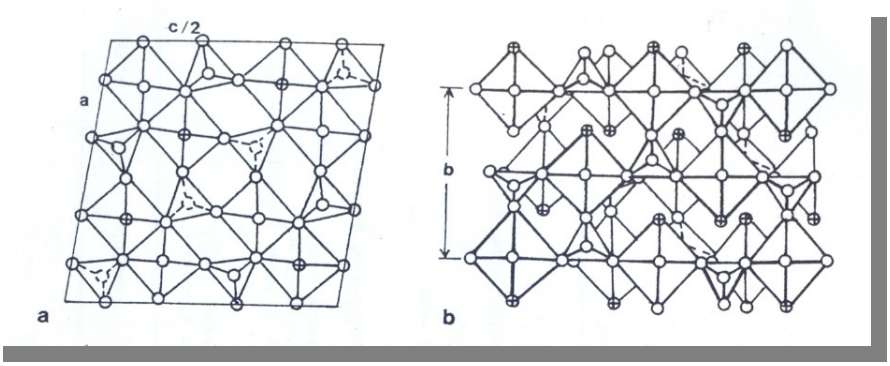

Fig.2.5: The hypothetic framework of λ-$VOPO_4$. (a) (010) plane; (b) (100) plane.[1]

2.2.2 The mechanism of reduction of the α, β, and γ-$VOPO_4$ phases

α -$VOPO_4$

The reduction of α-$VOPO_4$ and β-$VOPO_4$ proceeds via the crystallographic sheer plane mechanism (CS) found in ReO_3-type oxides. This mechanism has been found as the only one capable of explaining the same behavior of the α- and β-$VOPO_4$. In the CS mechanism, the initial step is the diffusion of oxygen vacancies followed by their aggregation into planar disks forming elements of shear planes.

For cooperative diffusion of these vacancies along a given direction the resulting CS planes will be ordered, resulting in the formation of definite structures and not extended defects. The cooperative movement of VO_6 in the [22] direction of the (001) α-$VOPO_4$ results in the edge-sharing position, where the V=O bonds are already in the trans-position and the PO_4 groups rotate to fuse as the pyrophosphate groups in the upper sheets as well as in the lower sheets (Fig.2.6a).

β -$VOPO_4$

The same cooperative movement of VO_6 is encountered but occurs along the {211} direction of the (201) β-$VOPO_4$ cleavage plane perpendicular to the V=O bonds (Fig.2.6b). Slabs of (001) α-$VOPO_4$ and (201) β-$VOPO_4$ closely resemble the (100) plane of $(VO)_2P_2O_7$, A crystallographic mismatch of 2 and 3% has been reported for α-$VOPO_4$ and β-$VOPO_4$, respectively.[1]

γ - $VOPO_4$

The CS mechanism is not considered in the reduction of γ-$VOPO_4$ to $(VO)_2P_2O_7$, the transformation for this compound proceeds via the gliding mechanism. The small displacements of the atoms lying in the (010) planes result in their connections to the PO_4 groups as well as the formation of VO_6 pairs.[6]

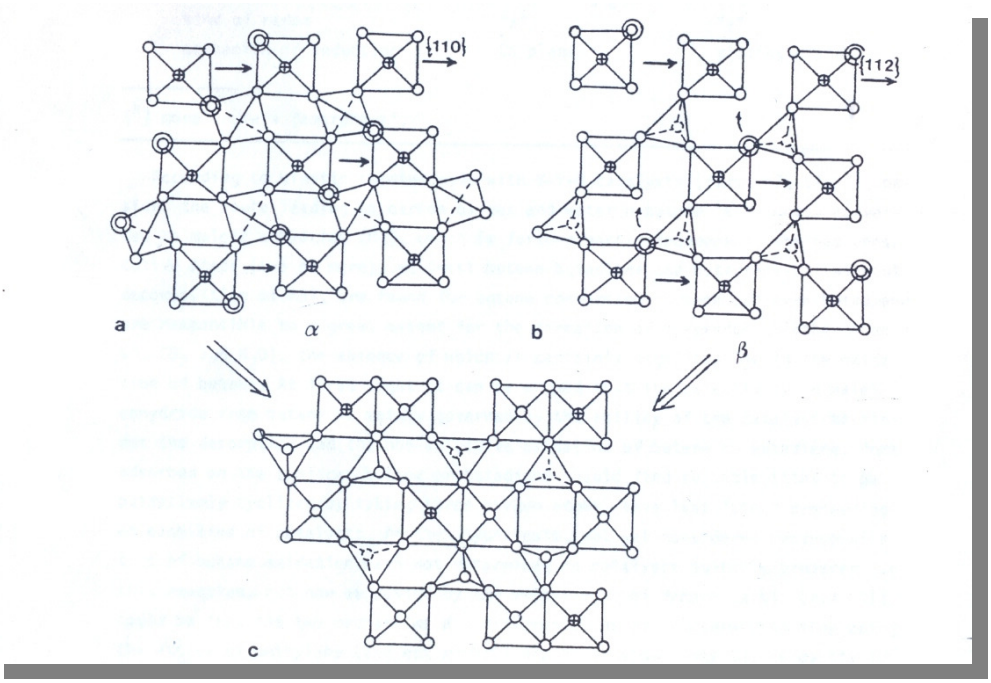

Fig.2.6: Reduction of $VOPO_4$ to (100) $(VO)_2P_2O_7$ by the CS mechanism. (a) (001) α-$VOPO_4$: sharing of VO_6 octahedra in the {100} direction; (b) (201) β-$VOPO_4$: sharing of VO_6 in the {211} direction. Double circles correspond to V-O-P bonds to be broken.[1]

2.2 Models for the active sites for n-butane transformation on VPO catalysts

The existence of various V^{4+} and V^{5+} species, and $(VO)_2P_2O_7$ has been reported in the VPO literature. These phases are known to interconvert depending on several factors such as the redox properties of the reaction stream, the time of activation, as well as the temperature of reaction. The existence of these phases can be in either crystalline or amorphous state depending on the conditioning procedure or the degree of catalyst equilibration. The solid-state chemistry of the VPO catalysts is considered very complex and this has led to a number of possible active and selective phases being reported in the literature.

Several authors have suggested models for the active and selective phases for the VPO catalysts.[1, 7-10] Bordes explained the model of a non-equilibrated VPO catalyst. In this model, the active sites involved in the *n*-butane to maleic anhydride transformation are found at the interface between the $VOPO_4$ (001) and the $(VO)_2P_2O_7$ (200) planes along the (001) and the (201) planes respectively.[1] Volta *et al*. also reported a model of a non-equilibrated VPO catalyst. Contrary to what Bordes reported, Volta *et al.*[11] did not support the association of the active sites with the interfaces between the crystalline phases. They believe that the active sites consist of a mixture of a well crystallized $(V^{4+}O)_2P_2O_7$ and an amorphous $V^{5+}OPO_4$, which they interpreted as the precursor for the high temperature *b*-$VOPO_4$.

Hutchings *et al.*[12] suggested the V^{4+}/V^{5+} couple dispersed on the surface of VPO phases, e.g. $(VO)_2P_2O_7$ for the equilibrated catalysts or the $V^{5+}OPO_4$ for the non-equilibrated catalysts, as the active site for *n*-butane oxidation to maleic anhydride. The $VO(H_2PO_4)_2$ was also reported by Yamazoe *et al*.[10] as the precursor for the active phase, whereby $VO(H_2PO_4)_2$ transforms to the $VO(PO_3)_2$ phase which is less active but displays similar capabilities as the selective vanadyl pyrophosphate, $(VO)_2P_2O_7$. However, although Yamazoe *et al*.[10] reported $VO(H_2PO_4)_2$ as the active precursor to the active phase, previous reports have also reported this phase as an impurity phase, which can affect the catalytic performance. The presence of this impurity phase was identified by a lower temperature water loss, which amounts to *ca.* 10% by mass. The removal of this impurity results in improved catalytic performance.[13]

The necessity for a presence of a controlled amount of V^{5+} phases was reported by Trifirò *et al*,[8] as the selective phases in the presence of the active $(VO)_2P_2O_7$ as shown in Fig. 2.7 C.

The presence of the defects in structure, reported by Gai and Koutakis,[9] is another possibility of the active sites, as well as the interfaces between the $VOPO_4$ (microcrystalline) and the well crytstalline $(VO)_2P_2O_7$.

In other studies[14-17] the pure $(VO)_2P_2O_7$ has been reported as the active phase since no other impurity phases could be detected in these catalysts. For a well crystallized $(VO)_2P_2O_7$ the steady state was attained following the removal of a thin layer of an amorphous layer found on the (200) surface plane of the $(VO)_2P_2O_7$. Cavani and Trifiro illustrated the four types of surface termination of the (200) planes to explain the models of the active phases as illustrated in Fig. 2.7.[18]

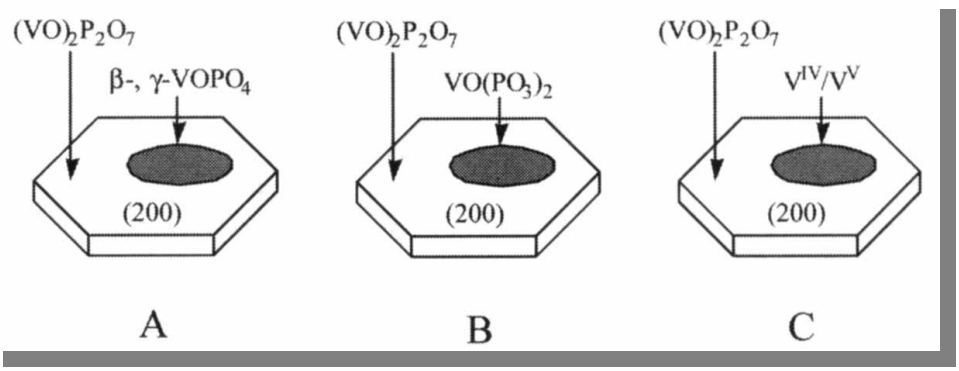

Fig. 2.7: Models of the active sites for the vanadyl pyrophosphate according to various authors (taken from ref. 18).[18] (A) Volta *et al.*[7] (B) Yamazoe *et al.*[10] (C) Trifirò *et al.*[8]

Type A termination envisage the model for catalysts with a P/V<1 leading to high activity but low selectivity catalysts. This model thus presents the termination where only vanadium species are present on the surface of the catalyst. According to Ebner and Thompson, [19] this type of termination is the least probable, since excess phosphate is always required in the VPO catalysts

For Type B termination every phosphate tetrahedron facing up the bulk (200) plane is replaced by the pyrophosphate groups, such that pairs of vanadyl dimers are separated by the pyrophosphate from other pairs which are known to be beneficial towards maleic anhydride selectivity. This, however, strongly affects the selectivity.

In type C termination every phosphate tetrahedron facing up in the bulk (200) planes corresponds to a surface HPO_4^- group. The vanadyl dimers are easily accessed from the gas phase in this type of termination and the possible formation of the $V^{5+}OPO_4$ can occur.

Type D termination involves the (200) surface termination with $VO(PO_3)_2$ when excess of phosphate is present. This results in an overall lower catalytic activity.

2.3 Proposed active sites for the vanadyl pyrophosphate catalysts for maleic anhydride synthesis

Section 2.1 discussed some of the proposed models for the active sites during the n-butane transformation. The models were based on the experimental data obtained by various authors. The reported models discussed the active sites found in both the equilibrated and the non-equilibrated VPO catalysts. However, other authors indicated that the best VPO catalysts preferentially expose the (200) plane of the $(VO)_2P_2O_7$,[6, 20, 21] such that the models for the hypothetical active sites need to be associated with this crystallographic plane.

2.3.1 Hypothetical active sites on the surface of the (200) plane of the $[(VO)_2P_2O_7]$[7]

i. Brønsted acid sites, Probably the -POH
ii. Lewis acid sites, Probably the V^{4+} and V^{5+}
iii. One electron redox couple, V^{5+}/V^{4+} and V^{4+}/V^{3+}
iv. Two electron redox couple, V^{5+}/V^{3+}
v. Bridging oxygen species, V-O-V, V-O-P, P-O-V_2
vi. Terminal oxygen species, V^{5+} = O, V^{4+} = O
vii. Activated molecular oxygen, θ^1-peroxo and θ^2-superoxo species

2.3.2 The proposed roles for the hypothetical active sites on the surface of the (200) plane of the $[(VO)_2P_2O_7]$

The above mentioned active sites are believed to exist on the *trans*-oxo vanadium(IV) dimer present in the (200) plane of the vanadyl pyrophosphate.[18] The rate determining step in the *n*-butane to maleic anhydride transformation is the activation of the C-H methylene bonds, i.e. the removal of two methylene hydrogen atoms in the 2- and 3-positions of n-butane. The V^{4+} site can effectively discriminate between the stronger methyl C-H bonds and the methylene bonds assisting in the homolytic cleavage of the latter. This is made possible by the lower reactivity of its d_x^2- $_y^2$ orbitals.

$$V^{4+} + C_4H_{10} \longrightarrow C_4H_9\bullet + V^{3+}$$

Centi *et al.*[8] proposed a mechanism through which the V^{4+} Lewis acid site and the bridging oxygen can abstract two hydrogen atoms of the methylene groups from *n*-butane according to the mechanism in Fig.2.8. This hydrogen abstraction step may be broken up according to the following steps:

$$C_4H_{10} = C_4H_9\bullet + H\bullet, \qquad \Delta H^o = +\,411 kJ / mol \text{ [12]}$$

$$V^{4+} + H\bullet = (VH)^{4+}, \qquad \Delta H^o = -200 kJ / mol \text{ [12]}$$

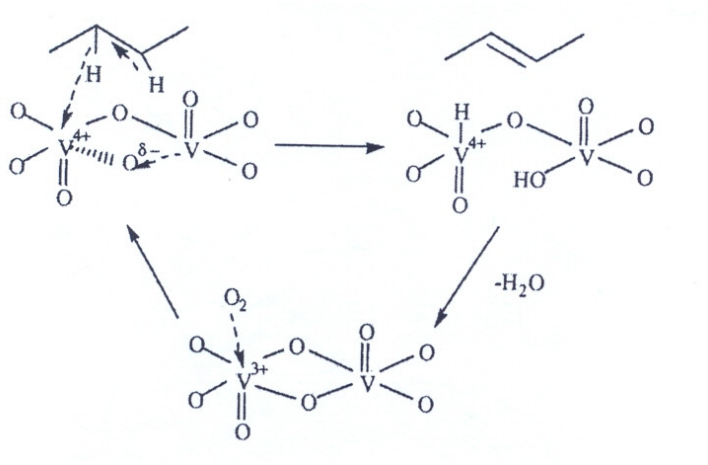

Fig.2.8: Mechanism of n-butane activation on $(VO)_2P_2O_7$ according to Centi *et al.*[8]

Centi *et al.*[8] further reported that following the initial activation of *n*-butane, the Brønsted acid sites may be involved in the final transformation steps. Thompson *et al.*[19] detected the Brønsted acid sites by IR spectroscopy, which they attributed to the P-OH groups belonging to terminal HPO_4^- and $H_2P_2O_7$ species. These P-OH groups may function to facilitate the removal of water formed during the partial oxidation of *n*-butane, to form the surface phosphate esters (P-O-C), thereby stabilizing the reaction intermediates and preventing their desorption.[21] Conversely, these surface intermediates can facilitate desorption of maleic anhydride from the catalyst surface, thus preventing over-oxidation of this compound.[22]

The activation and transformation of *n*-butane to 1,3-butadiene at the active sites located on the (200) plane of the pyrophosphate was proposed by Grasselli *et al.*[23] They deduced a mechanism based on the formation of the vanadyl dimeric clusters on the surface, whereby each cluster is separated from the other clusters by the pyrophosphate groups $[O_3P\text{-}OPO_3H_2]^{2-}$. These pyrophosphate groups are the Brønsted acid sites participating in the overall oxidation mechanism and also function as diffusion barriers preventing over-oxidation of the surface-bound intermediates by excess oxygen from neighboring clusters.

According to Grasseli *et al.*[23] the four vanadium dimers within each cluster can assume one of the four states, S_o to S_3. When molecular oxygen coordinatively adsorbs on the unsaturated V^{4+} in the dimer to form the peroxo or the superoxo speies, S_1 gets transformed into S_3. The superoxo species in the S_3 is responsible for hydrogen abstraction forming a surface-bound hydroperoxy group. Following this, the adjacent vandyl group simultaneously captures the alkyl radical to give a surface-bound alkoxy group. This hydroperoxy group then abstracts either the α-methylene or the β-methylene hydrogen, forming a metal-bound S_1-ketaloxy or S_2-glycoloxy group, respectively (Fig.2.9).

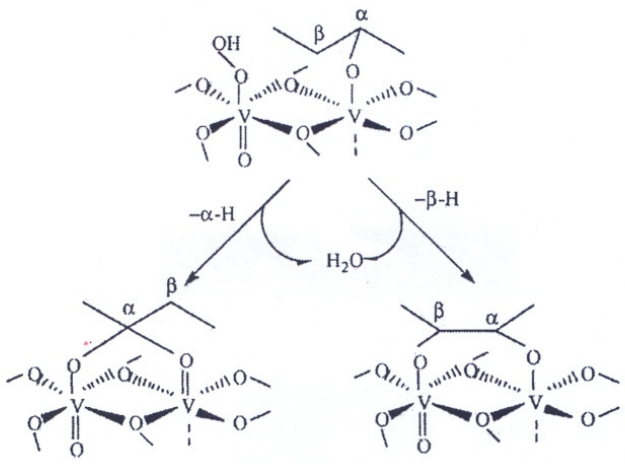

Fig. 2.9: Activation of *n*-butane on a vanadyl dimer site in state S_3 according to Grasselli *et al.*[23]

Following the steps outlined in Fig.2.9, the participation of the Brønsted acid sites $[O_3P\text{-}OPO_3H_2]$,$^{2-}$ in the acid catalyzed dehydration reaction leads to the formation of 1,3-butadiene and the regeneration of the S_1 state (Fig.2.10). Further oxidation of 1,3-butadiene to maleic anhydride is explained according to the model of Schiøtt and Jørgersen.[24]

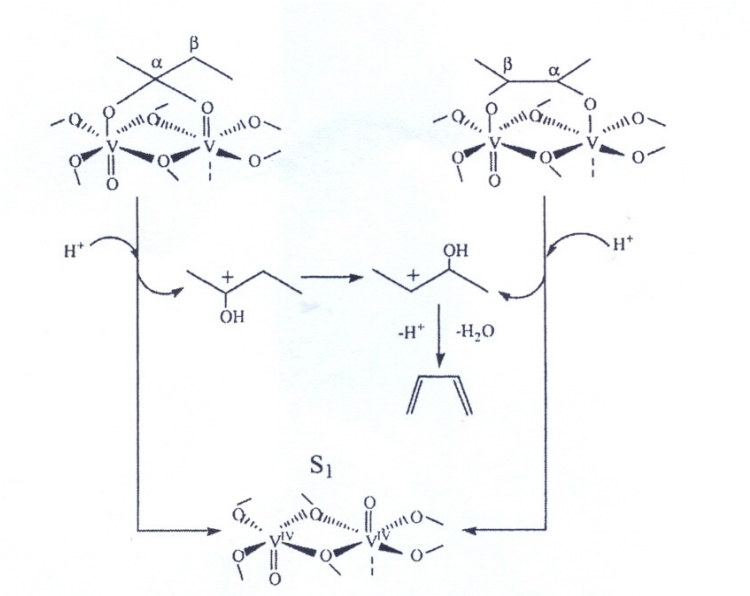

Fig. 2.10: Acid catalyzed conversion of surface-bound ketaloxy and glycoloxy intermediates to 1,3-butadiene according to Grasselli *et al*.[23]

Through the use of frontier molecular orbital theory and extended Hückel calculations Schiøtt and Jørgersen[24] deduced that the V^{4+}=O is involved in the [2+4]-like cycloaddition of 1,3-butadiene in the formation of 2,5-dihydrofuran on a vanadyl dimer present on the (200) plane of the $(VO)_2P_2O_7$, according to (Fig.2.11). In this model, molecular oxygen, which is adsorbed on the adjacent vanadium atoms, either as the η^1-superoxo or the η^2-peroxo species in the dimer, activates the C-H bond in the 2-position of the 2,5-dihydrofuran. This leads to a hydrogen atom transfer to the peroxo species giving a surface bound hydoperoxide group. The hydroxyl group in the hydroperoxo species is then transferred to the neighboring 2,5-dihydrofuran derivative to yield the 2-hydroxy derivative.

Hydrogen atom transfer to the adjacent oxovanadium site to form λ-butyrolactone occurs, such that further oxidation of λ-butyrolactone on the 5-position, followed by desorption of a water molecule, leads to maleic anhydride formation.

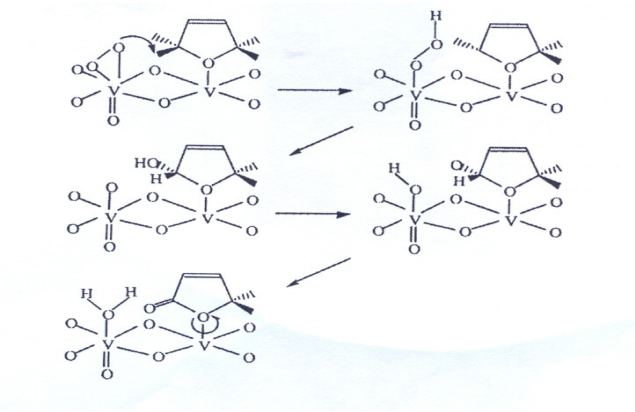

Fig.2.11: Oxidation of n-butane on the (200) plane of the $(VO)_2P_2O_7$ according to Schiøtt and Jørgersen[24]

The (200) plane of the vanadyl pyrophosphate displays the *trans*-oxovanadium(IV) dimers arranged such that the V^{4+}atoms and the apical coordination site are always next to each other in the chain. The comparable distance between the oxygen atoms (3.5Å) and the methylene H-H distance of (2.3Å) allows for contemporaneous abstraction of two methylene hydrogen atoms. From these observations, Guliants and Holmes[25] proposed and studied the activation of C_4-probe molecules on the cis-peroxo oxovanadium(V) dimeric active site in Fig.2.12. The formation of maleic anhydride from *n*-butane on the cis-peroxo oxovanadium(V) dimeric active site, as studied by Guliants and Holmes indicates that the activation step proceeds via the homolytic C-H bond cleavage and the formation of the 2,3-diradical (2) intermediate to form 2-butene (Fig.2.13).

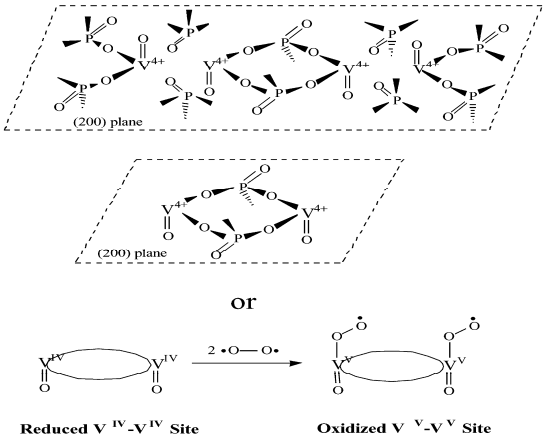

Fig. 2.12: The proposed cis-peroxo oxovanadium(V) dimeric active site for n-butane oxidation to maleic anhydride according to Guliants and Holmes.[25]

The olefin thus formed (2-butene) then undergoes dihydroxylation by an abstraction recombination mechanism, via the 1,4-alkenyl diradical (5), to form but-2-ene-1,4-diol (6). The V^{5+}-O• site oxidizes but-2-ene-1,4-diol, forming 4-hydroxy-but-2-enal (7) and V^{4+}.

The dehydration of 4-hydroxy-but-2-enal by the surface HPO_4^- and $H_2P_2O_7^{2-}$ groups allows the formation of furan (9). Furan undergoes cycloaddition with singlet oxygen yielding 5-hydroxy-2(5H)-furanone (11) which is further oxidized to maleic anhydride (12) by the V^{5+}-O• species as illustrated in Fig. 2.13.[25]

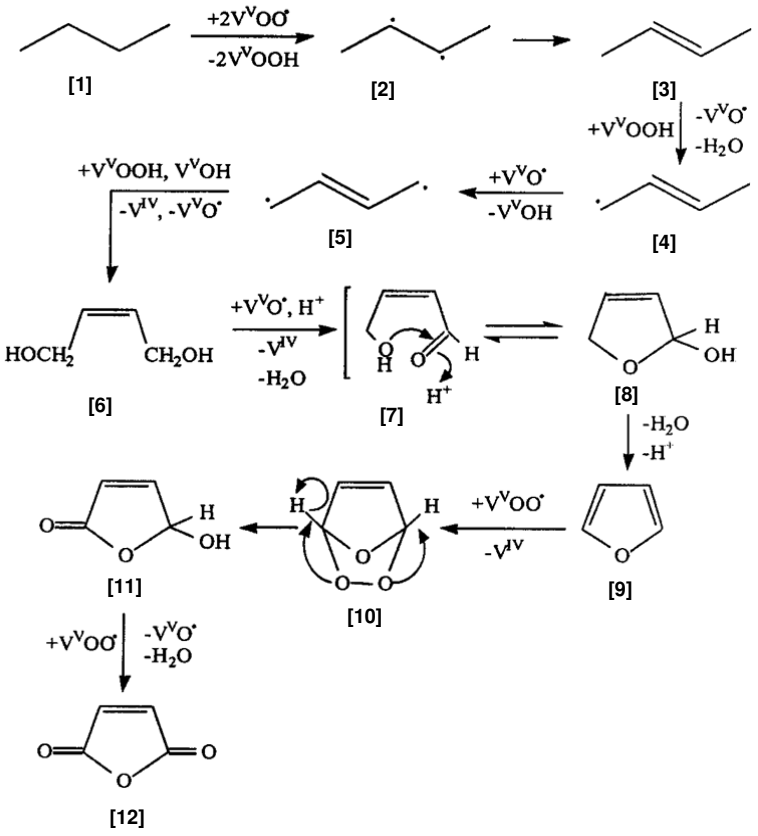

Fig.2.13: Proposed oxidation of *n*-butane to maleic anhydride over the *cis*-peroxo oxovanadium(V) dimer sites present in the (200) planes of $(VO)_2P_2O_7$.[25]

2.4 The poly-functional nature of VPO catalysts

2.4.1: The transformation of C_4- probe molecules on VPO catalysts

The proposed reaction steps for the *n*-butane to maleic anhydride transformation, following *n*-butane activation via the contemporaneous abstraction of two methylene hydrogen atoms on the *trans*-oxo vanadium(IV) dimer present in the (200) plane of the vanadyl pyrophosphate, are given in Table.2.1. None of these reaction intermediates are, however, detected under typical reaction conditions. Rapid transformation of the reaction intermediates is encountered prior to desorption from the catalyst surface. Therefore, in order to detect these reaction intermediates, conditions which prevent further oxidation of these intermediates must be chosen.

Two factors to be considered when the reaction intermediates are to be observed include: The use of a higher *n*-butane concentration (30%) and the utilization of fast non-equilibrium transient experiments that are possible in a TAP reactor. The reaction intermediates such as butenes, butadiene, and other oxygenates similar to those observed in the partial oxidation of olefins could be observed under such conditions.

The concentration of these by-products was reported to increase with oxygen concentration up to a 100% oxygen concentration: the amount of oxygen on the catalyst surface is very important in the formation of by-products.[5] It has been observed that the highly reduced metal oxide surface modifies the distribution of the surface sites, thus limiting the rate of consecutive oxidation of the reaction intermediates, hence allowing desorption into the gas phase.

Table.2.1: The proposed reaction steps in the *n*-butane to maleic anhydride transformation

Step	Reaction
n-butane → butenes	Oxidative dehydrogenation
Butenes → butadiene	Allylic oxidation
Butadiene → 2,5-dihydrofuran	1,4-oxygen insertion
2,5-dihydrofuran → furan	Allylic oxidation
Furan → γ-butyrolactone	Electrophilic insertion
γ-butyrolactone → maleic anhydride	Electrophilic oxygen insertion

From the TAP studies, two conclusions regarding desorption and detection of intermediates were reached. When insufficient oxygen is directed to the active sites, the reaction intermediates may desorb and react at other sites to form other partial oxidation products, which can thus be detected. However, in the presence of high oxygen concentration, once *n*-butane is activated it remains bound on the surface of the catalyst and desorbs from the surface as maleic anhydride.

Relative to other catalysts (e.g. MoO_3), which can activate *n*-butane with lower selectivity towards maleic anhydride, VPO catalysts possesses unique features that allow them to perform the reaction steps given in Table.2.1 to maleic anhydride without any desorption of the reaction intermediates into the gas phase, hence resulting in high selectivity towards maleic anhydride. This reaction pathway demonstrates the poly-functional nature of the active sites found on the (200) plane of the VPO catalysts.

Table.2.2: The polyfunctional nature of VPO catalysts

Reaction	Probe Molecule	Product
Oxidative dehydrogenation	Isobutyric acid Cyclohexane Succinic anhydride Hexahydrophthalic anhydride Paraffin	Methacrylic acid Benzene Maleic anhydride Phthalic anhydride Olefin
Allylic oxidation (H-abstraction)	Olefin 2,5-dihydrofuran Tetrahydrophthalic anhydride	Diolefin Furan Phthalic anhydride
1,4-oxygen insertion	Benzene Naphthalene	Maleic anhydride Naphthaquinone
Electrophilic oxygen insertion	Methacrolein *o*-xylene	Mathacrylic acid Phthalic anhydride

The poly-functional nature of the active sites was further demonstrated by Guliants and Holmes[25] on different C_4-hydrocarbons. The hydrocarbons investigated include: Unsaturated hydrocarbons, 5-membered heterocycles, alcohols and diols, *i*-butane and *n*-butane. These amounted to a total of 16 probe molecules investigated. In their study, they discovered that all the C_4-molecules could be transformed into maleic anhydride with variable yields. From their results, they established the ability of the VPO catalysts to selectively oxidize different functionalities to maleic anhydride and hence the poly-functional nature of the VPO catalysts. Other examples of probe molecules which illustrate these characteristics are given in Table.2.2.

2.4.2 Reaction pathways of C_4 to C_8 n- and cycloalkanes to maleic and phthalic anhydrides on VPO catalysts

From the results obtained in the oxidation of different probe molecules over VPO catalysts, a general reaction pathway for the transformation of paraffins over VPO catalysts can be derived.[17]

The combination of acidic and oxidizing properties of these catalysts enhances different reactions leading to a variety of products, such that the nature of the prevailing products will depend on the kinetically favored reaction under aerobic conditions. Two competitive pathways exist for ethane oxidation. Ethylene formation from oxidative dehydrogenation or the formation of acetic acid through direct oxidation of one methyl group occurs on the VPO catalysts. For the oxidation of propane and isobutane, oxidative dehydrogenation, followed by allylic oxidation are the favored pathways, since dimerization is thermodynamically unfavored at the activation temperatures required to activate these hydrocarbons.

In the *n*-butane oxidation, the formation of maleic anhydride outweighs the formation of by-products through other parallel reactions. This is achieved by the available oxygen-insertion centres which exist on the active VPO catalysts. The parallel pathways of dimerization of the intermediate olefins lead to the formation of carbon oxides by-products. However, these parallel pathways lead to the formation of phthalic anhydride in the partial oxidation of *n*-pentane via 1,4 O-insertion on the diolefin

The selectivity to maleic anhydride when cyclo paraffins (cyclohexane, cycloheptane, cyclooctane) are used is affected due to the prevalence of carbon oxides arising from the rapid transformation of the diolefins to unstable oxygenated compounds which are then thermally degraded to carbon oxides at the required activation temperatures.

2.4.3 The acidity and properties of VPO catalysts

The presence of acid centres on the surface of the VPO catalysts have been reported to exist as the Brønsted-type from pendant P-OH groups and the Lewis-type arising from V^{4+} ions.[10,19] Some of the reaction transformations, e.g. skeletal isomerization of cycloparaffins, can be explained by the presence of these acid sites. The free P-OH have also been reported to play a role in the high-pressure alkylation of benzene with propylene,[26] giving a similar product profile as the commercially employed silica-supported phosphoric acid catalysts.

During the partial oxidation of *n*-pentane to phthalic anhydride, tests were carried out to elucidate the role played by surface acidity in VPO catalysts under anaerobic conditions. Cavani and Trifirò[17] established the mechanism of the formation of a C_{10}-alkyl aromatic compound (phthalic anhydride precursor) from pentadiene. From these studies, it was established that the acid centres can dimerize, cyclize the dimer, and dehydrogenate the dimer to form the corresponding C_{10}-alkyl aromatic. Following decarboxyllation of the two carbon atoms on the C_{10}-alkyl aromatic, the precursor towards phthalic ahydride could be formed. The possible mechanism of the acid-catalyzed dimerization and transformation of pentadiene is illustrated in Fig.2.8 according to Cavani and Trifirò.[17]

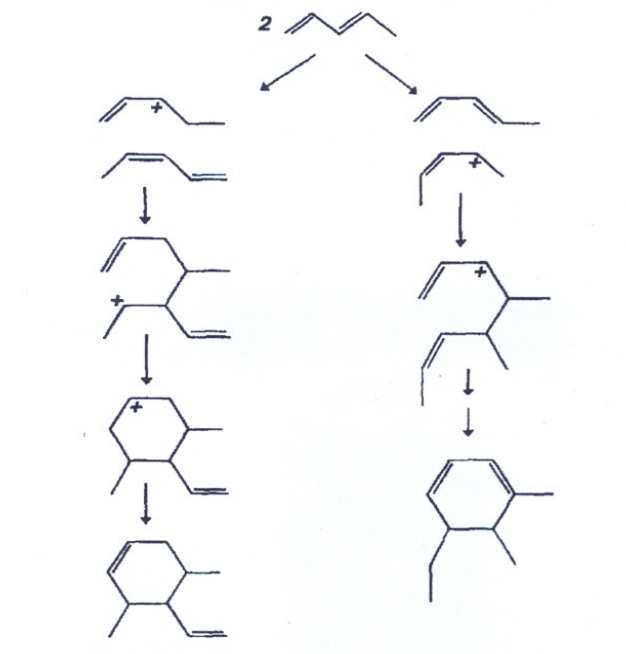

Fig.2.14: Mechanism of the acid-catalyzed dimerization of pentadiene and transformation to a cyclic unsaturated C_{10} compound.[17]

Some of the properties associated with this system are:

a. The ability to undergo oxidative dehydrogenation of paraffins, e.g. a high selectivity to benzene from cyclohexane, as well as the formation of olefins and diolefins from paraffins is achieved (in low selectivity, except when molecular oxygen is a limiting reagent).
b. The presence of active sites necessary to undergo allylic oxidation explains the high selectivity of oxygenated compounds relative to olefins on these catalysts under oxygen rich conditions.
c. A certain amount of oxidized vanadium sites is necessary and plays a role in the transformation of the olefins and diolefins to oxygenated compounds. However, a highly oxidized surface leads to a lower selectivity due the consecutive degradation of these oxygenated compounds to carbon oxides.
d. VPO catalysts are able to undergo reversible structural inter-conversions between the $(V^{4+}O)_2P_2O_7$ and $V^{5+}OPO_4$ phases.[8]
e. VPO catalysts possess acid centres to promote different transformations such as dimerization and isomerization reactions.
f. Bimolecular reactions, which are not acid catalyzed but depend on the geometry of sites at which molecules are adsorbed, can also be encountered. One such example is the formation of a phthalic anhydride precursor from a pentadiene intermediate.[17]

REFERENCES

1. E. Bordes, *Catal. Today.*, 1987, **1**, 499.
2. M. E. Leonowicz, J. W. Johnson, J. F. Brody, H. F. Shannon and J. M. Newsam, *J. Solid State Chem.*, 1985, **56**, 370.
3. C. C. Torardi and J. C. Calabrese, *Inorg. Chem.*, 1984, **23**, 1308.
4. B. C. Tofield, G. R. Crane, G. A. Pasteur and R. C. Sherwood, *J. Chem. Soc. Dalton. Trans.*, 1979, **245**, 584.
5. E. Bordes and P. Courtine, *J. Catal.*, 1979, **57**, 236.
6. E. Bordes and P. Courtine, *J. Chem. Soc. Chem. Commun.*, 1985.
7. L. Cornaglia, S. Irusta, E. A.. Lombardo, M. C. Durupty, J. C. Volta, *Catal. Today*, 2003, **78**, 291.
8. G. Centi, F. Trifiro, J. B. Ebner and V. M. Franchetti, *Chem. Rev.*, 1988, **88**, 55.
9. P. Gai and K. Kourtakis, *Science.*, 1995, **267**, 661.
10. H. Morishige, J. Tamaki and N. Yamazoe, *Chem. Lett.*, 1990, **9**, 1513.
11. G. Bergert, M. David, J. P. Boyer, C. Volta and G. Hequet, *Catal. Today*, 1987, **1**, 37.
12. G. J. Hutchings, C. J. Kiely, M. T. Sananes-Shulz, A. Burrows and J. C. Volta, *Catal. Today.*, 1998, **40**, 273.
13. G. J. Hutchings and R. Higgins, *J. Catal.*, 1996, **162**, 153.
14. G. Centi, F. Cavani and F. Trifiro, eds., *Fundamental and applied catalysis*, Kluwer Academic/Planum Publishers: New York, 2001.
15. H. Horowitz, C. M. Blackstone, A. W. Sleight and G. Teufer, *Appl. Catal.*, 1988, **38**, 193.
16. J. W. Johnson, D. C. Johnson, A. J. Jacobson and J. F. Brody, *J. Am. Chem. Soc.*, 1984, **106**, 8123.
17. F. Cavani and F. Trifirò, *Appl. Catal.* A., 1997, **157**, 195.
18. V. V. Guliants and A. Carreon, *Catalysis.*, 2005, **18**, 1.
19. J. B. Ebner and M. R. Thompson, *Catal. Today.*, 1993, **16**, 51.
20. L. Sartoni, A. Delimitis, J. K. Bartley, A. Burrows, H. Roussel, J. M. Herrmann, J. C. Volta, C. J. Kiely and G. J. Hutchings, *J. Mater. Chem.*, 2006, **16**, 4348.
21. S. Sajip, J. K. Bartley, A. Burrows, M. T. Sananes-Shulz, A. Tuel, J. C. Volta, C. J. Kiely and G. J. Hutchings, *New. J. Chem.*, 2001, **25**, 125.

22. G. Centi, F. Trifiro, G. Busca, J. R. Ebner and J. Gleaves, *Faraday Discuss. Chem. Soc.*, 1989, **87**, 215.

23. P. A. Agaskar, L. De Caul and R. K. Grasselli, *Catal. Lett.*, 1994, **23**, 339.

24. B. Schiøtt and K. A. Jørgensen, *Catal. Today.*, 1993, **16**, 79.

25. V. V. Guliants and S. A. Holmes, *J. Mol. Catal. A.*, 2001, **175**, 227.

26. F. Cavani, A. Colombo, F. Giuntoli, F. Trifirò, E. Gobbi and P. Vasquez, *Catal. Today.*, 1996, **32**, 125.

CHAPTER 3

3.1 Reactor setup

The reactor set-up was carried out using a fixed-bed continuous flow micro reactor and a gas chromatograph for analytical and quantification purposes. The partial pressure of 0.75% (below the lower explosion limit) *n*-butane in air, was employed to avoid the possibility of hot-spots formation which can render the reaction gas mixtures flammable.[1] Literature has reported the use of partial pressures lower than 2% when fixed-bed reactors are used during the *n*-butane partial oxidation, a partial pressure of 4% for the fluidized-bed reactors and percentages higher than 10% for the circulating fluidized-bed reactors.[2] The advantages of using a fixed-bed reactor include low operation costs and a continuous operation of the process.[3]

The reactor set-up comprised of 1/8th inch copper tubing feed lines and a 1/8th inch stainless steel tubing product lines. 1/16th inch stainless steel tubing was used to send the product from the gas-sampling valve to the GC. The flow rate of the feed-gas was controlled by a pressure gauge, a needle valve and the rotameter, all being mounted onto the control panel. A constant supply pressure of 100 KPa was used for all the catalytic runs and for calibration purposes.

A 300 mm long block furnace was used to supply heat during the partial oxidation of *n*-butane in air. The stainless steel tubing employed after the reactor was heated to 160 ^{o}C to prevent the condensation of the product stream (MA) in the lines at room temperature. The reactor tubing had a 7 mm inner diameter and a 10 mm outer diameter. 24 gritt carborandum powder was packed on either side of the catalyst to allow mixing of the feed stream gases and to pre-heat the gases before they reach the catalyst bed to allow for a constant temperature. Glass wool was packed on either side of the reactor tube to prevent particulate matter from entering the product stream and the valves down stream from the reactor. The temperature of the catalyst was monitored by a thermocouple placed on the outside of the reactor wall inside the furnace block. A schematic diagram of the set-up is given in Fig.3.1.

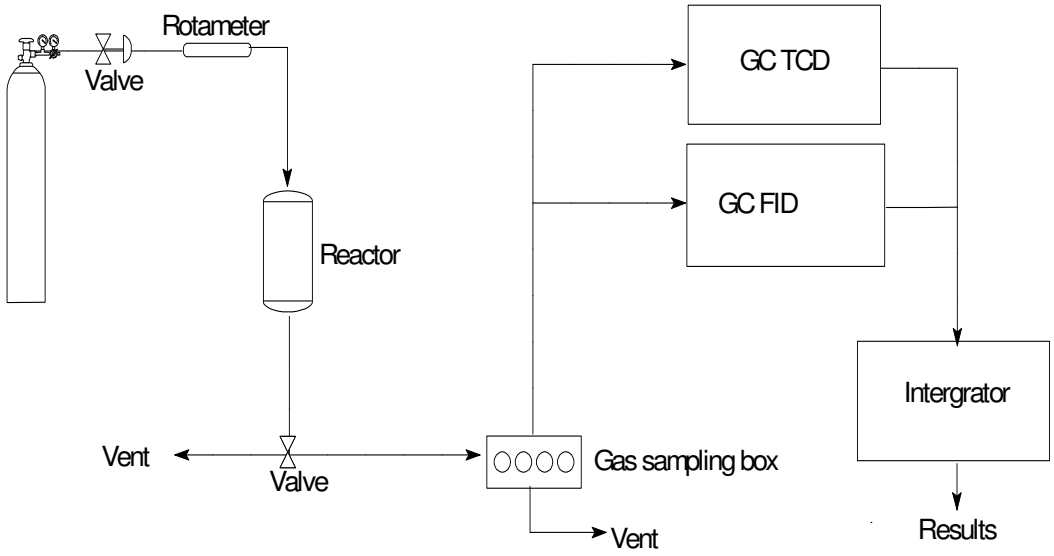

Fig.3.1: Schematic representation of the analytical system. (Refer to the text)

3.2 The gas-sampling box

The gas-sampling box contained two Valco rotary valves connected to the electronic switches. These two Valco rotary valves comprise of a 6 port rotary valve and a 10 port rotary valve attached to a heater plate as illustrated in Fig.3.2. The heater plate is continuously kept at a constant temperature of 160 ^{o}C to prevent condensation of the products from the reactor in these valves.

The gas-sampling box is connected to two GC's; the first GC is an isothermal Varian 3700 GC which is employed for the separation and analysis of air, carbon monoxide and carbon dioxide. The second GC is a Perkin Elmer XL auto system GC, which functions to separate and analyze the hydrocarbons e.g. *n*-butane and maleic anhydride. The gas-sampling box consists of entrance lines (to the gas-sampling box) and exit lines.

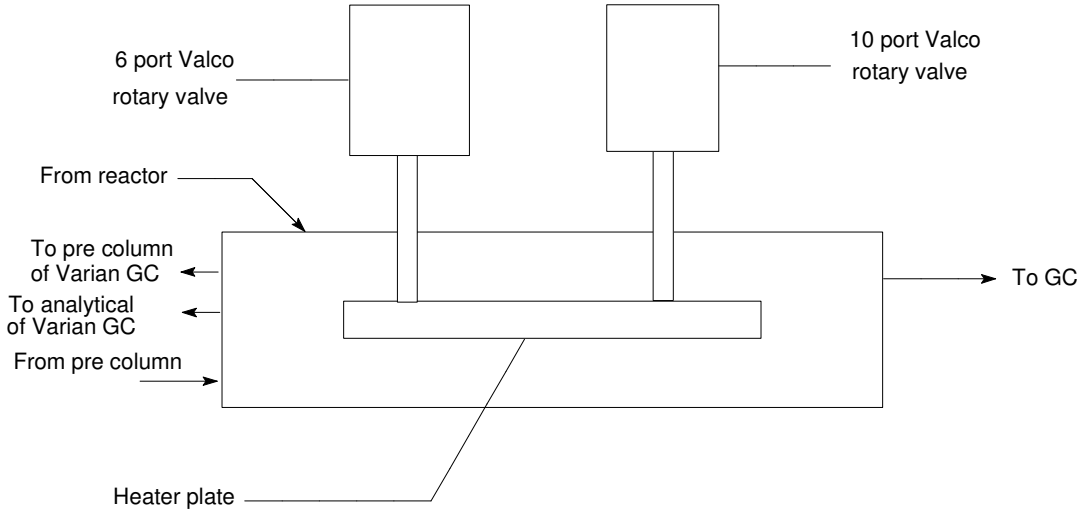

Fig.3.2: The gas sampling box equipped with a 6 port and a 10 port rotary valve

The entrance lines include the reactor product stream and the return line from the pre-column of the Varian 3700 GC, whereas the exit lines comprises of the sample feed to the pre-column and the feed line to the analytical column of the Varian 3700 GC. Both the 6 port and the 10 port rotary valves are employed with a 500 μL sampling loop. The 10 port rotary valve sampled to the Varian 3700 GC, whilst the 6 port rotary valve sampled to the Perkin Elmer GC. The pre-column in the Varian 3700 GC functioned to trap all the components that are solid at room temperature; this was maintained at room temperature to allow only gaseous products to pass through to the analytical column, thereby trapping all the other components which are solid particles at room temperature e.g. maleic anhydride.

3.2.1 Operation of the gas-sampling box

The valves were operated electronically by the Perkin Elmer GC. The valves were turned on electronically utilizing pressurized air through pressure build-up and release in the valves. Fig.3.3 illustrates the operation of the 10 port Valco rotary valve in the standby mode and the sampling mode respectively. Helium was used as a carrier gas in the Varian 3700 GC.

Valves in a stand-by mode (10 port Valco rotary valve):

The carrier gas was carried into the valves through port 7, towards port 6 and this was further carried into the analytical column, followed by the detector. The mobile phase flowed in through port 4 and then out of port 5, through the injector and through the pre-column into port 9, and further out through port 8, through a restrictor (which functions to regulate the pressure in the system) and then vented out to waste. Sample from the reactor was sent out to waste following its flow through port 1 and the sample loop.

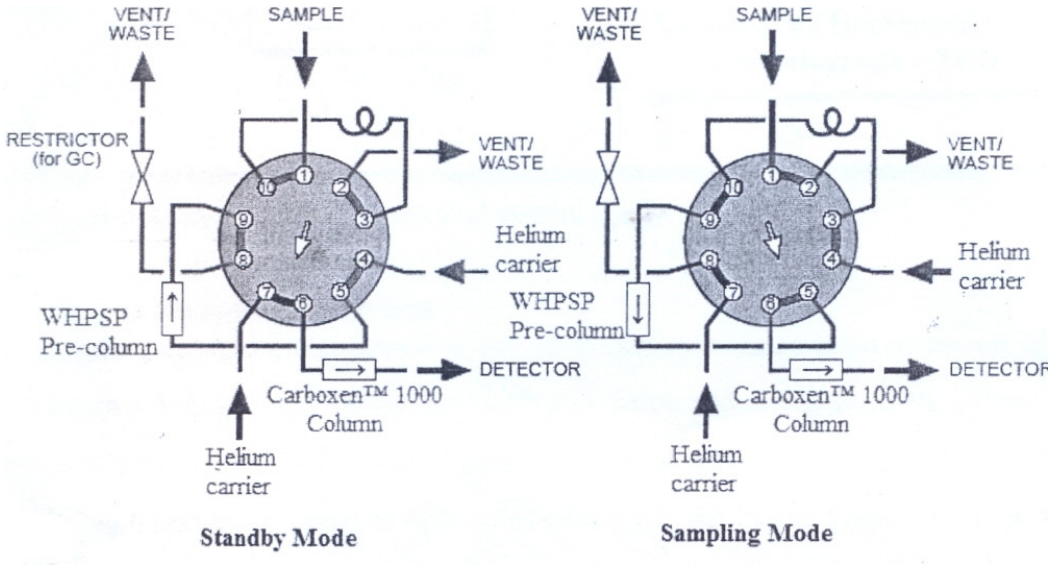

Fig. 3.3: The 10 port valco rotary valve in the standby mode.

Valves in a sampling mode (10 port Valco rotary valve):

In this mode, the valve was automatically turned clockwise allowing the carrier gas to flow through port 7 and out to waste. When the sample is being sent to the detector for analysis, the carrier gas flows through port 4, then through the sample loop with the sample from the reactor, enters the pre-column, the analytical column and the detector.

The 6 port rotary valve operated the Perkin Elmer GC in the same manner as the 10 port rotary valve except that no pre-column is attached (Fig.3.4). When the 6 port rotary valve is in the sampling mode the sample was being directed to the analytical column in the Perkin Elmer GC.

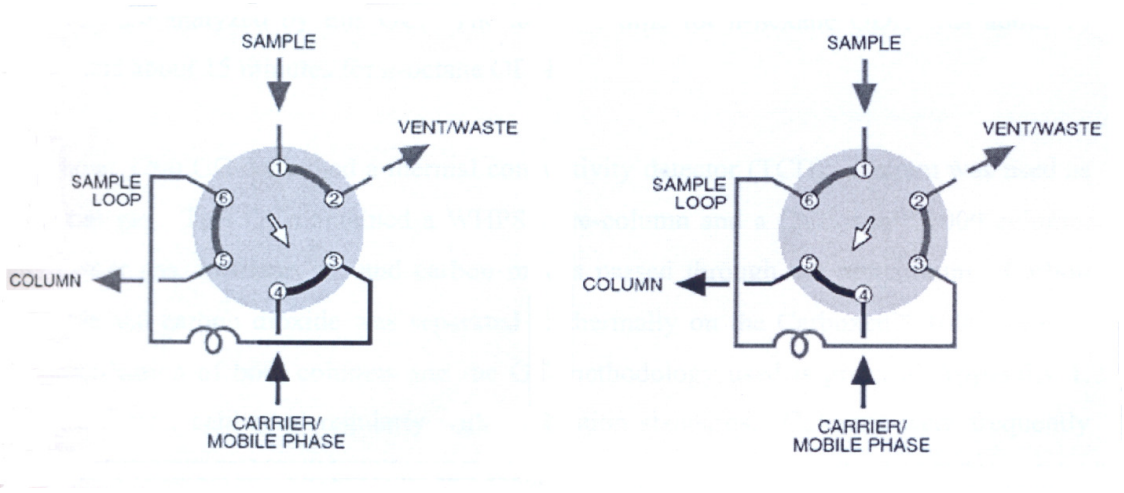

Fig. 3.4: The illustration of the 6 port rotary valve for the Perkin Elmer GC in the standby mode and the sampling mode.

3.2.2 Chemicals utilized for testing and analysis

Table.3.1: The percentage purity of the chemical used in the catalyst synthesis.

CHEMICALS	% PURITY	USES	MOLECULAR WEIGHT ($g.mol^{-1}$)	SUPPLY
Butane (special gas mixture)	0.75% *n*-butane, 19.5 O_2, balance N_2	Feed gas / Calibration	58.12	Afrox
Maleic anhydride	>98%	Calibration	98.06	Saarchem
Carbon monoxide	5% balance nitrogen	Calibration	28.01	Afrox
Carbon dioxide	15% balance nitrogen	Calibration	44.01	Afrox

3.3 Gas chromatography-mass spectrometry (GC-MS) analysis

A gas sample was obtained from the reactor (off-line) and analyzed via GC-MS to determine the product composition in the sample. Comparison to the library data confirmed the presence of maleic anhydride in the sample. An Agilent 6890 series GC system; 5973 network mass selective detector was utilized using a 30.0 x 250 µm 25 HP-5 5% Phenyl siloxane capillary column.

3.4 Gas chromatography (GC)

Analysis and quantification of *n*-butane and the other products were obtained by the aid of a flame ionization detector (FID) GC and a thermal conductivity detector (TCD) GC for the analysis of hydrocarbons and carbon oxides respectively. The parameters used are outlined in section 3.4.

3.5 Analysis of the unreacted feed gas and the reaction products

The separation of the unreacted feed, as well as the reaction products, was carried out by the use of a CP-sil24CB column installed in the Perkin Elmer GC. The products obtained in this study include: maleic anhydride, propane, CO and CO_2. The retention times of the feed (*n*-butane) and the products are shown in Table 3.2.

Table.3.2: Retention times of the feed-gas and products as obtained from the FID.

COMPOUND	RETENTION TIMES (min)
Propane	6.2
n-butane	6.3
Maleic anhydride	17.6

The carbon oxides were separated using the carboxen^{Tm} 1000 column installed in a Varian 3700 GC. A chromosorb WHPSP pre-column was installed in the Varian 3700 GC to separate gaseous products from other products at room temperature, allowing only the carbon oxides and air to pass through to the analytical column and flushing all the other products out to waste. The retention times of the carbon oxides are shown in Table 3.3 as obtained from the thermal conductivity detector GC.

Table.3.3: Retention times of the carbon oxides as obtained from the TCD.

COMPOUND	RETENTION TIME
Carbon monoxide	1.83
Carbon dioxide	13.36

3.6 The specifications for the columns used are listed below:

Table.3.4: The specifications of the columns used in the Varian 3700 and the Perkin Elmer XL auto system GC.

*SPECIFICATIONS FOR A COLUMN USED IN THE **VARIAN 3700 ISOTHERMAL GC***		
Specifications	Pre-column	Analytical column
Support	Chromosorb WHPSP	Carboxen^{TM} 1000
Dimension	Length: 1m; OD: 1/8"; ID: 2.2mm	Length: 2.5m; OD: 1/8"; ID: 2.2mm
Maximum temperature	20-275 ^{o}C	225^{o}C
*Specifications for the column used in the **Perkin Elmer XL auto system GC***		
Coating	No pre-column	CP-Sil 24CB
Dimensions		Length: 30; OD: 0.32mm ID: 0.45mm
Maximum temperature		225^{o}C

GC parameters used for testing

Isothermal Varian 3700

Temperature of the detector: 130^{o}C

Temperature of the column: 22^{o}C

Temperature of the injector: 150^{o}C

Temperature of the TCD filament: 150^{o}C

Perkin Elmer XL Autosystem

Temperature of the detector: 130^{o}C

Injector A: 220^{o}C

CarrierA: 9.0 psig

Split flow: 50.2

The column temperature program for the Perkin Elmer XL auto system was ramped as follows: an initial temperature of 40 ^{o}C was held for 8 minutes to a set point of 200 ^{o}C and heated at a rate of 7 ^{o}C.min^{-1}. Both the carrier gas (N_2) and the flame gases (H_2 and O_2) were supplied by Afrox.

3.7 Catalyst synthesis

The catalysts were prepared according to the organic solvent procedure, whereby a V^{5+} species was reduced in *iso*-butanol in the presence of *ortho*-phosphoric acid to obtain the required phosphorus to vanadium mole ratio. Following the synthesis, the resulting blue solid was recovered by vacuum filtration, washed, dried and activated under a stream of nitrogen at 450^{o}C for 6 hours (Fig.3.5). The promoted catalysts were prepared in a similar manner. The promoter salts were added during the first step of the synthesis (see Fig.3.5) to obtain the required metal to vanadium mole ratio. The chemicals used for the synthesis and their purity are given in Table.3.5.

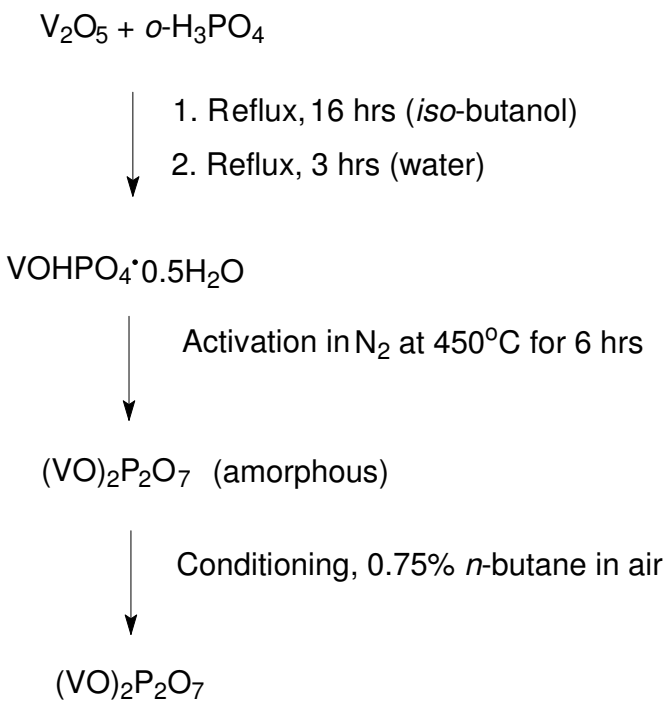

Fig.3.5: Schematic representation illustrating the synthetic route toward a VPO catalyst.

Table.3.5: Reagents used for catalyst synthesis.

REAGENTS	SUPPLIER	% PURITY	MOLECULAR WEIGHT ($g.mol^{-1}$)
V_2O_5	Sigma-Aldrich	98+ %	181.88
O-H_3PO_4	Riedel-deHaen	99+ %	98
Iso-butanol	Saarchem	98 %	74.12
$RuCl_3.xH_2O$	Alfa Aesar	99.9 %	261.47
$FeCl_3$	Saarchem	99 %	162.21

The un-promoted catalyst was prepared by adding V_2O_5 (11.80 g) to *iso*-butanol (250 mL). *o*-H_3PO_4 was introduced and the mixture was refluxed for 16 hours. After 16 hours reflux, the blue solid was recovered by vacuum filtration and washed with *iso*-butanol (200 mL) and ethanol (150 mL). The resulting solid was allowed to reflux in water for 3 hours (9 mLg^{-1} solid), filtered hot and dried in air (110 ^oC, overnight).

The ruthenium-promoted catalysts were prepared by dissolving the required amount of ruthenium trichloride hydrate in a mixture of V_2O_5 (11.80 g) and *iso*-butanol (250 mL) to obtain a 0.1% Ru/V, 0.3% Ru/V and a 1% Ru/V ruthenium-promoted VPO catalysts. *o*-H_3PO_4 was then introduced and the mixture was refluxed for 16 hours. After 16 hours reflux, the blue solid was recovered by vacuum filtration and washed with *iso*-butanol (200 mL) and ethanol (150 mL). The resulting solid was allowed to reflux in water for 3 hours (9 mLg^{-1} solid), filtered hot and dried in air (110 ^oC, overnight).

The iron-promoted catalysts were prepared by dissolving the required amount of iron trichloride to a mixture of of V_2O_5 (11.80 g) and *iso*-butanol (250 mL) to obtain a 0.1% Fe/V, 0.3% Fe/V and a 1% Fe/V iron-promoted VPO catalysts. *o*-H_3PO_4 was then introduced and the mixture was refluxed for 16 hours. After 16 hours reflux, the blue solid was recovered by vacuum filtration and washed with *iso*-butanol (200 mL) and ethanol (150 mL). The resulting solid was allowed to reflux in water for 3 hours (9 mLg^{-1} solid), filtered hot and dried in air (110 ^oC, overnight).

Following the synthesis and drying of the catalysts, these catalysts were then activated under nitrogen atmosphere at 450 ^oC for 6 hours at a temperature ramp of 10 $^oC.min^{-1}$.

3.8 Catalyst testing

Approximately 1 mL of 300-600 μm catalyst pellets were packed in the middle of a 350 mm stainless steel reactor tube with quartz wool placed on either end of the reactor tube. Inert SiC carborandum was packed in the reactor on either side of the catalyst to completely fill the reactor tube and quench any free radical gas phase reactions which would otherwise occur with the void spaces of the reactor tube. Different gas hourly space velocities were investigated to obtain a range of *n*-butane conversion at a constant temperature. These catalysts were allowed to stabilize for a period of approximately 200 hours on stream. The optimum conditions for each catalyst were thus established.

3.9 Catalyst characterization

The un-promoted catalysts and the promoted catalysts were characterized with the aid of various techniques, these include: attenuated total reflectance (ATR), inductively coupled plasma-optical emission spectroscopy (ICP-OES), X-ray diffraction (XRD), Brunauer-Emmet Teller surface area (BET), redox titrations, energy dispersive X-ray spectroscopy (EDS), temperature programmed reduction (TPR) and solid state phosphorus nuclear magnetic resonance spectroscopy (^{31}P NMR).

3.9.1 Attenuated total reflectance (ATR)

The catalysts surfaces were analyzed by the Perkin Elmer spectrum 100 spectrophotometer, whereby an infrared transmitting crystal (ZnSe) with a refractive index of (n=2) was employed to reflect the infrared radiation within an ATR element. In this technique, no sample preparation is required. The catalysts powders are merely pressed onto the top surface of the crystal to maintain an intimate optical contact with the refracting crystal (ZnSe). The IR radiation from the spectrometer once reflected by the crystal enters and penetrates a finite amount of this radiation into the sample with each reflection via the “evanescent” wave. At the end of the crystal the beam is then redirected back to the spectrometer and the signal sent to the detector for spectrum recording.[4]

3.9.2 Inductively coupled plasma-optical emission spectroscopy (ICP-OES)

Quantitative and qualitative analysis of the catalysts were performed on a Perkin Elmer ICP-OES Optima 5300 DV. The molar ratios of the elements, P/V ratios as well as the mole percentage of the promoting elements (Fe and Ru) were determined using this technique. The catalyst powders were digested in aqua-regia (1.5 mL HNO_3: 3.5 mL HCL) to release the metal elements into solution for analysis.

The multi elemental standards of the elements under study were prepared in the 10 to 50 ppm concentration range for vanadium and phosphorus and a 1 to 5 ppm range for the promoting elements. The actual concentrations of the promoting elements in the samples were determined from this range of standards using the calibration graphs obtained from the elemental standards. The range of elemental standards used and the spectral lines selected for the analysis are given in Table 3.6.

Table.3.6: The selected spectral lines and the range of calibration standards utilized in the ICP-OES.

ELEMENT	**SPECTRAL LINE (nm)**	**CONCENTRATION RANGE (ppm)**				
P	213	10	20	30	40	50
V	310	10	20	30	40	50
Ru	249	1	2	3	4	5
Fe	259	1	2	3	4	5

In this technique, the sample is aspirated into an inductively coupled plasma discharge. The analyte is converted into the gas-phase atoms in their excited states. Following this, the emitted light produced by the excited atoms is measured relative to the concentration range of the standards to give the sample concentration.

3.9.3 Powder X-ray diffraction (XRD)

The catalyst powders were analyzed on a Philips PW 1730-10 X-ray diffractomer to determine the 2-D diffraction patterns.

Table.3.7: The calculated d-spacings and the corresponding hkl values for $VOHPO_4 \cdot 0.5H_2O$ and $(VO)_2P_2O_7$.[5]

$VOHPO_4.0.5H_2O$		$(VO)_2P_2O_7$	
d-spacing	hkl	d-spacing	hkl
5.901	110	6.266	021
5.719	001	5.651	111
4.818	020	4.786	002
4.535	101	4.069	131
4.099	111	3.863	200
3.684	200	3.133	042
3.300	121	3.005	202
3.116	201	2.904	113
2.944	211	2.433	232
2.796	031	2.393	242
2.663	102	2.393	004
2.615	131	2.358	223
2.567	112	2.267	331
2.454	022	2.203	171
2.405	040	2.088	063
2.263	301	1.976	224
2.234	231	1.931	400

About a gram of the catalyst powder was placed onto a sample holder and smeared uniformly to create a flat upper surface. This is needed to achieve a random distribution of lattice orientations. A powder XRD scan was then recorded as a plot of scattering intensity vs. the scattering angle (2θ). The corresponding d-spacing can thus be calculated using Bragg's law form the equation $n\lambda = 2d \sin\theta$.

The identification of the VPO phases as well as the hkl for the different phases was obtained by comparing to the literature values reported by Bordes *et al.*[5] The different phases are given in Table.3.7 for the catalyst precursor, $VOHPO_4 \cdot 0.5H_2O$ and the vanadyl pyrophosphate, $(VO)_2P_2O_7$.

3.9.4 Brunauer-Emmet-Teller (BET)

The surface area of the catalysts was determined by the use of a Micromeritics Gemini flow prep 060. The powders were heated and degassed in a flow of nitrogen gas to remove any adsorbed foreign molecules prior to analysis. During the analysis, the sample was placed inside a vacuum chamber at a constant temperature of liquid nitrogen. The sample was then subjected to a wide range of pressures in order to generate adsorption/desorption isotherms.

Once the area occupied by one adsorbate molecule is known, e.g. $\sigma = 16.2$ Å^2 for nitrogen, then the surface area of the material can be determined using the BET equation for multilayer adsorption[6]:

$$\frac{P}{n(P_0 - P)} = \frac{1}{cn_m} + \frac{c - 1}{cn_m}\frac{P}{P_0}$$

Where, P = adsorption pressure

Po = saturation vapor pressure

c = a constant

n = moles per gram of adsorbent

n_m = monolayer capacity

3.9.5 Redox titration

Redox titration was performed to determine the average oxidation state of vanadium in the samples according to a method similar to that reported by Namakura *et al*.[7] About 0.1g of the catalyst sample was dissolved in 17 mL of 12 M H_3PO_4 and heated until all the catalyst powder has dissolved to give a clear blue solution. This solution was then added to 10 mL of concentrated H_2SO_4 in 250 mL water. The content of vanadium was then determined by titration with 0.05 N $KMnO_4$ and 0.05 N $(NH_4)_2Fe(SO_4)_2$ for V^{4+} and V^{5+} determination respectively. 1% diphenyl ammine (in concentrated H_2SO_4) was used as an indicator for the reduction process. This indicator undergoes a color change from deep violet in the oxidizing medium to colorless in the reducing medium. For the oxidation process, $KMnO_4$ was employed as a self indicator. The average oxidation state of vanadium was expressed as $5-(V_1/V_2)$, where V_1 = the volume of the oxidizing agent ($KMnO_4$) and V_2 = the volume of the reducing agent $(NH_4)_2Fe(SO_4)_2$.

3.9.6 Scanning electron microscope (SEM) and Energy dispersive X-ray spectroscopy (EDS)

The catalyst's structure, as well as the elemental composition, was determined using the Hitachi S520 scanning electron microscope equipped with an ISIS energy dispersive X-ray analytical system. A small amount (spatula tip) of the catalyst sample was used in both the analyses. For EDS characterization, the atoms on the surface of the catalyst powders are excited by the electron beam from the SEM, emitting specific wavelengths which are characteristic of the atomic structure of the elements.

The SEM analysis involved coating the surface with a thin layer of gold metal for conductive purposes during the analysis. The procedure involves focusing a finely collimated beam of electrons into a small probe, which scans across the surface of the specimen. The interaction between the beam and the sample result in the emission of the electrons and photons, as the electrons penetrates the surface of the sample. Following this, the emitted particles are then collected and sent to the detector to provide information regarding the surface morphology.

3.9.7 Temperature programmed reduction (TPR)

The number of reducible species present in the VPO catalyst as well as the reduction temperature was determined and recorded on the Micromeritics Auto Chem II 2920 analyzer equipped with a TCD detector. Prior to analysis, the catalysts were pretreated in a vacuum oven to remove the unwanted adsorbates from the catalyst surface. The analysis involved the flow of a reducing gas (5% H_2 in argon) through the sample (50 mg) at ambient temperature. The temperature was then raised at a rate of 5 ^{o}C min^{-1} to a temperature of 850 ^{o}C. Hydrogen consumption was monitored and the detector gave hydrogen uptake volume relative to the temperature of reduction (or time) signal.

3.9.8 Solid state Phosphorus nuclear magnetic resonance (^{31}P NMR)

The solid state ^{31}P NMR spectra was recorded to provide information about the different oxidation states of vanadium surrounding the phosphorus atoms in the $(VO)_2P_2O_7$ catalyst. The catalyst samples were analyzed at Bruker Biospin, Germany using a Bruker Avance III 500 WB NMR spectrometer with a 3.2mm probe at 20 KHz.

REFERENCES

1. S. Mota, M.Abon, J. C. Volta and J. A. Dalmon, *J. Catal.*, 2000, **193**, 303.
2. G. Centi, F. Trifiro, J. B. Ebner and V. M. Franchetti, *Chem. Rev.*, 1988, **88**, 55.
3. S. Buchanan, J. Apostolakis and S. Sundaresan, *Appl. Catal.*, 1985, **19**, 66.
4. http://www.nuance.northwestern.edu/keckII/ftir, Accessed 9/5/2008.
5. E. Bordes, *Catal. Today.*, 1987, **1**, 499.
6. http://www.beckmancoulter.com, Accessed 02/03/2008.
7. M. Namakura, K. Kawai and Y. Fujiwara, *J. Catal.*, 1974, **34**, 345.

CHAPTER 4

4.1 Characterizations

4.1.1 Attenuated total reflectance spectroscopy (ATR)

4.1.1.1 ATR of the un-promoted and the promoted VPO precursor, $VO(HPO_4)\cdot 0.5H_2O$

The ATR spectra of the unpromoted, iron and the ruthenium-promoted VPO precursor, $VO(HPO_4)\cdot 0.5H_2O$ are given in Fig.4.2 and Fig.4.3 respectively. This technique was used to analyze the influence of the promoter elements on the V=O species in the VPO matrix.

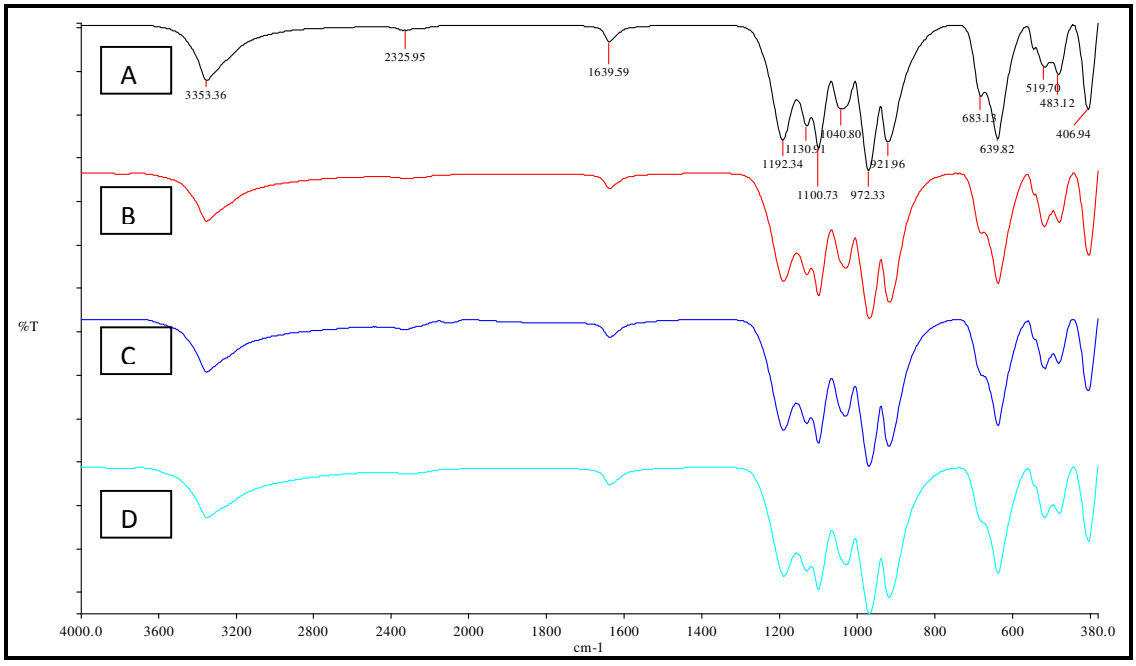

Fig.4.1: ATR of a VPO [A]and Fe-VPO precursors at 0.1%-Fe [B], 0.3%-Fe [C] and 1.0%-Fe [D] loading respectively

The bands for coordinated water at 3350 and 1639 cm^{-1} are clearly distinguished. These bands correspond to O-H stretching vibrations of structural water bound to vanadium (IV) in the face shared VO_6 di-octahedra in the lattice of the hemihydrate, and the O-H bending vibrations respectively.[1] The P-O stretching vibrations occur in the 900-1200 cm^{-1} region.[2]

Similar results were obtained for both ruthenium and the iron promoted VPO catalysts, thus no information could be obtained on the band vibrations of the promoted precursor catalysts relative to the unpromoted VPO precursor. The ATR spectra of the activated precursors in Figs.4.4 and 4.5 are used to further study the influence of these metals on VPO catalysts

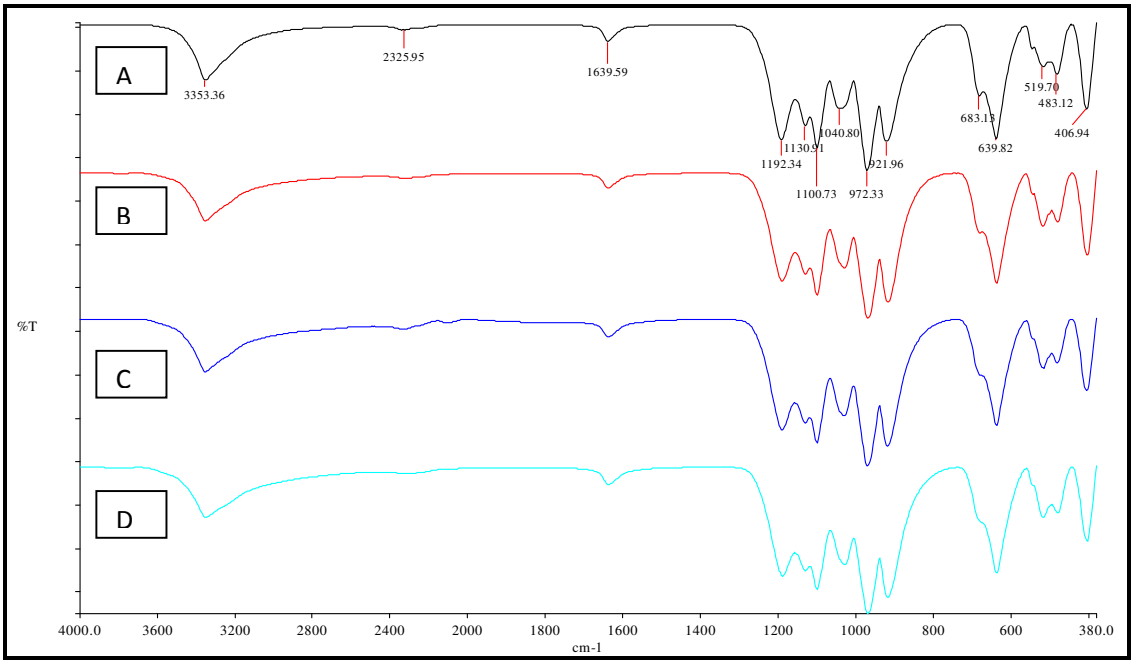

Fig.4.2: ATR of a VPO [A] and Ru-VPO precursors at 0.1%-Ru [B], 0.3%-Ru [C] and 1.0%-Ru [D] loading respectively.

4.1.1.2 ATR of the activated un-promoted and the Fe- and Ru-promoted VPO catalysts

Following thermal activation of the precursor catalyst under a stream of nitrogen at 450^{o}C for 6 hours, and subsequent catalytic testing, coordinated water molecules could no longer be observed in the ATR spectra. This corresponds to the weight loss of ~ 10.48% according to equation (1):

$$2VO(HPO_4)\cdot 0.5H_2O \rightarrow (VO)_2P_2O_7 + 2H_2O \ldots\ldots\ldots\ldots (1)$$

The influence of iron and ruthenium metals on the V=O species in the VPO matrix is determined in the activated catalysts. Typical VPO bands are observed for the un-promoted and the promoted catalysts, however a distortion can be observed in the bands shifting from 950 cm^{-1} to 935 cm^{-1} in the iron-

promoted catalysts (at 0.1% to 0.3% loading). This shift may explain the location of iron in the matrix of the vanadyl pyrophosphate.[3]

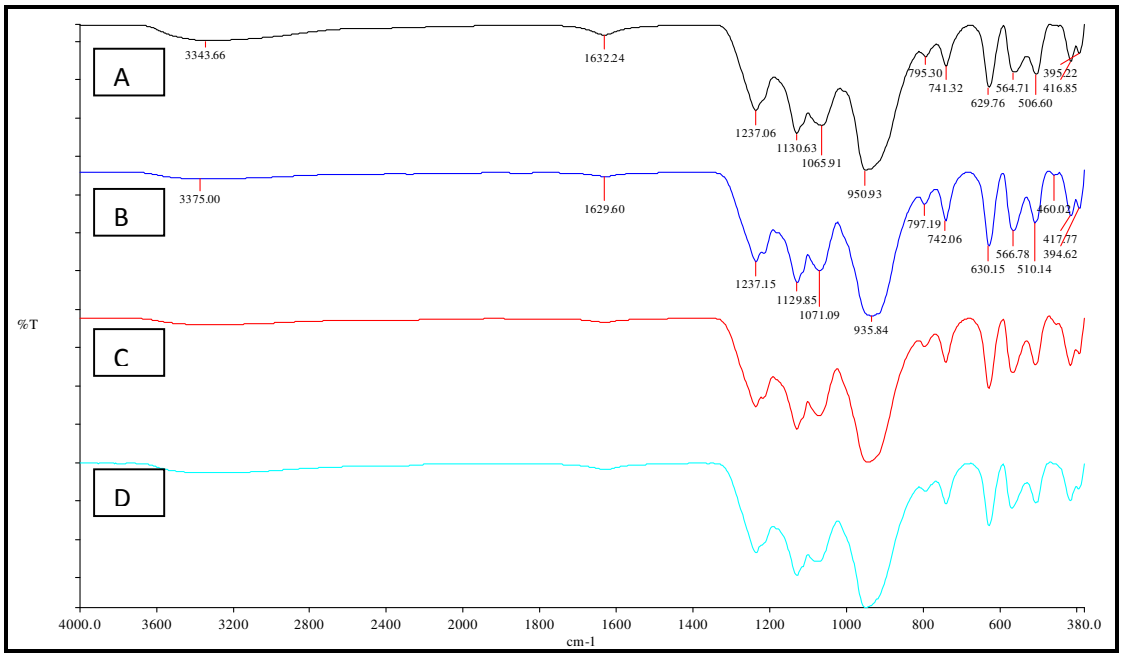

Fig.4.3: ATR of a used VPO and the used Fe-VPO catalysts; for the VPO [A], 0.1%-Fe [B], 0.3%-Fe [C], and 1.0%-Fe [D] VPO catalysts respectively.

In the ruthenium promoted catalysts, a shift for the V=O vibration is not observed. This observation may suggest that ruthenium is not incorporated within the lattice but rather that ruthenium is dispersed on the surface of the vanadyl pyrophosphate, and therefore can act as a structural promoter rather than an electronic promoter. However, if iron is indeed incorporated within the lattice of the vanadyl pyrophosphate, then iron can effectively act as an electronic promoter for $(VO)_2P_2O_7$, enabling catalyst re-oxidation by forming solid solutions of the form $(VO)_{2-x}Fe_xP_2O_7$ reported by Otake *et al.*[4]

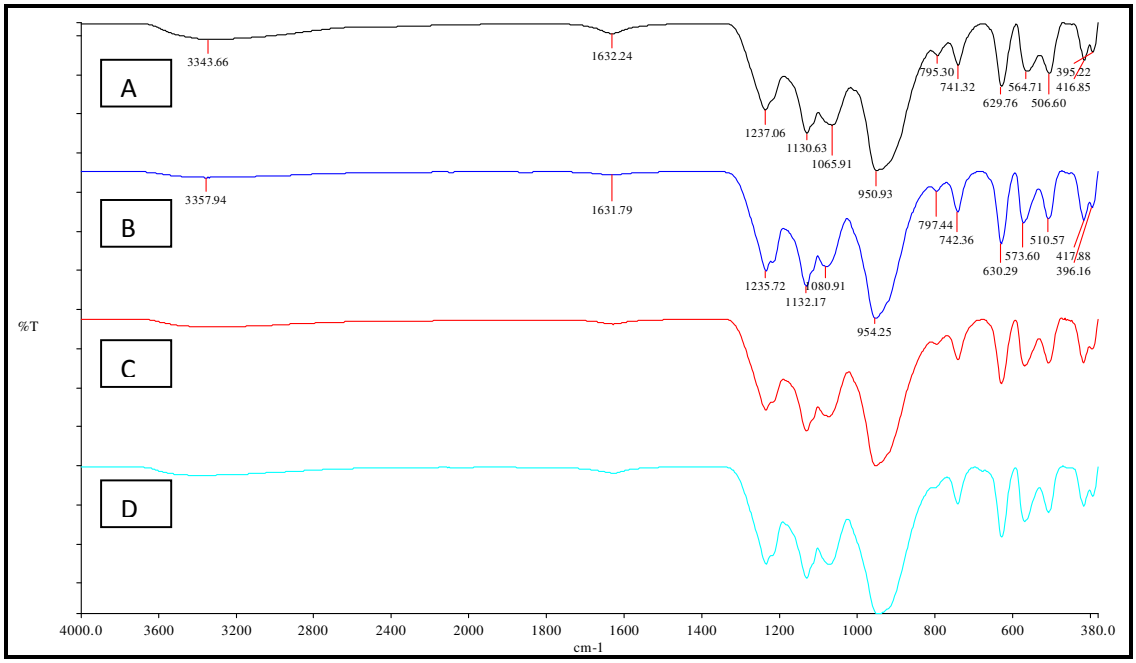

Fig.4.4: ATR of a used VPO and the used Ru-VPO catalysts; for the VPO [A], 0.1%-Ru, 0.3%-Ru [B], and 1.0%-Ru [D] VPO catalysts.

4.1.2 Inductively coupled plasma-Optical emission spectroscopy (ICP-OES)

A slight excess of phosphate (P/V = 1.04-1.06) was obtained for all the catalysts studied (see Tables.4.1 and 4.2). The optimal catalysts are characterized with a slight excess of phosphate with respect to the empirical formula of the precursor, $VO(HPO_4)\cdot 0.5H_2O$.[5-7] Phosphate deficiency e.g. P/V = 0.95 in VPO catalysts results in high relative rates of V^{4+} and V^{5+} oxidation and reduction, respectively. VPO catalysts characterized with a high V^{5+}content have high activity but low selectivity, whereas catalysts rich in phosphate concentration results in low activity catalysts.

A reasonable compromise between the reducibility and the oxidizability of the catalysts is needed for active and selective VPO catalysts, and this has been reported for catalysts with a slight excess of phosphate e.g. P/V = 1.05.[8]

Table.4.1: Elemental molar ratios (mol %) for the un-promoted and the iron promoted VPO catalysts

CATALYSTS	PRECURSOR		USED	
Name	P/V	Fe/V	P/V	Fe/V
VPO	1.06	------	1.03	------
0.1% Fe-VPO	1.04	0.14	1.03	0.13
0.3% Fe-VPO	1.04	0.33	1.03	0.34
1% Fe-VPO	1.05	1.19	1.06	1.14

Table.4.2: Elemental molar ratios (mol %) for the un-promoted and the ruthenium promoted VPO catalysts

CATALYSTS	PRECURSOR		USED	
Name	P/V	Ru/V (%)	P/V	Ru/V (%)
VPO	1.06	------	1.03	------
0.1% Ru-VPO	1.06	0.13	1.04	0.11
0.3% Ru-VPO	1.05	0.35	1.05	0.32
1% Ru-VPO	1.06	1.35	1.04	1.16

4.1.3 X-ray diffraction (XRD)

4.1.3.1 X-ray diffractogram of the un-promoted $VO(HPO_4)\cdot 0.5H_2O$

An XRD diffractogram of the un-promoted VPO precursor catalyst in Fig.4.6 shows a pure crystalline $VO(HPO_4)\cdot 0.5H_2O$. The broadening of the (001) interlayer spacing reflection is exposed relative to the in-plane (220) reflection. This is a characteristic of un-promoted VPO catalysts prepared via the organic route of synthesis.[9 10]

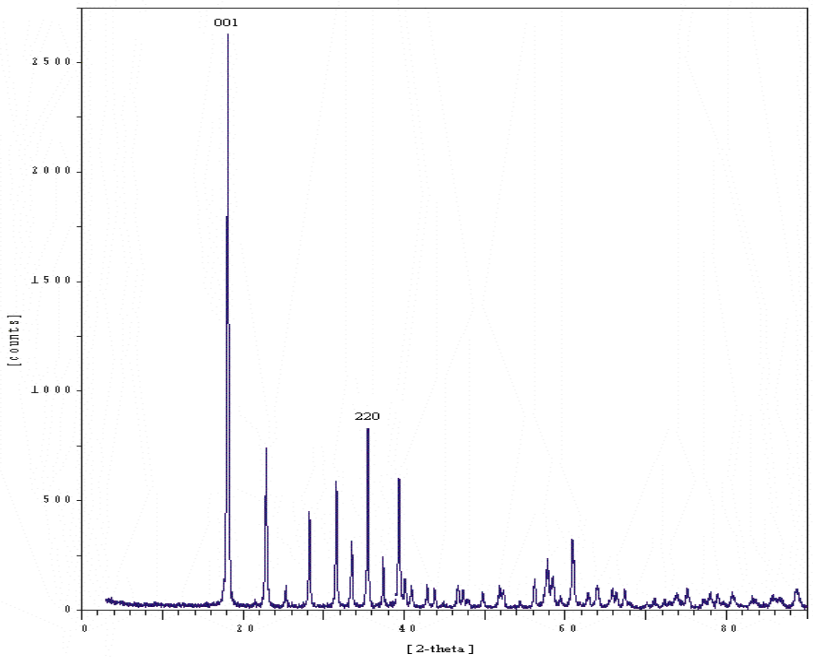

Fig.4.5: XRD pattern of the VPO precursor

4.1.3.2 X-ray diffractogram of the Fe- and Ru-promoted $VO(HPO_4)\cdot 0.5H_2O$

The XRD pattern of the iron-promoted catalysts (0.1% to 1%) is given in Fig.4.7. All the reflections in the iron-doped VPO catalysts are attributed to $VO(HPO_4)\cdot 0.5H_2O$. The introduction of the iron leads to a slight modification in the [001] ^{hemi} / [220] ^{hemi} relative intensity ratio, such that the [220] in-plane reflection is more pronounced relative to the [001] interlayer reflection. This effect was also observed and reported by Hutchings *et al.*[11] for cobalt and iron promoted catalysts.

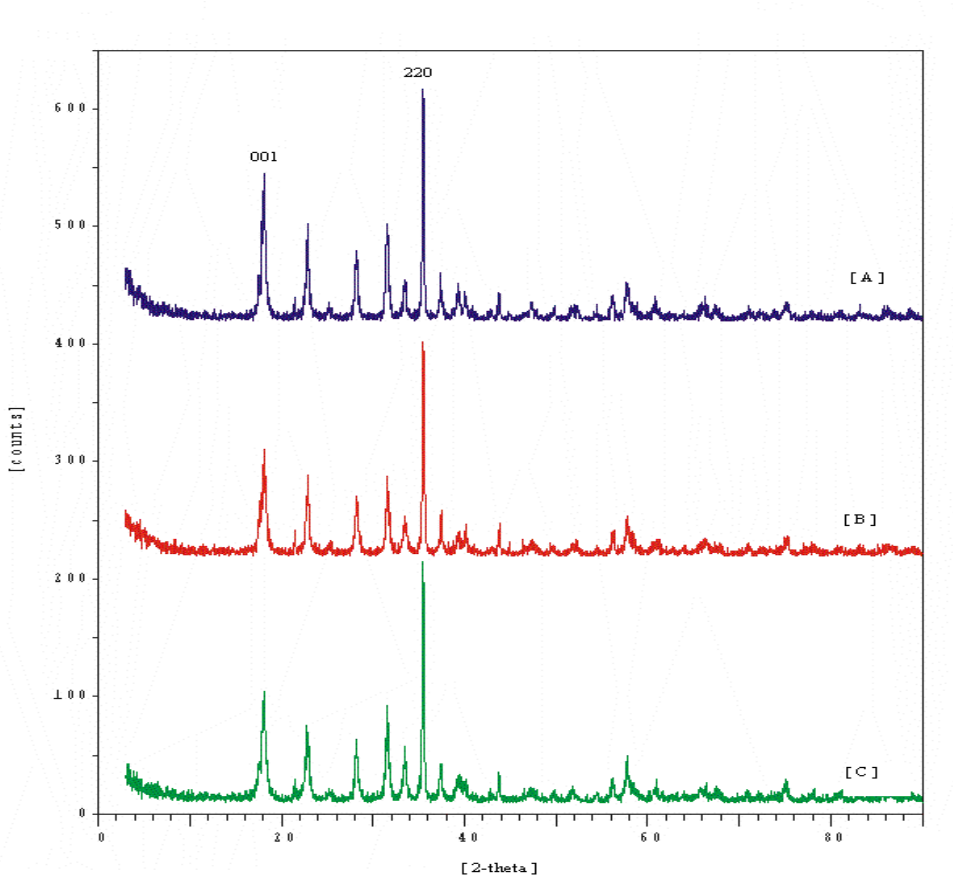

Fig.4.6: XRD patterns of the Fe-VPO precursors for the 0.1% Fe [A], 0.3% Fe [B], and 1.0% Fe [C] VPO catalysts

The XRD pattern of the ruthenium-promoted catalysts (0.1% to 1%) in Fig.4.8 displays the same trend as observed for the iron-promoted catalysts. The presence of ruthenium leads to a modification in the [001] ^{hemi} / [220] ^{hemi} relative intensity ratio, leading to a high exposure of the [220] in-plane reflection relative to the [001] interlayer reflection. Other phases were not observed for the catalyst precursors, especially the non-selective $VO(H_2PO_4)_2$ which could be removed during the water extraction step.

Furthermore, the diffractograms obtained for these promoted catalysts resemble literature patterns for the catalysts prepared via the VPD route of synthesis [The reduction of $VOPO_4{\cdot}2H_2O$ in an organic solvent to form $VO(HPO_4){\cdot}0.5H_2O$].[12] This provides information about the role played by these promoters on the catalyst structure, such that these promoters may be playing a similar role to that played by alcohols during the reduction of $VOPO_4{\cdot}2H_2O$.

Moreover the structure of the precursor catalysts can be deduced from the characteristic diffractograms. A dominant (001) reflection corresponds to the basal plane of $VO(HPO_4)\cdot 0.5H_2O$, indicative of a stacked platelet morphology, whereas a dominant (220) reflection is associated with platelets agglomerated into rosette-type morphology.[13]

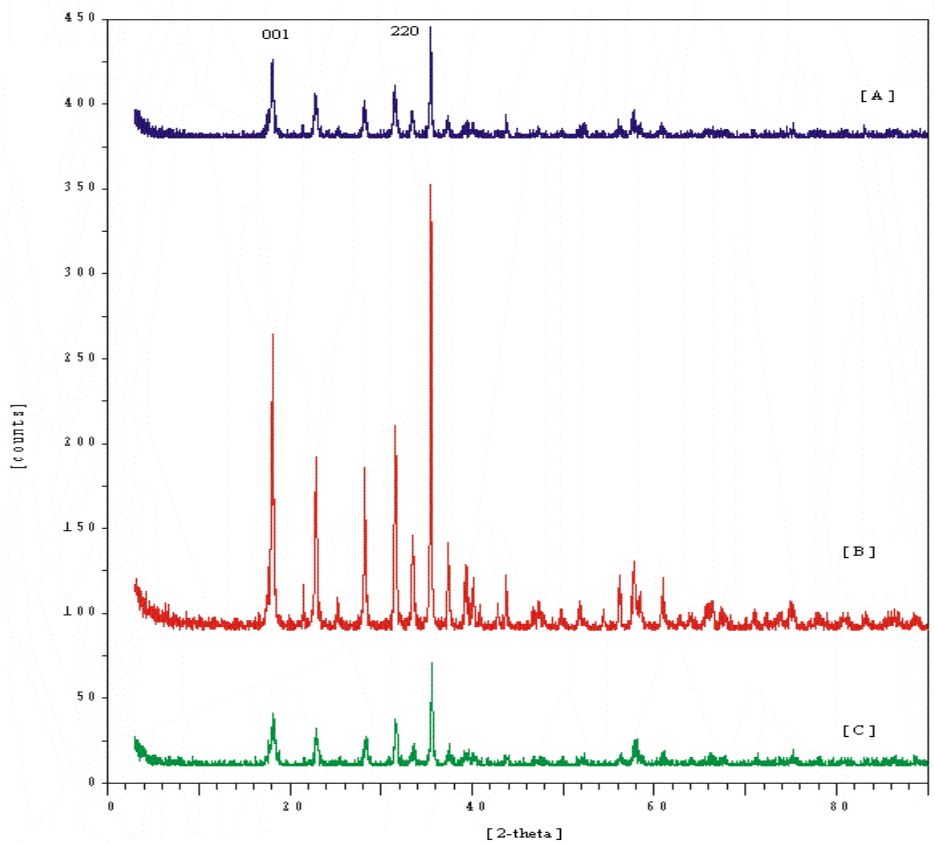

Fig.4.7: XRD patterns of the Ru-VPO precursors for the 0.1% Ru [A], 0.3% Ru [B], and 1.0% Ru [C] VPO catalysts

4.1.3.3 X-ray diffractogram of the Fe- and Ru-promoted $(VO)_2P_2O_7$

Fig.4.9 and Fig.4.10 illustrate the x-ray diffractograms for the un-promoted, iron-promoted and the ruthenium-promoted VPO catalysts after catalysis. All the catalyst samples are crystalline in nature relative to the samples activated under nitrogen for 6 hours at 450^{o}C, which displayed the characteristic of a poorly crystalline $(VO)_2P_2O_7$, and these thus crystallized with time in the reactant mixture in agreement with the results obtained by Hutchings *et al.*[14]

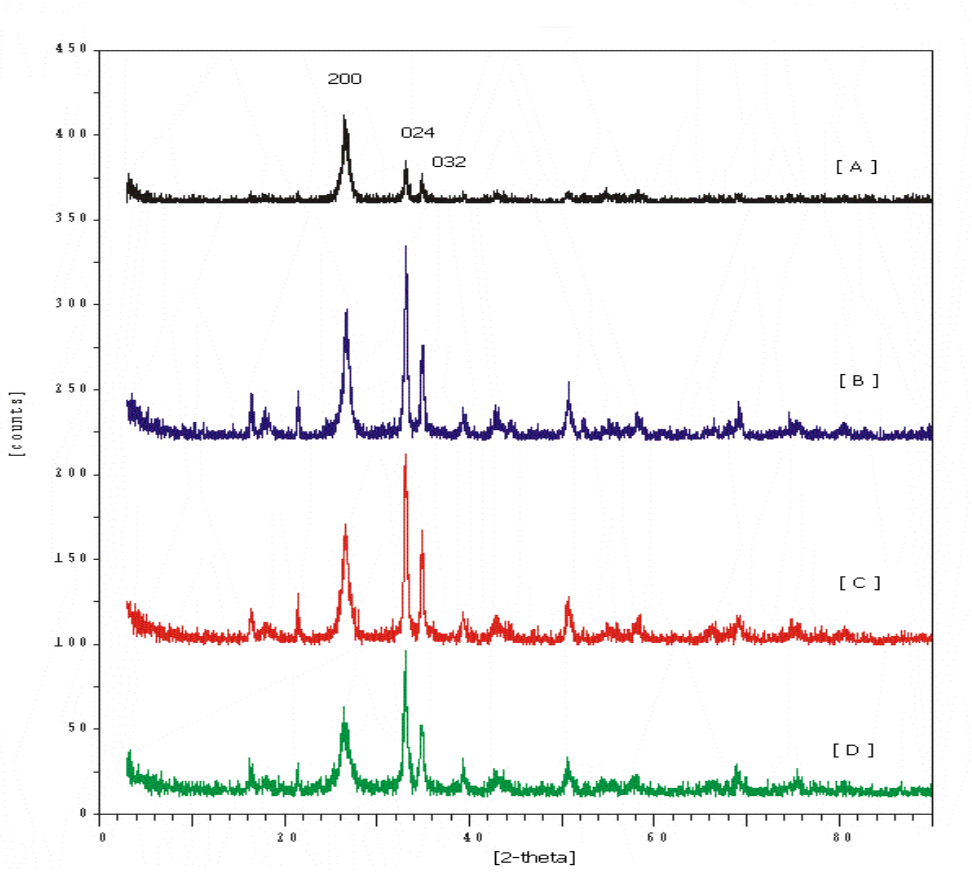

Fig.4.8: XRD patterns of the used VPO and Fe-VPO catalysts: VPO[A], 0.1% Fe- [B], and 0.3% Fe- [C] and 1% Fe- [D] VPO catalysts

Moreover the un-promoted VPO catalyst preferentially exposes the interlayer (200) reflection relative to the in-plane (024) reflection; this observation suggests that the crystals in the vanadyl pyrophosphate are stacked along the [100] direction.[15] The opposite trend is observed for the promoted catalysts which preferentially expose the in-plane (024) reflection relative to the interlayer (200) reflection, thus suggesting that the morphology of the catalyst is modified with promoter incorporation. Furthermore the concept of topotactic transformation from the precursor phase to the active pyrophosphate as reported by Bordes *et al.*[16] is well illustrated here. This is based on the observed broadening of the interlayer spacing reflections in both the $VOHPO_4 \cdot 0.5H_20$ ((001) vs. the in-plane 130 reflection) and $(VO)_2P_2O_7$ ((200) vs. the in-plane (024) reflection.[16]

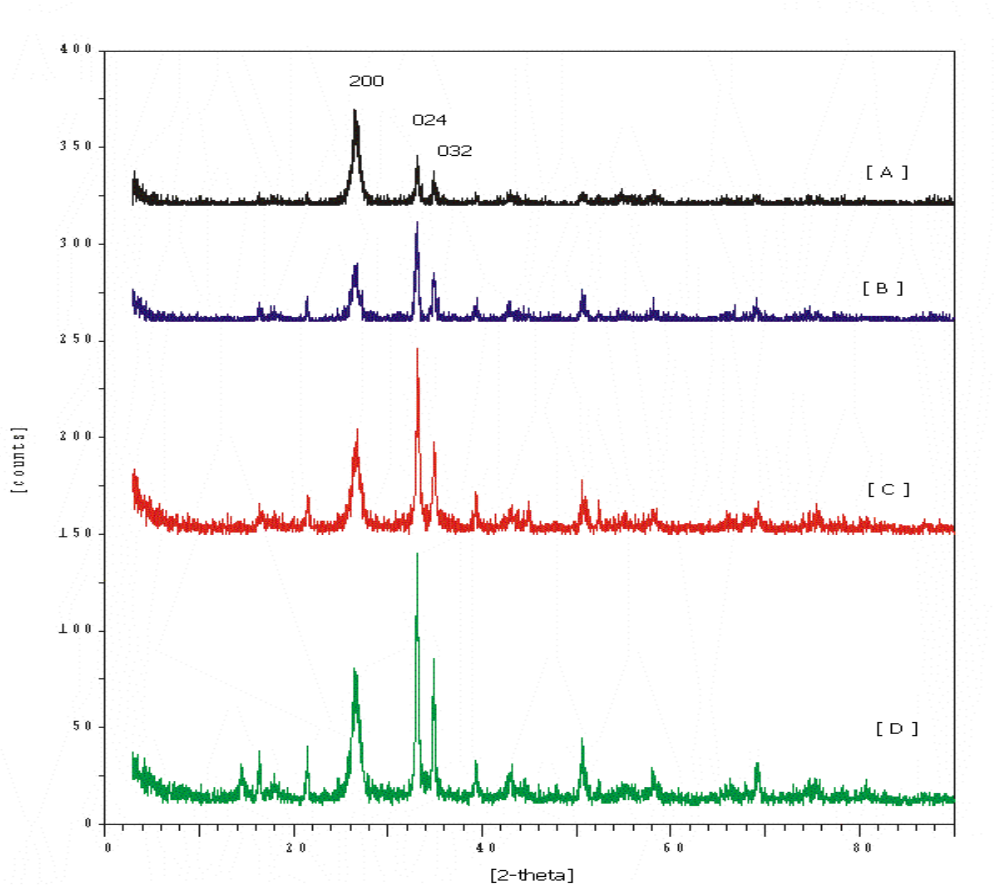

Fig.4.9: XRD patterns of the used VPO and Ru-VPO catalysts: VPO[A], 0.1% Ru- [B], and 0.3% Ru- [C] and 1% Ru- [D] VPO catalysts

4.1.4 BET surface area

Comparison of the surface areas in Table.4.3 of the promoted catalysts with an un-promoted precursor catalyst indicates a slight increase in the surface area with the incorporation of the metal salts. This effect is more pronounced in the ruthenium promoted catalysts. Following catalytic testing under *n*-butane-air mixture, the surface areas are further increased for all the catalysts studied. However, a correlation between the surface area and the promoter loading was not observed. This increase in surface area after catalysis is due to the catalyst being conditioned under the reaction mixture in the reactor. This aid to remove the V(V) impurity phases and hence increased the surface area. The same trend was not observed for the 1%-Ru-promoted catalysts and this can be explained by the oxidizing property of the metal with the given loading, such that the impurity phases cannot be removed at the same rate as for the other catalysts.

Table.4.3: BET-surface area analysis of the VPO catalysts

CATALYST NAME	PRECURSOR ($m^2.g^{-1}$)	USED ($m^2.g^{-1}$)
Un-promoted VPO	10	17
0.1%Fe-promoted VPO	16	22
0.3%Fe-promoted VPO	11	21
1%Fe-promoted VPO	10	27
0.1%Ru-promoted VPO	16	29
0.3%Ru-promoted VPO	10	23
1%Ru-promoted VPO	27	25

4.1.5 Redox titrations: Determination of the average vanadium oxidation state (AV)

Redox titrations were performed on the VPO samples to determine the average oxidation state of vanadium in the samples. From the data obtained in Table.4.4 the average oxidation state lies close to 4.00 for both the un-promoted and the promoted catalysts.

Table.4.4: Average oxidation states of the precursor and the used catalysts

CATALYST NAME	PRECURSOR	USED
Un-promoted VPO	4.04	4.09
0.1%Fe-promoted VPO	4.00	4.03
0.3%Fe-promoted VPO	4.08	4.05
1%Fe-promoted VPO	4.06	4.05
0.1%Ru-promoted VPO	4.12	4.08
0.3%Ru-promoted VPO	4.09	4.12
1%Ru-promoted VPO	4.08	4.10

The data shown in Table.4.4 correlates well with the information from the x-ray diffraction patterns in Figs.4.6 to 4.10 which displayed no traces of V^{5+} species, e.g. $VOPO_4$. Furthermore, the data supports the

results obtained from the ICP-OES in Table.4.1 and 4.2. Literature has reported the necessity for a slight excess of phosphate (P/V=1.05) to maintain the right compromise between the reducibility and the oxidizability of the catalysts, thereby stabilizing the V^{4+} phases relative to V^{5+} phases.[8]

4.1.6 Energy dispersive x-ray Spectroscopy (EDS)

To confirm the results obtained from ICP-OES, energy dispersive spectroscopy was utilized. This technique provides information about the elemental ratio at the catalyst surface. The difference between the results of this analysis and ICP-OES is low indicating that most of the phosphorus is at the surface. This provides evidence of surface phosphorus enrichment in the catalyst for both the un-promoted and the promoted catalysts as has been observed for alkali-promoted catalysts.[17] Furthermore, the lower P/V ratio observed in the energy dispersive x-ray spectroscopy was also expected since EDS is a surface technique, penetrating a few microns of the catalyst surface.

Table.4.5: P/V elemental molar ratios of the VPO catalysts from EDS

CATALYST NAME	PRECURSOR	USED
Un-promoted VPO	0.95	0.97
0.1%Fe-promoted VPO	0.92	0.95
0.3%Fe-promoted VPO	0.98	0.92
1%Fe-promoted VPO	1.00	0.91
0.1%Ru-promoted VPO	0.92	0.96
0.3%Ru-promoted VPO	0.96	1.02
1%Ru-promoted VPO	0.92	0.94

4.1.7 Scanning electron microscopy (SEM)

4.1.7.1 Scanning electron microscopy of the un-promoted VPO catalyst

The scanning electron microscope image of the un-promoted VPO after catalysis in Fig.4.11 shows the characteristic stacked platelet morphology. This data corroborates the x-ray diffractograms obtained in Fig.4.6, where a dominant (001) reflection obtained is associated with a VPO precursor having a stacked platelet morphology.

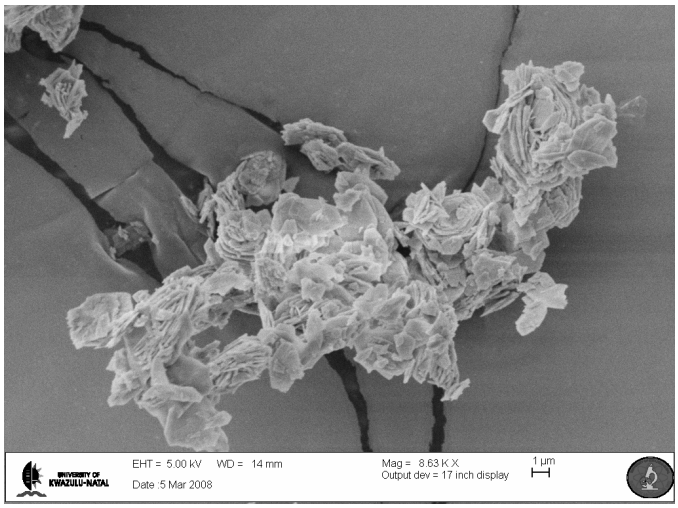

Fig.4.10: Scanning electron micrographs of an un-promoted VPO catalyst

4.1.7.2 Scanning electron microscope of the Fe-promoted VPO catalyst

Promoting the catalysts with iron modifies the morphology of the catalysts from stacked platelet to agglomerated rosettes, Fig.4.12. The x-ray patterns of the promoted catalysts also had a stronger (220) reflection corresponding to a characteristic agglomerated rosette-type morphology.

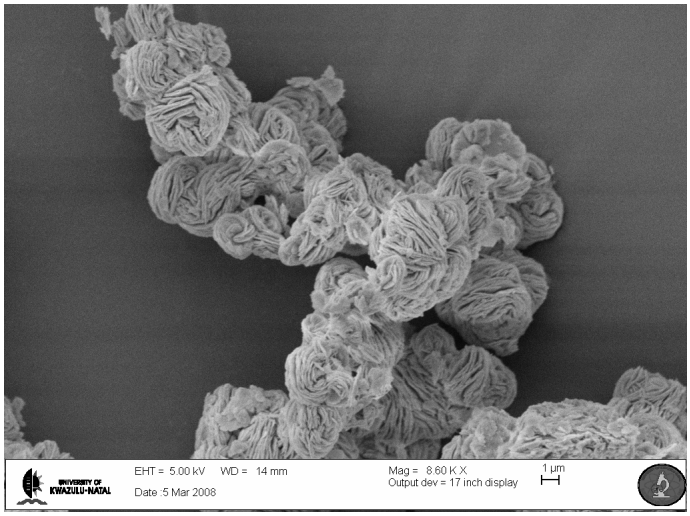

Fig.4.11: Scanning electron micrographs of the Fe-promoted VPO catalysts

4.1.7.3 Scanning electron microscope of the Ru-promoted VPO catalyst

The inclusion of ruthenium also modifies the catalyst morphology to agglomerated rosettes as was expected from the XRD patterns. This indicates that the inclusion of these metal-salts functions to modify the morphology of the catalysts from a stacked platelet to agglomerated rosettes morphology.

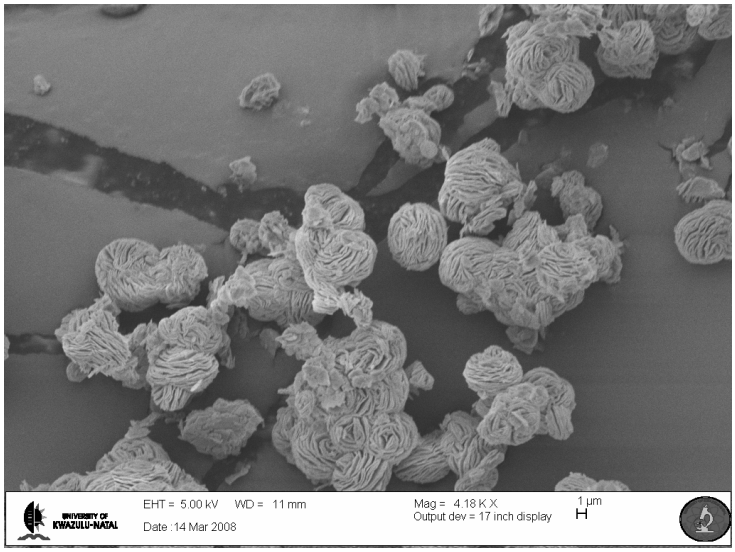

Fig.4.12: Scanning electron micrographs of the Ru-promoted VPO catalysts

4.1.8 Temperature programmed reduction (TPR) profiles of the VPO catalysts

The TPR profile of the studied catalysts is given in Fig.4.14. In this profile, the un-promoted VPO shows the maximum reduction peak at a temperature of 840^{o}C. This peak shifted to a lower reduction temperature of 780^{o}C in the Ru-promoted VPO catalysts, but remains in the same position for the Fe-promoted VPO catalysts. The un-promoted VPO and the Fe-promoted VPO catalysts shows one peak corresponding to a characteristic $V^{4+} \rightarrow V^{3+}$ reduction, whereas the Ru-promoted analogue shows a shoulder at a temperature of 540^{o}C which can be ascribed to $V^{5+} \rightarrow V^{4+}$ reduction. Furthermore, hydrogen consumption by the Ru-promoted VPO catalyst was the highest compared to the un-promoted and the Fe-promoted catalysts. This data show that the inclusion of a ruthenium cation in the VPO formulations leads to a modification of the vanadium oxidation state. However, this effect is not as pronounced (Fig.4.14). Furthermore this data corroborates the XRD patterns (absence of $VOPO_4$ phases). Therefore, this metal cation may function to modify the V^{4+}/V^{5+} ratio leading to a slight increase in the average oxidation state of vanadium, as was indeed observed (Table.4.4).

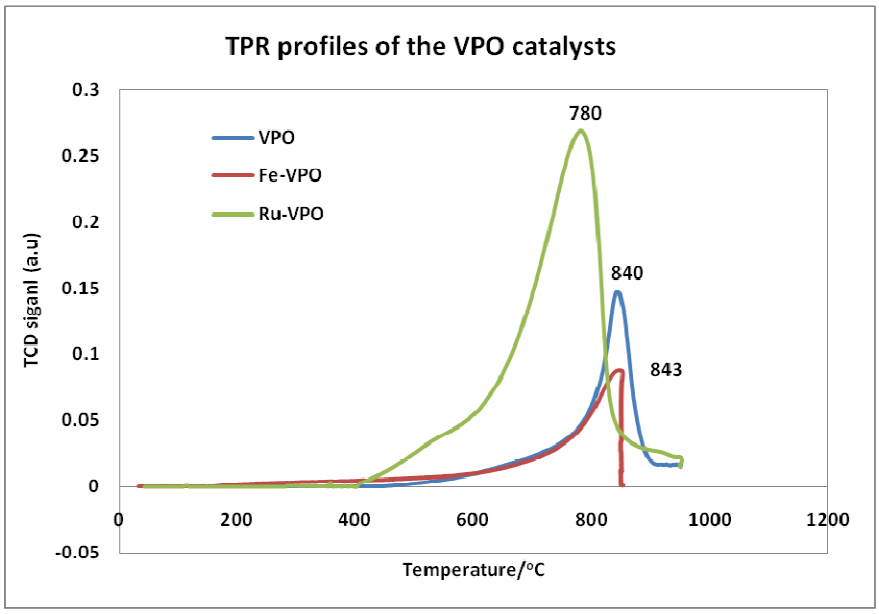

Fig.4.13: TPR profiles of the used un-promoted and promoted-VPO catalysts (catalysts compared at 0.1% loading)

4.1.9 Solid state ^{31}PNMR spectra of the VPO catalysts

The ^{31}P NMR spectra of the catalysts are given in appendix1. The ^{31}P NMR spectra of the un-promoted VPO catalyst shows signals at (i) 0 ppm indicative of P atoms connected to V^{5+} in the orthophosphate phases and (ii) between 200 to 400 ppm range indicative of P atoms in the vicinity of V^{4+}- V^{5+} dimers. These dimers have been reported to exist in the poorly crystalline $(VO)_2P_2O_7$ matrix, however, ^{31}P NMR spectra of the un-promoted catalyst in appendix 1 shows a crystalline nature. On the contrary to what is observed in the un-promoted catalyst, the ^{31}P NMR spectra of the Fe-VPO and the Ru-VPO catalysts shows signals in the regions mainly close to 0 ppm. This gives an indication of the presence of $V^{5+}OPO_4$ in these catalysts. This data corroborates the redox titration results; where by the average oxidation states of vanadium in the samples is higher than an oxidation state of 4+. Furthermore, in the XRD patterns of the catalysts, only the reflections attributed to $(VO)_2P_2O_7$ were observed. The absence of the $VOPO_4$ phases in the XRD patterns could be due to their amorphous nature such that they were not detected since XRD is a technique for the characterization of crystalline surfaces. An improved yield observed when 0.1%Fe-VPO was used can be explained in terms of two models proposed by (i) Volta *et al.*[18] and (ii) Trifirò *et al.*[19] In the first model, Volta *et al.*[18] believe that the active sites consist of a mixture of a well crystallized $(V^{4+}O)_2P_2O_7$ and an amorphous $V^{5+}OPO_4$, while in the latter model, Trifirò *et al.*[19] reported

the importance of the presence of a controlled amount of V^{5+} phases as the selective phases in the presence of the active $(VO)_2P_2O_7$.

REFERENCES

1. A. Datta and M. A. Agarwal, *J. Mater. Chem.*, 2002, **12**, 1892.
2. J. W. Johnson, D. C. Johnson, A. J. Jacobson and J. F. Brody, *J. Am. Chem. Soc.*, 1984, **106**, 8123.
3. S. Irusta, A. Boix, B. Perini, C. Caspani and J. Petunchi, *J. Catal.*, 1999, **187**, 298.
4. M. Otake, in *US Patents.,* 4337 173 (to Mitsubishi Chem. Ind), 1982.
5. L. M. Cornaglia, C. Caspani and E. A. Lombardo, *Appl. Catal.*, 1991, **74**, 15.
6. B. K. Hodnett, F. Dason and M. O'Connor, *Appl. Catal.*, 1990, **64**, 161.
7. H. Horowitz, C. M. Blackstone, A. W. Sleight and G. Teufer, *Appl. Catal.*, 1988, **38**, 193.
8. I. Matsuura and M. Yamazaki, eds., In new developments in selective oxidation, Elsevier, Amsterdam, 1990.
9. S. Albonetti, F. Cavani, F.Trifiro, P. Venturoli, G. Calestani, M. Lopez-Granados and J. L. Fierro, *J. Catal.*, 1996, **160**, 52.
10. V. V. Guliants, J. B. Benzinger, S. Sundaresan, I. E. Wachs, J. M. Jehng and J. E. Roberts, *Catal. Today.*, 1996, **28**, 275.
11. S. Sajip, J. K. Bartley, A. Burrows, M. T. Sananes-Shulz, A. Tuel, J. C. Volta, C. J. Kiely and G. J. Hutchings, *New. J. Chem.*, 2001, **25**, 125.
12. M. T. Sananes-Schulz, A. Tuel, G. J. Hutchings and J. C. Volta, *J. Catal.*, 1997, **166**, 388.
13. L. Sartoni, A. Delimitis, J. K. Bartley, A. Burrows, H. Roussel, J. M. Herrmann, J. C. Volta, C. J. Kiely and G. J. Hutchins, *J. Mater. Chem.*, 2006, **16**, 4348.
14. G. J. Hutchings, C. J. Kiely, M. T. Sananes-Shulz, A. Burrows and J. C. Volta, *Catal. Today.*, 1998, **40**, 273.
15. D. Wang, H. K. Kung and M. A. Barteau, *Appl. Catal.* A., 2000, **201**, 203.
16. E. Bordes, *Catal. Today.*, 1987, **1**, 499.
17. V. A. Zazhigalov, J. Haber, J. Stoch, I. V. Bacherikova, G. A. Komashko and A.I. Pyatnitskya, *Appl. Catal.* A., 1996, **134**, 225.
18. G. Bergeret, M. David, J. P. Boyer, C. Volta, G. Hequet, *Catal. Today*., 1987, **1**, 37.
19. G. Centi, F. Trifiro, J. B. Ebner, V. M. Franchetti, *Chem. Rev*., 1988, **88**, 55.

CHAPTER 5

5.1 Results and Discussion

5.1.1 Conversion vs. Temperature

Preliminary investigations to find the optimum reaction temperature were carried out. The catalysts were investigated from a temperature of 250°C to a temperature of 450°C. The selectivities to different products are displayed for the tested catalysts at a constant GHSV of 3051h^{-1} for the un-promoted VPO, the promoted iron and the promoted ruthenium catalysts at 1% metal loading.

VPO: 250-450°C

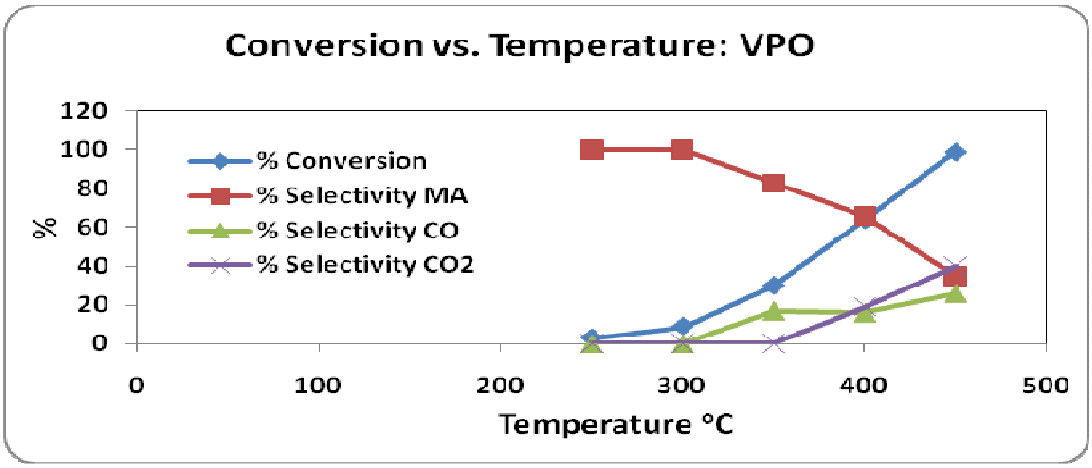

Fig.5.1 Conversion vs. Temperature: VPO

For un-promoted VPO, conversion was found to increase with temperature; a 66 mol% conversion obtained at 400°C increased to 100 mol% conversion at 450°C. The selectivity to maleic anhydride decreases with temperature with a corresponding increase to the carbon oxides which are favored at higher temperatures. An optimum yield towards MA under these conditions was observed at 400°C, corresponding to a yield of 42 mol% at 64 mol% conversion. The selectivity towards carbon oxides is lower than the selectivity to MA for the entire temperature range.

1% Fe-VPO: 250-450°C

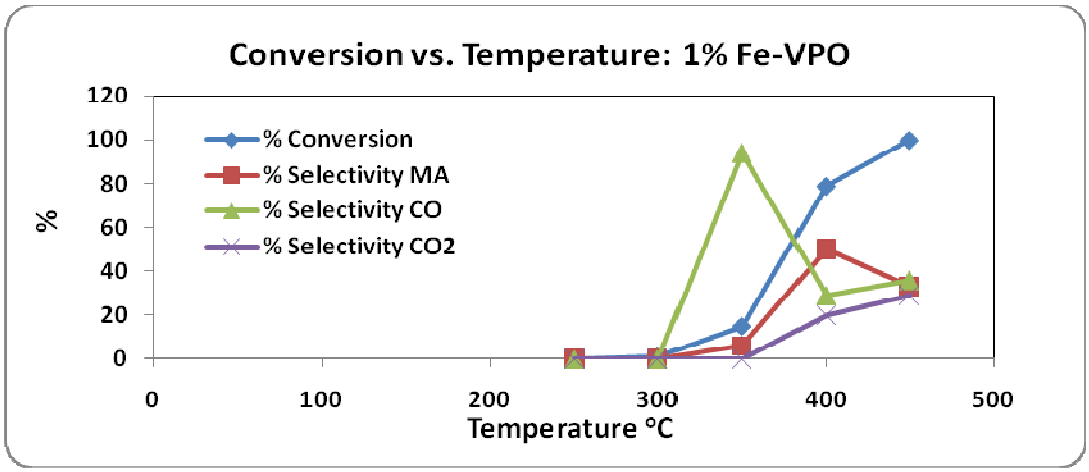

Fig.5.2: Conversion vs. Temperature: 1% Fe-VPO

The 1% iron promoted catalyst shows the same trend as the ruthenium (1%) promoted catalyst. Conversion is further increased from 73 mol% in the 1% Ru-VPO to 79 mol% conversion at 400°C and a GHSV of 3051/h. This increased conversion affected maleic anhydride selectivity, resulting in 50 mol% selectivity at 79 mol% conversion leading to maleic anhydride production of 40mol%. In general these graphs show that ruthenium and iron doped VPO catalysts increases n-butane conversion relative to the unpromoted VPO catalyst while increasing the selectivity of carbon oxides at the expense of maleic anhydride under the given conditions.

1% Ru-VPO: 250-450°C

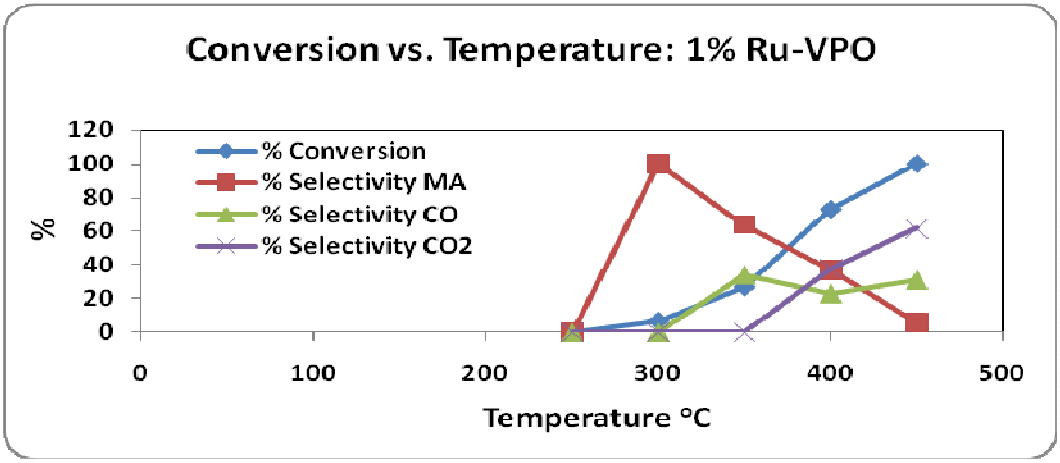

Fig.5.3: Conversion vs. Temperature: 1% Ru-VPO

An improved conversion was encountered for 1% Ru-VPO relative to the un-promoted VPO catalyst. Conversion of n-butane increased from 64 mol% to 73 mol% conversion at the same temperature and the same GHSV of 3051h^{-1}. Maleic anhydride selectivity was drastically affected at a temperature of 450^{o}C, allowing carbon oxides to be the only major products at this temperature. The optimum maleic anhydride yield obtained for 1% ruthenium promoted VPO catalyst was 37 mol% at 400^{o}C.

5.1.2 Product distribution data as a function of n-butane conversion

Following the preliminary catalyst testing over the 250 to 450^{o}C temperature range to determine an optimum temperature for maleic anhydride production, an optimum temperature of 400^{o}C was established. The catalysts were then tested at this temperature (400^{o}C) while varying the gas hourly space velocities (The optimum GHSV's to produce optimum selectivities for a given conversion per catalyst is given in Table.4.6 and 4.8).

5.1.2.1 VPO: Selectivity vs. Conversion (product distribution)

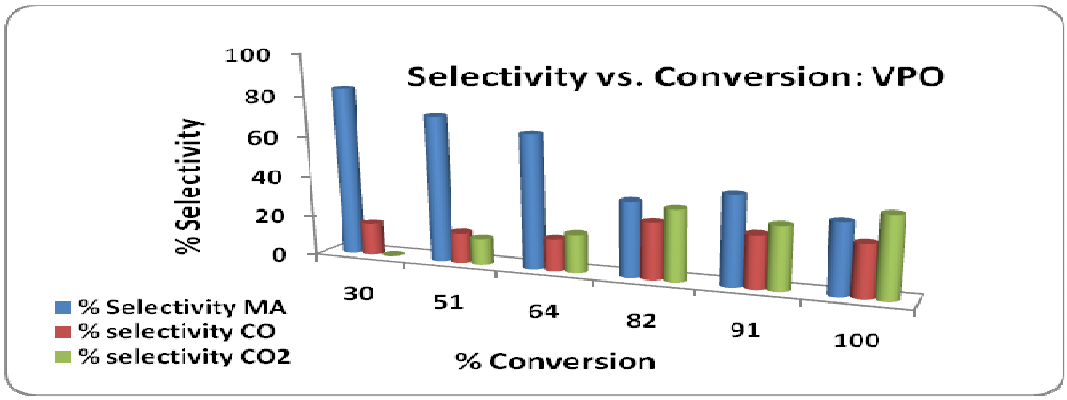

Fig.5.4: Selectivities towards different products as a function of n-butane conversion over an un-promoted VPO catalyst

For the un-promoted catalyst, high selectivity towards carbon oxides is apparent at conversions higher than 80 mol%, while the selectivity towards maleic anhydride is high at lower conversions. An approximate constant selectivity is obtained for all the products at conversions higher than 80 mol%. The above plot indicates that maleic anhydride productivity will be most favored at lower conversions, where the carbon oxide production is limited. Hence maleic anhydride production should be optimal at conversions within the 60 to 70 mol% range.

5.1.2.2 0.1% Fe-VPO: Selectivity vs. Conversion (product distribution)

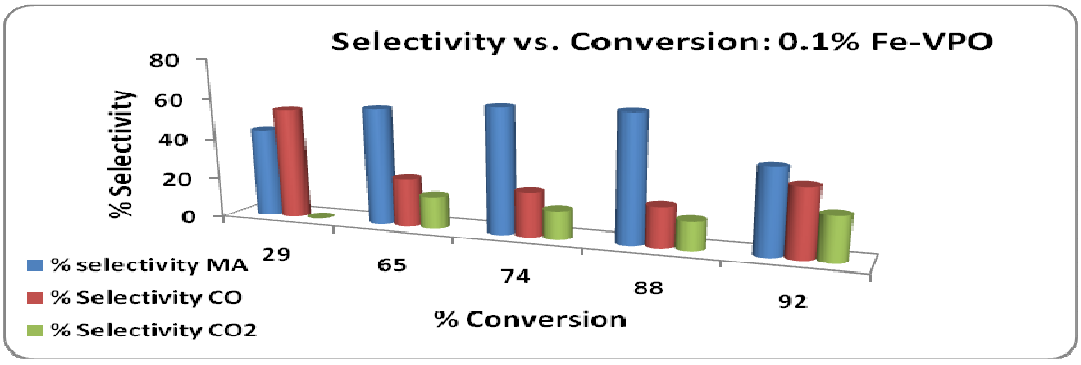

Fig.5.5: Selectivities towards different products as a function of n-butane conversion over 0.1% Fe-VPO catalyst

The 0.1% Fe-VPO catalyst improved the selectivity towards maleic anhydride by suppressing the carbon oxides formation. An average selectivity to carbon oxides of approximately 35 mol% was obtained up to about 88 mol% conversion, giving an average maleic anhydride selectivity of *ca.* 60 mol%. It can be observed from Figure.5.5 that while the selectivity towards carbon oxides stabilizes within the studied conversion range, maleic anhydride selectivity was found to increase within the very same range. In comparison to the ruthenium-promoted and the un-promoted VPO, the 0.1% Fe-VPO led to an improved catalytic behavior by improving the selectivity towards maleic anhydride and giving a 10% yield improvement relative to the reference catalyst.

5.1.2.3 0.3% Fe-VPO: Selectivity vs. Conversion (product distribution)

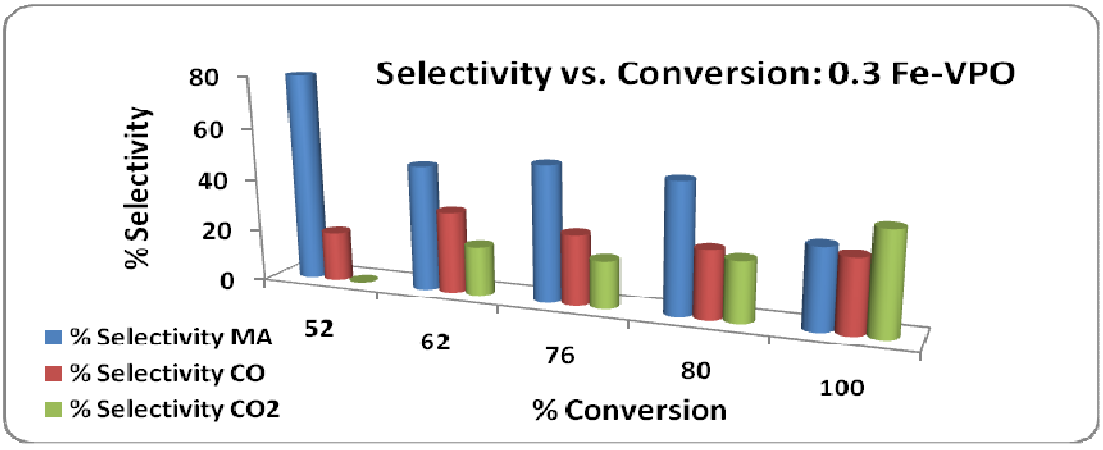

Fig.5.6: Selectivities towards different products as a function of n-butane conversion over 0.3% Fe-VPO catalyst

The selectivity towards maleic anhydride is favored by the 0.3% Fe-VPO up to a conversion of 80 mol%, thereafter carbon dioxide becomes favored. An improved yield is visible from 70 to 80 mol% conversion. In comparison to the results obtained for the un-promoted catalyst, the 0.3% Fe-VPO improves the selectivity at higher conversions. An optimum yield was established at conversions within the range 70 to 80 mol%.

5.1.2.4 1% Fe-VPO: Selectivity vs. Conversion (product distribution)

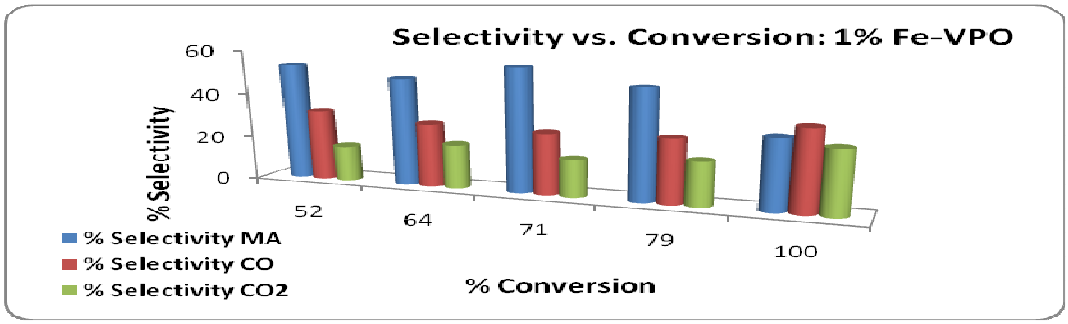

Fig.5.7: Selectivities towards different products as a function of n-butane conversion over 1.0% Fe-VPO catalyst

The 1% Fe-VPO catalyst displays similar behavior to the 0.3% Fe-VPO; however, for the former catalyst maleic anhydride selectivity was lower than the un-promoted catalyst. The 1% Fe-VPO catalyst also displays improved maleic anhydride selectivity within the 70 to 80 mol% range. Therefore it is seems that the iron promoter functions to promote the VPO catalyst at higher conversions and improves the selectivity to maleic anhydride at these conversions.

5.1.2.5 0.1% Ru-VPO: Selectivity vs. Conversion (product distribution)

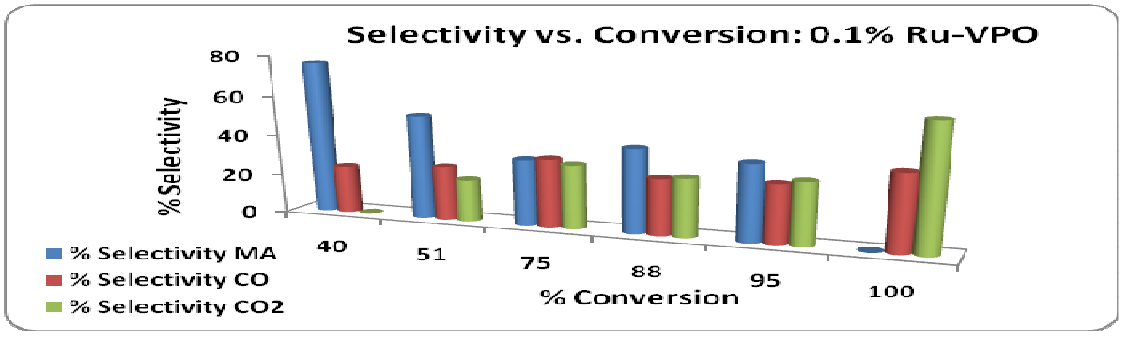

Fig.5.8: Selectivities towards different products as a function of n-butane conversion over 0.1% Ru-VPO catalyst

The selectivity towards maleic anhydride decreased for the 0.1% Ru-VPO relative to the reference un-promoted catalyst. Total conversion resulted in total combustion, since no other products could be observed at 100 mol% conversion for the 0.1% Ru-VPO. Selectivities towards carbon oxides increased to almost 50% at lower conversions (40 to 60 mol%) when related to the reference catalyst. This catalyst displays considerable oxidizing properties as can be observed from the high carbon oxides formation even at lower conversions. However, no other phases except $(VO)_2P_2O_7$ were detected from the x-ray diffractograms, but the average vanadium oxidation state in Table.4.4 indicated a slightly higher oxidation state relative to the other catalysts under study.

5.1.2.6 0.3% Ru-VPO: Selectivity vs. Conversion (product distribution)

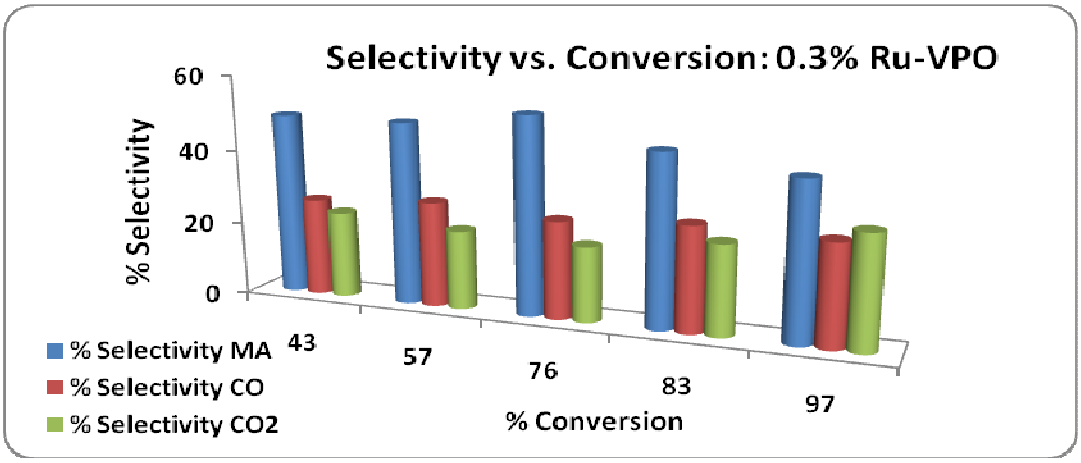

Fig.5.9: Selectivities towards different products as a function of n-butane conversion over 0.3% Ru-VPO catalyst

An approximately constant selectivity towards all the products is observed for 0.3% Ru-VPO over the range of conversions studied. An average maleic anhydride selectivity of *ca.* 48 mol% was obtained within this range of conversion. Another observation that is apparent from this data is the approximate equal selectivities to the carbon oxides, even at high conversions i.e. carbon dioxide was not favored at higher conversions (with the exception of 97 mol%) in contradiction to what was encountered for the un-promoted VPO catalyst.

5.1.2.7 1% Ru-VPO: Selectivity vs. Conversion (product distribution)

For the 1% Ru-VPO catalyst, a small decrease is observed in maleic anhydride selectivity and this decrease is accompanied by a constant increase in the formation of the carbon oxides within the range 40 to 70 mol% conversion relative the un-promoted reference catalyst.

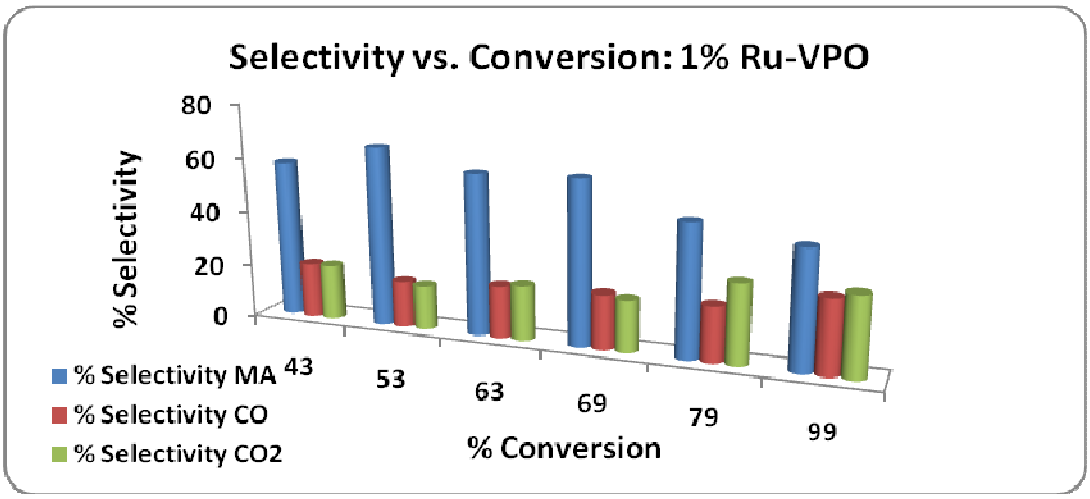

Fig.5.10: Selectivities towards different products as a function of n-butane conversion over 1.0% Ru-VPO catalyst

At conversions higher than 80 mol%, the selectivity to carbon oxides increases leading to ≥ 50% contribution. This, however, does not affect maleic anhydride selectivity, since relative to the reference catalyst, the selectivity improved at 80 mol% and 100 mol% conversions, improving the yield at those conversions. The three ruthenium-promoted catalysts gave similar results (yield: to the un-promoted VPO and promotion proved to be beneficial only at conversions higher than 70 mol%). Hence one can deduce that the ruthenium-promoted catalysts are selective at higher conversions.

5.2 Selectivity vs. Conversion

5.2.1 Comparison of the catalytic behavior for the un-promoted VPO and the Fe-VPO catalysts at constant temperature of 400°C.

From the data obtained in section 4.2, the performance of the different catalysts could thus be established and compared graphically, at a constant temperature of 400°C.

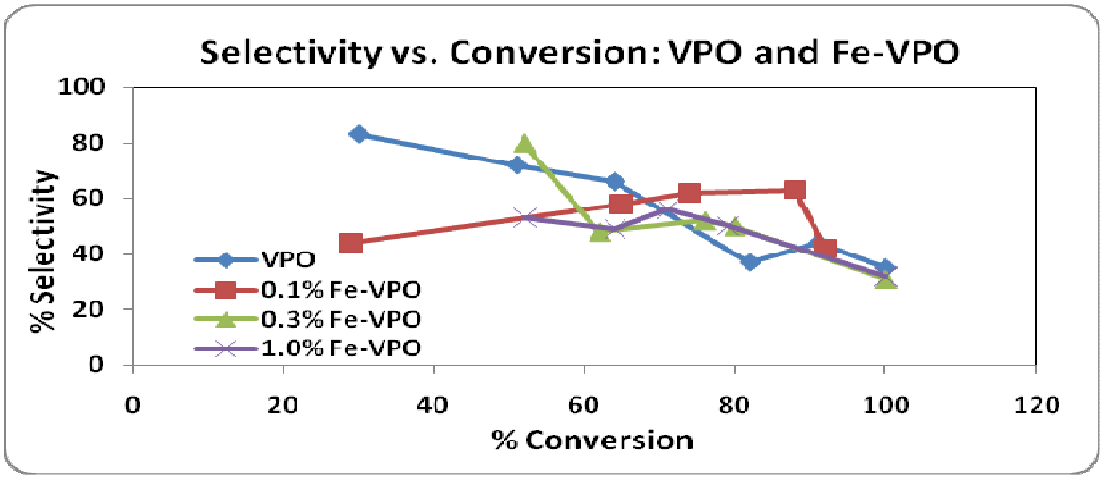

Fig.5.11: Selectivity vs. Conversion: VPO and Fe-VPO

In the iron promoted series, improved maleic anhydride selectivity relative to the un-promoted VPO was observed at conversions greater than 70 mol%. These results show a decrease in maleic anhydride selectivity with increasing conversion for the 0.3% and 1% iron promoted catalysts. However, the 0.1% iron loaded catalyst shows the opposite trend, the selectivity was found to increase with conversion. An optimum yield of 55% was obtained at 88 mol% conversion. The optimum percentage yield obtained for the different catalysts are given in Table.5.1 for direct comparative purposes.

Table.5.1: The optimum percentage yield (MA) for the iron promoted and the un-promoted VPO catalyst at 400°C.

CATALYST NAME	**% CONVERSION**	**GHSV (H^{-1})**	**MA % YIELD**
VPO (Reference)	***64***	***3051***	***42***
0.1% Fe-VPO	74	2573	**46**
0.1% Fe-VPO	88	1450	**55**
0.3% Fe-VPO	52	6360	42
0.3% Fe-VPO	80	3579	40
1.0% Fe-VPO	71	2833	40
1.0% Fe-VPO	79	3029	40

Table.5.2: The specific activity and specific selectivity data for Fe-VPO catalysts at 50% and 80% conversion (MA %Yield given in brackets)

CATALYST NAME	**SPECIFIC ACTIVITY 50% (X)**	**SPECIFIC SELECTIVITY 50% (X)**	**SPECIFIC ACTIVITY 80% (X)**	**SPECIFIC SELECTIVITY 80% (X)**
VPO(Reference)	***3.0***	***4.2(37)***	***4.8***	***2.2(37)***
0.1% Fe-VPO	2.3	2.4(**27**)	3.7	2.7(**49**)
0.3% Fe-VPO	2.5	3.8(**42**)	4.0	2.2(**38**)
1.0% Fe-VPO	2.0	2.0(**28**)	3.0	1.7(**38**)

The specific activity and the specific selectivity for the catalysts were calculated based on the surface areas of the catalysts and they are given in Tables.5.2 and 5.3. The specific activity and specific selectivity of the iron modified samples did not improve at 50% conversion, though the surface area has increased in these samples. At 80% conversion, the specific selectivity increased in the 0.1% and the 0.3% Fe-VPO catalysts, giving an improved yield of 49 and 38% respectively, relative to the un-promoted VPO (37). This shows that, the presence of iron as a modifier increases the surface area, and the beneficial effect is observed at higher conversions giving an improved maleic anhydride production relative to the un-promoted VPO catalyst.

Table.5.3: The specific activity and specific selectivity data for Ru-VPO catalysts at 50% and 80% conversion (MA %Yield given in brackets)

CATALYST NAME	**SPECIFIC ACTIVITY 50% (X)**	**SPECIFIC SELECTIVITY 50% (X)**	**SPECIFIC ACTIVITY 80% (X)**	**SPECIFIC SELECTIVITY 80% (X)**
VPO(Reference)	***3.0***	***4.2(37)***	***4.8***	***2.2(37)***
0.1% Ru-VPO	1.8	1.8(27)	2.8	1.3(30)
0.3% Ru-VPO	2.2	2.1(35)	3.6	2.0(38)
1.0% Ru-VPO	2.1	2.5(25)	3.2	1.8(38)

The results obtained for the Ru-VPO catalysts in Table.4.8, indicated that both the specific activity and the specific selectivity of the catalysts were affected at 50% and 80% conversions. The surface area of these catalysts increased relative to the un-promoted VPO (Table.4.3). This finding illustrates that the presence of ruthenium in these samples was to increase the surface area of the catalysts; however, an improved performance did not follow. From the results in Table.5.2 and 5.3, it shows that the inclusion of iron in the VPO formulations improves the performance of the catalyst at higher conversions relative to the un-promoted VPO (see Table.5.1), whereas a lower yield was obtained for the ruthenium promoted catalysts for all the range of conversions studied. Moreover the improved yield obtained for the iron promoted catalyst was observed at relatively higher conversions.

5.2.2 Comparison of the catalytic behavior for the un-promoted VPO and the Ru-VPO catalyst at constant temperature

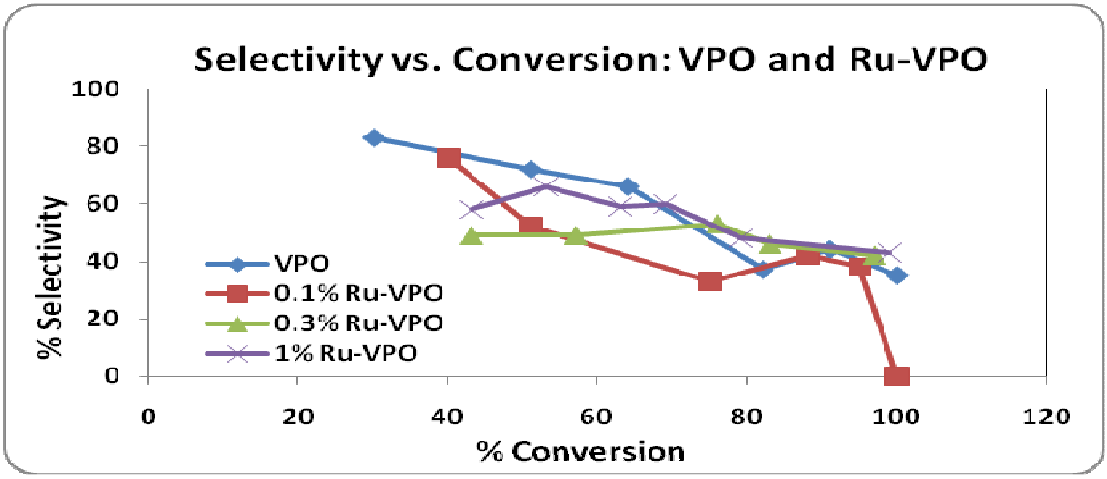

Fig.5.12: Selectivity vs. Conversion: VPO and Ru-VPO

The above plot (Fig.5.12) represents the effect of ruthenium loading on the VPO catalysts. For all the catalysts displayed in Figure 5.12, the selectivity to maleic anhydride was found to decrease with conversion. A negligibly improved selectivity is observed with ruthenium loading from 0.1 to 1% Ru-VPO at 80 mol% conversion relative to 64 mol% conversion in the un-promoted VPO. However, the ruthenium promoted catalysts display an overall lower yield towards MA relative to the un-promoted VPO catalysts.

At conversions above 70 mol%, all the ruthenium promoted catalysts gave an overall MA yield within the range 37 to 42 mol%, hence no promotional effect can be associated with the ruthenium promoted catalysts, even though the surface area has improved. The optimum percentage yield obtained for the different ruthenium-promoted catalysts are given in Table.5.2 for direct comparative purposes.

Table.5.4: The optimum percentage yield (MA) for the ruthenium promoted and the un-promoted VPO catalyst at 400°C.

CATALYST NAME	% CONVERSION	GHSV (H^{-1})	% YIELD
VPO (Reference)	***64***	***3051***	***42***
0.1% Ru-VPO	88	4918	37
0.3% Ru-VPO	76	3680	40
1.0% Ru-VPO	69	4762	41

5.3 Comparison of the metal promoted VPO catalysts at the same loading at 400°C

5.3.1 Selectivity vs. Conversion for the 0.1% promoted VPO catalysts

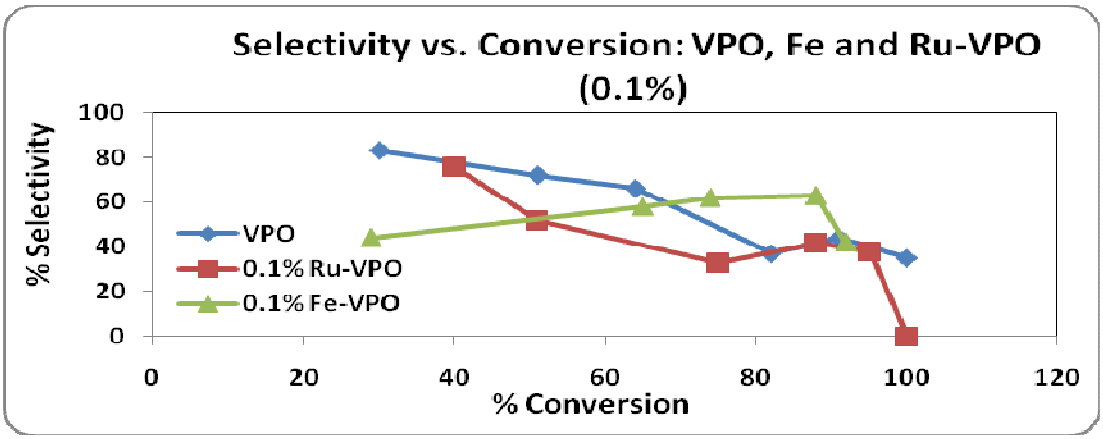

Fig.5.13: Selectivity vs. Conversion: Fe and Ru-VPO at 0.1% loading

Ruthenium and iron metal promoters were studied and compared at 0.1% metal loading. From the results obtained, ruthenium at 0.1% loading did not improve the performance of the catalyst relative to the un-promoted catalyst. At the same loading, an iron promoter improved the catalytic performance by increasing the yield of maleic anhydride at high conversions.

5.3.2 Selectivity vs. Conversion for the 0.3% promoted VPO catalysts

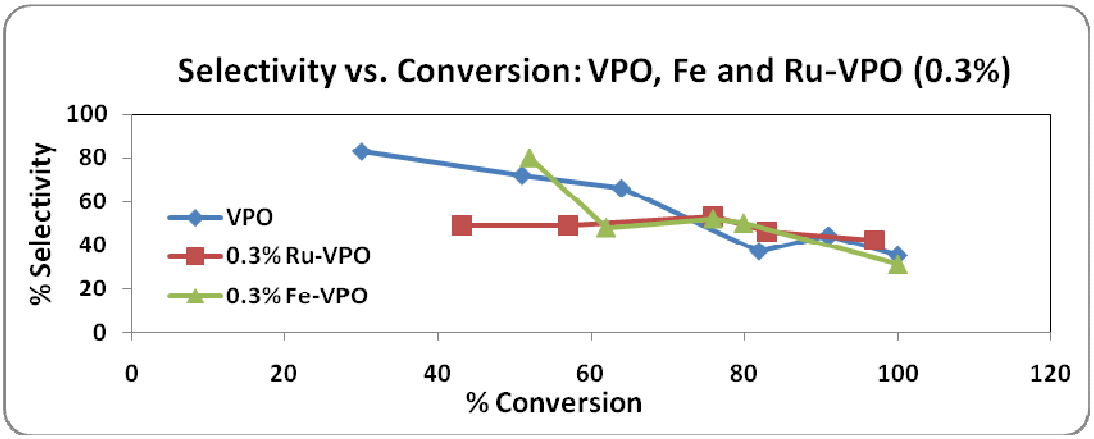

Fig.5.14: Selectivity vs. Conversion: Fe and Ru-VPO at 0.3% loading

The improved catalytic performance resulting from the 0.3% ruthenium and iron promoted catalysts relative to the un-promoted catalyst is almost negligible. The observed selectivity towards maleic anhydride is lower for these catalysts at conversions lower than 70 mol%. There is, however, a slight improved selectivity at 80 mol% conversion relative to the un-promoted VPO, thus increasing the yield of maleic anhydride.

5.3.3 Selectivity vs. Conversion for the 1% promoted VPO catalysts

The same trend as above is furthermore illustrated in the 1% ruthenium and iron promoted catalysts (Fig.5.15)

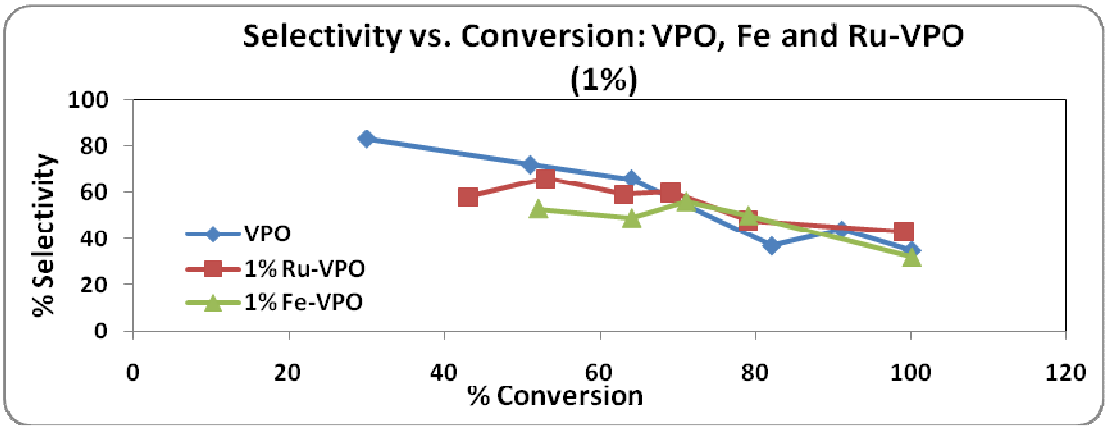

Fig.5.15: Selectivity vs. Conversion: Fe and Ru-VPO at 1% loading

An un-promoted catalyst shows a reasonable selectivity to maleic anhydride at lower conversions, reaching an optimum yield at 64 mol% conversion, whereas the promoted catalysts displays similar characteristics at higher conversions. However, the optimum yields obtained for these catalysts at higher conversions amounts to similar yields to those obtained for the un-promoted catalyst at lower conversions i.e. 64 mol% conversion relative to 70, 80 and 90 mol% conversion. Therefore, only a 0.1%-Fe VPO catalyst increased maleic anhydride yield relative to the unpromoted VPO.

5.3.4 MA Selectivity plots for the studied VPO catalysts at constant conversions of 50% and 80%

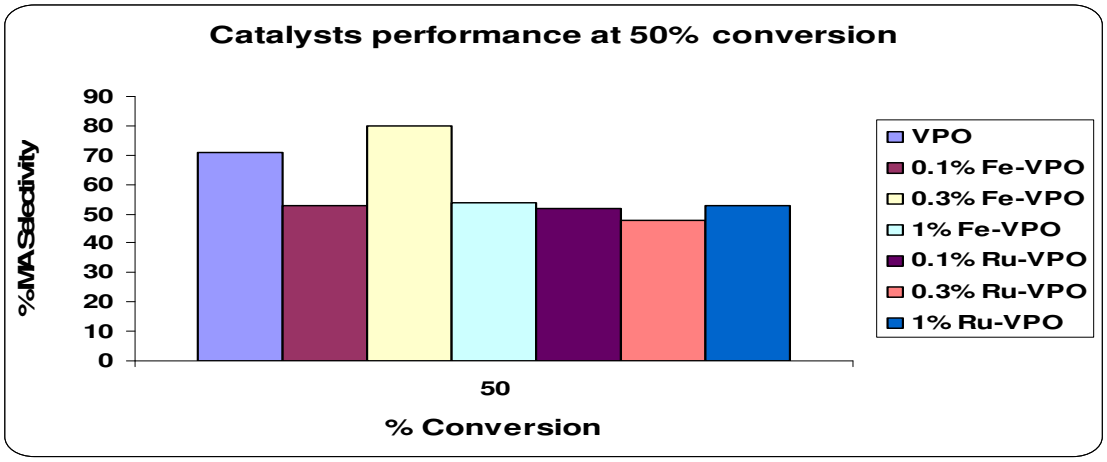

Fig.5.16: The performance of catalysts at constant conversion (50%)

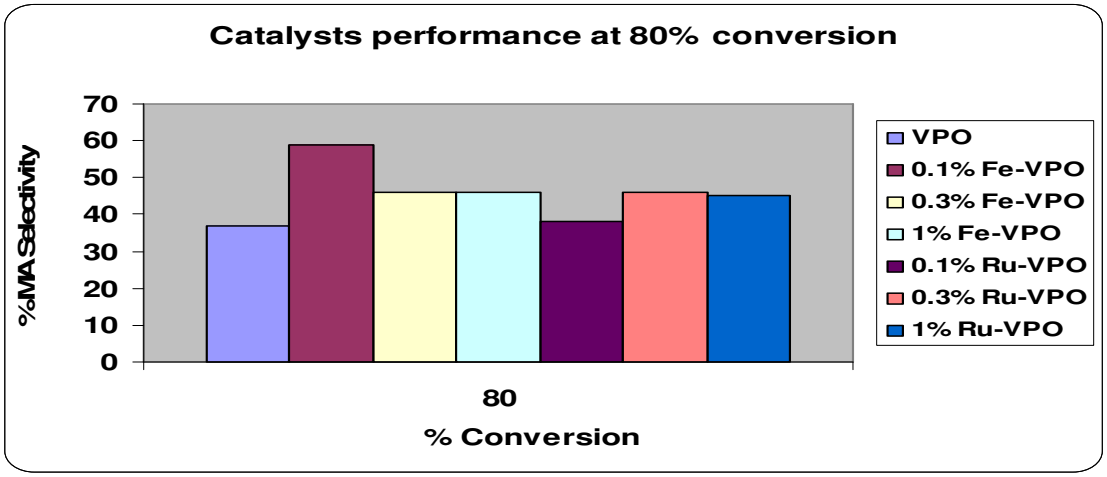

Fig.5.17: The performance of catalysts at constant conversion (80%)

The catalysts under study were then compared at the same conversions of 50% and 80% to determine their catalytic performances under similar conditions. It can be seen in Figure.5.16 that at a lower conversion of 50%, an un-promoted VPO catalyst, displays a relatively higher selectivity with respect to the promoted analogues. However, the opposite trend is observed as the conversion is further increased. The selectivity toward maleic anhydride diminishes with conversion for the un-promoted catalyst, as a result of the formation of carbon oxides as the conversion is increased. On the contrary, the promoted catalysts, shows an improved selectivity towards maleic anhydride as the conversion is increased (Fig.5.17). Moreover, highly improved maleic anhydride selectivity is observed in the 0.1% iron promoted catalyst. The selectivity for this catalyst, increase further to ca. 90% conversion. At conversions greater than 90%, the selectivity decreases as carbon oxides predominates in the product stream.

The improved catalytic performance of the 0.1%Fe-VPO can be explained in terms of the model described by Trifirò *et al.*[19] which states the importance of the presence of a controlled amount of V^{5+} phases as the selective phases in the presence of the active $(VO)_2P_2O_7$. The XRD patterns of this catalyst indicated the presence of a crystalline $(VO)_2P_2O_7$ whereas the ^{31}PNMR spectra indicated signals at a region close to 0 ppm, corresponding to P atoms in the vicinity of vanadium in a +5 oxidation state. Since the presence of V^{5+} phases were not observed in the XRD patterns and in the TPR profiles of the 0.1% Fe-VPO catalyst, we can deduce that this catalyst possess a crystalline $(VO)_2P_2O_7$ as well as a limited and controlled amount of V^{5+} species. Moreover, this data corroborates an average oxidation state greater than four obtained from redox titrations. Furthermore, the surface area increased with the inclusion of the promoting element and the morphology was modified from platelet morphology to agglomerated rosettes. This modification of the morphology correlates well with the XRD patterns, which indicated a modification in the [001] / [220] relative intensity (Fig.4.6), whereby the former indicates a stacked platelet morphology and the latter is characteristic of agglomerated rossettes.

CHAPTER 6
CONCLUSIONS

The iron-promoted VPO catalysts: An improved *n*-butane conversion was obtained for the promoted VPO catalysts relative to the un-promoted VPO catalyst at an optimum temperature of 400^{o}C. This improved conversion could be explained by an improved specific activity observed in the iron-promoted catalysts (Table.5.2). A higher value for the specific activity obtained in the iron-promoted VPO catalysts could be a result of the incorporation of the cation in the $(VO)_2P_2O_7$ lattice replacing one of the V^{4+} ions such that the next vanadium ion withdraws more electrons from the neighboring oxygen atoms and increasing the electron density on the V^{4+} ions relative to the oxygen atom. The resulting V=O bond weakens rendering the lattice oxygen more labile and hence increases the activity (the specific activity increases with decreasing the strength of the V=O bond). A modification of the catalyst morphology was observed in these promoted catalysts from stacked platelet to agglomerated rosettes. This observation was confirmed by the x-ray diffractograms which indicated a modification in the relative intensities of the (200) and the (024) plane of the $(VO)_2P_2O_7$, whereby the (200) crystal plane was more pronounced in the un-promoted VPO and the (024) plane being more pronounced in the promoted VPO catalysts. The iron-promoted catalysts did not modify the reducibility of the catalysts. The peak (Fig.4.14) obtained at 840^{o}C corresponds to a $V^{4+}\rightarrow V^{3+}$ reduction, this provides evidence of the absence of V^{5+} species in the un-promoted as well as the iron-promoted catalysts. The redox titrations of the vanadium materials indicated an average oxidation state close to 4.00 in these catalysts. This information was further confirmed by the x-ray diffractograms which showed the presence of $(VO)_2P_2O_7$ as the major phase and other phases were not observed. However, ^{31}PNMR spectra of the catalysts indicated the presence of V^{5+} species.

The optimum yield of 46 mol% and 55 mol% for maleic anhydride production was obtained at GHSVs of 2573 and 1450/h respectively corresponding to 74 and 88 mol% conversion for the 0.1% Fe-VPO. The specific selectivities of 3.7 and 2.7 were obtained in the 0.1%Fe-VPO, while specific selectivities of 4.8 and 2.2 were obtained in the un-promoted VPO catalyst at 50% conversion and 80% conversion respectively. This improved selectivity can be associated with the incorporation of the promoter cation in the $(VO)_2P_2O_7$ increasing the lability of the lattice oxygen, hence maleic anhydride yield or alternatively forming surface defects in the VPO structure. From the characterization data obtained for the Fe-VPO catalysts, we may conclude that this cation induced both structural (from scanning electron microscopy) and electronic effects from infra-red and specific activity data.

The ruthenium-promoted VPO catalysts: An increased *n*-butane conversion was also observed for the ruthenium-promoted VPO catalysts relative to the un-promoted VPO catalyst at an optimum temperature of 400^{o}C. This improved conversion could be associated with an increased surface area (Table.4.3). A decrease in both the specific activity and the specific selectivity was encountered for the ruthenium-promoted VPO catalysts (Table.5.4). Furthermore, the incorporation of ruthenium cation in the $(VO)_2P_2O_7$ was not observed, the band corresponding to V=O band did not shift in these catalysts. The V=O band is known to shift when elements of various electronegativities are incorporated into the VPO lattice by substitution of the V^{4+} ion by the promoting cation. A modification of the catalyst morphology was also observed in the ruthenium-promoted catalysts from stacked platelet to agglomerated rosettes. This observation was confirmed by the X-ray diffractograms which indicated a modification in the relative intensities of the (200) and the (024) plane of the $(VO)_2P_2O_7$, whereby the (200) crystal plane was more pronounced in the un-promoted VPO and the (024) plane being more pronounced in the promoted VPO catalysts. The ruthenium-promoted catalysts modified the reducibility of the VPO catalysts. In addition to the reduction peak (Fig.4.14) obtained at 840^{o}C corresponding to a $V^{4+}\rightarrow V^{3+}$ reduction, a shoulder was observed at a temperature of 540^{o}C corresponding to a $V^{5+}\rightarrow V^{4+}$ reduction. From this finding, we can deduce that, the ruthenium cation led to a slight increase in the vanadium oxidation state and probably forming an insignificant amount of the orthophosphate phases which could not be traced in the x-ray diffractograms. This observation can be supported by a slight increase (relative to the un-promoted VPO) in the average oxidation state observed in the ruthenium-promoted VPO catalysts (Table.4.4). A comparable optimum (MA) yield of 41 mol% was obtained at a GHSV of 4762/h and a conversion of 69 mol%. From this observation we can conclude that the presence of ruthenium in the VPO was mainly to increase the surface area of the catalysts relative to the un-promoted VPO, however the specific activity and specific selectivity did not improve as can be observed in Table.5.3, rather comparable yield toward maleic anhydride was obtained at relatively higher conversion.

OVERALL CONCLUSIONS

A range of iron and ruthenium promoted VPO catalysts were prepared and tested for n-butane oxidation to maleic anhydride. These catalysts were tested at 0.1, 0.3 and 1% loading. From the observations of characterization and testing, an iron modified catalyst at a loading of 0.1% led to an improved maleic anhydride selectivity, giving a yield of 46% and 55% at GHSVs of 2573 and 1450 per hour respectively and a temperature of 400^{o}C. Electronic and structural modifications were encountered leading to an improved catalytic performance. The performance of this catalyst is associated with a vanadyl pyrophosphate phase, with a limited and controlled amount of V^{5+} species as illustrated in the x-ray diffractograms, TPR, and ^{31}PNMR data. Moreover, this modification can be considered both structural and electronic in nature as observed in the SEM images and ATR spectra of this catalyst. Furthermore, this improved performance is possible at higher conversions 80 to 90% conversion.

Overall these catalysts show a similar trend to what has been reported in the literature i.e., to improve maleic anhydride selectivity by modifying the morphology and the reducibility of the catalysts. These have been discussed in chapter 1 under the title “the role played by metal elements in VPO catalysis”.

Appendices

APPENDIX 1: ^{31}PNMR Spectra of the used catalysts

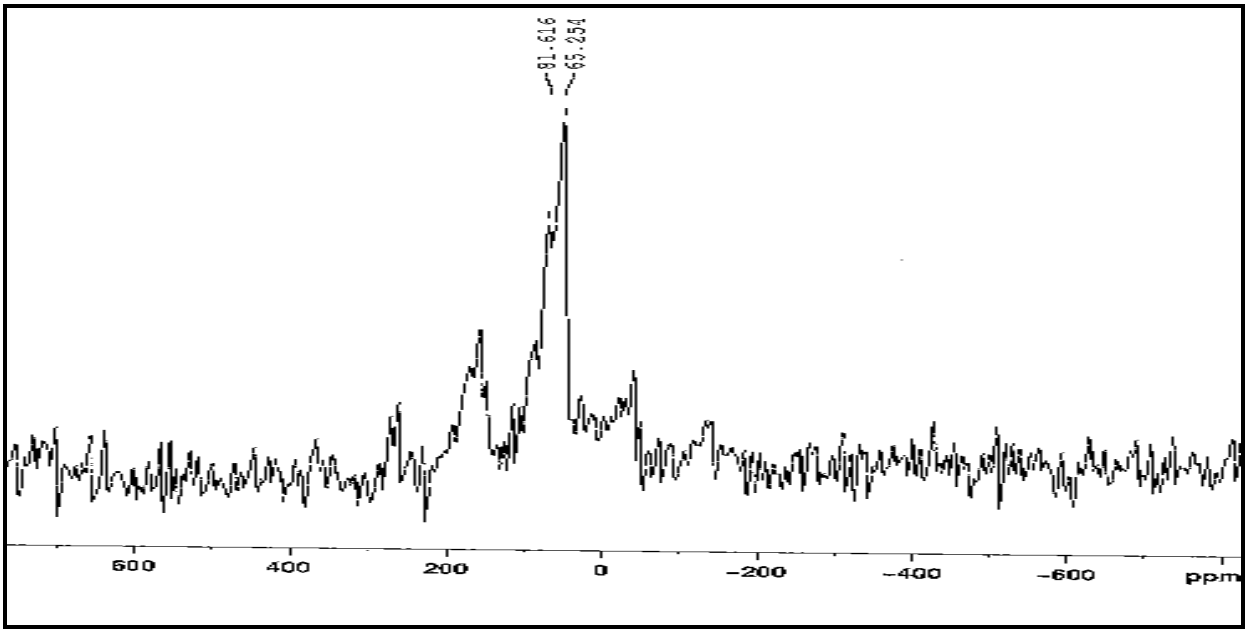

^{31}PNMR spectra 0.1% Fe-VPO

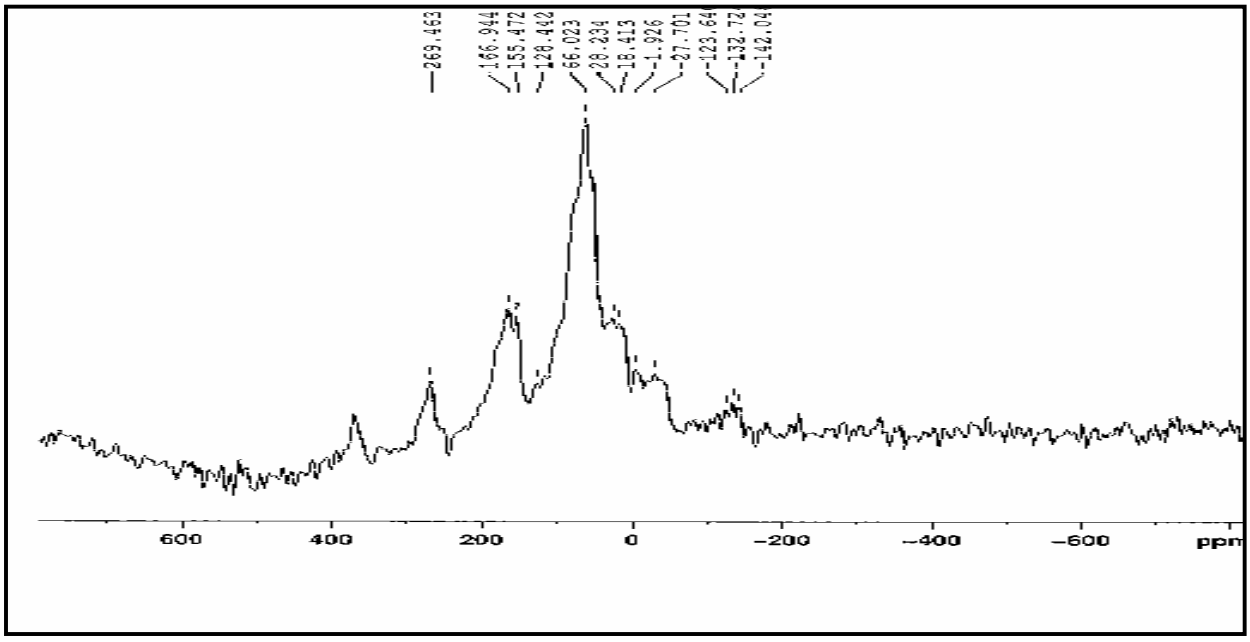

^{31}PNMR spectra of 0.3% Fe-VPO

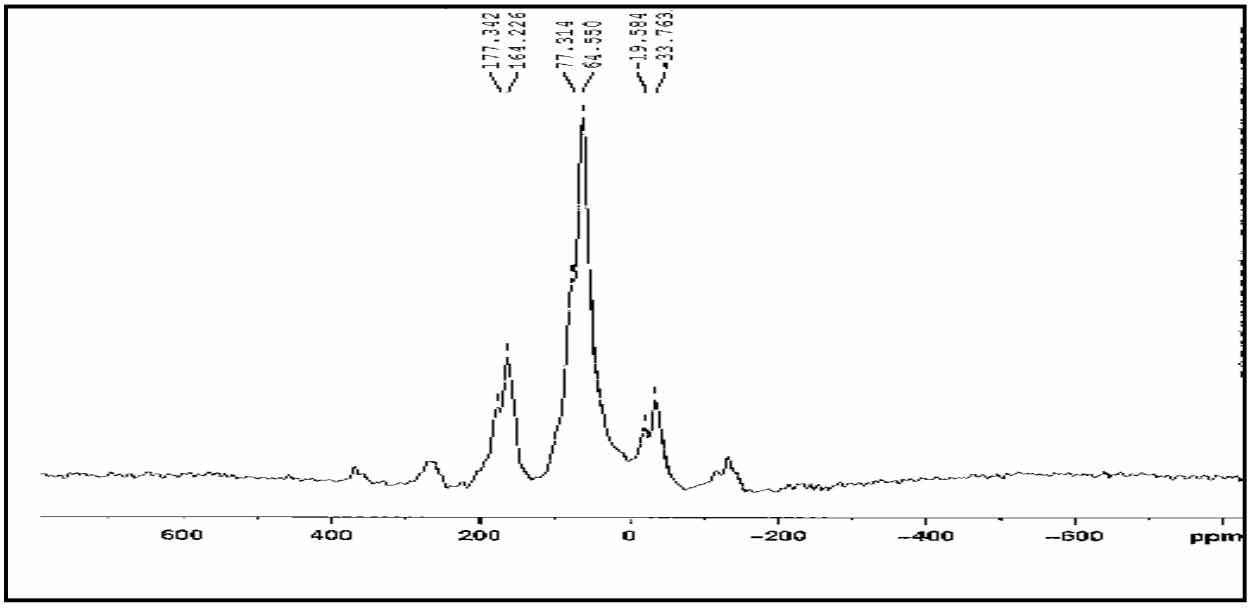

^{31}PNMR spectra of 1% Fe-VPO

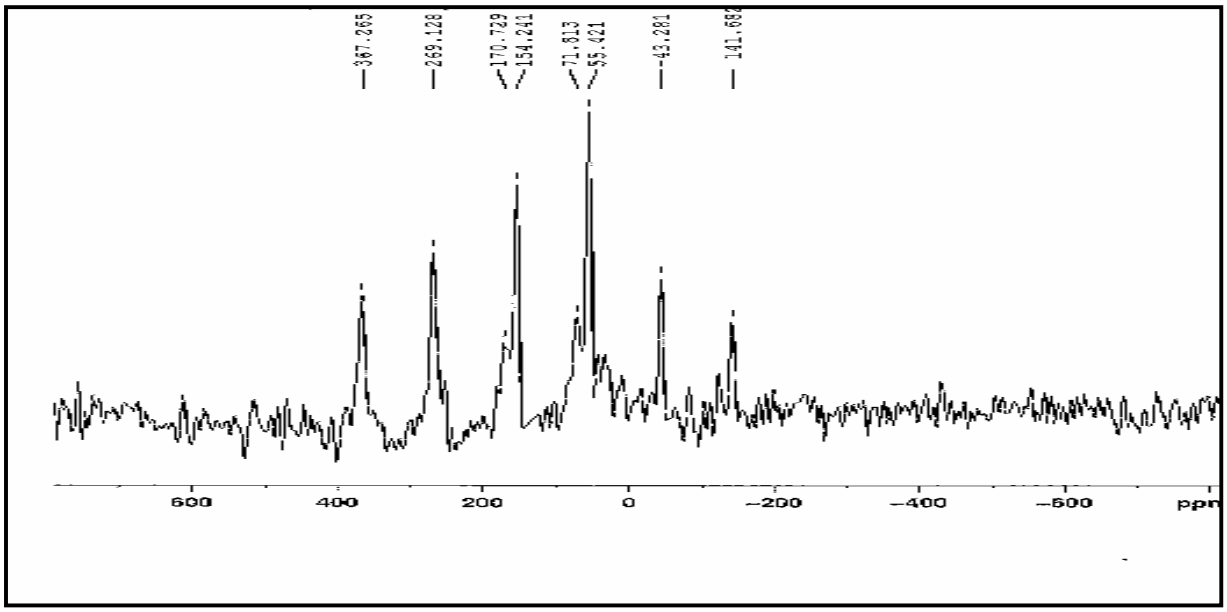

^{31}PNMR spectra of 0.1% Ru-VPO

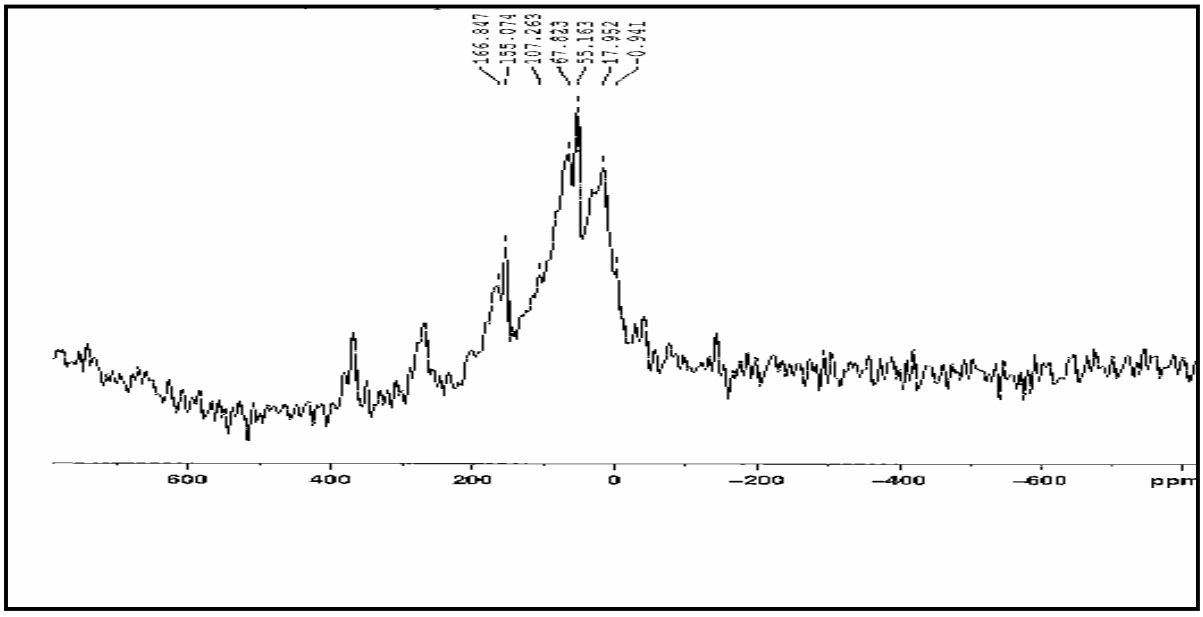

^{31}PNMR spectra of 0.3% Ru-VPO catalyst

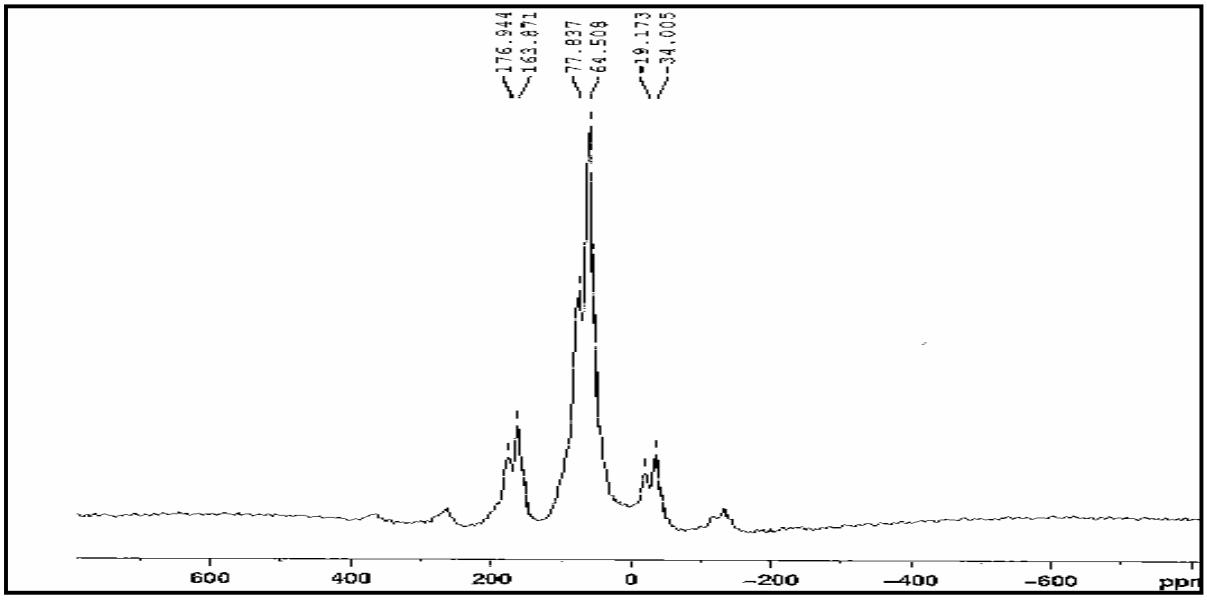

^{31}PNMR spectra of 1% Ru-VPO catalyst

APPENDIX 2: ANALYTICAL TOOLS

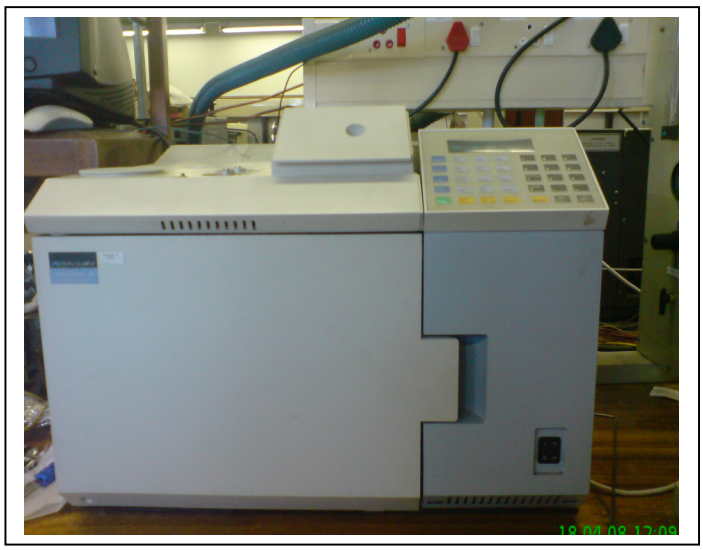

Gas chromatograph equipped with an FID detector

Gas chromatograph equipped with a TCD detector

Rotameters for controlling the feed gas flow rate

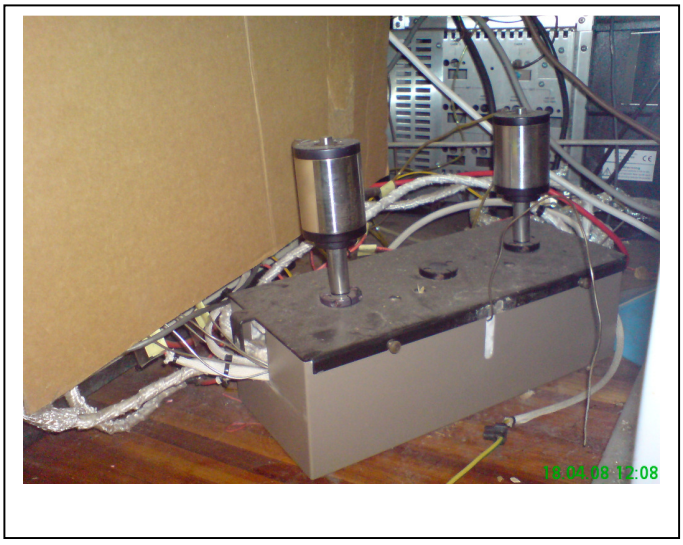

Sampling box with Valco rotary valves (see experimental)